On the Performance of Polypropylene

between synthesis and end-use properties

Claudia Stern

Stern, Claudia

On the Performance of Polypropylene / between systhesis and end-use properties
PhD thesis, University of Twente, Enschede 2005
ISBN: 90-365-2252-8

Cover: Albert Einstein (1879 - 1955)
Imagination is more important than knowledge...

ON THE PERFORMANCE OF POLYPROPYLENE

BETWEEN SYNTHESIS AND END-USE PROPERTIES

DISSERTATION

to obtain
the doctor's degree at the University of Twente,
on the authority of the rector magnificus,
prof. dr. W.H.M. Zijm,
on account of the decision of the graduation committee,
to be publicly defended
on wednesday 2nd of november 2005 at 15.00

by

Claudia Stern

born on 22nd april 1975
in Ellwangen, Germany

This dissertation is approved by the promoters:

prof. dr. G. Weickert and **prof. dr. A. Frick**

CONTENTS

LIST OF ABBREVIATIONS

a	exponent	[-]
a_T	shift factor	[-]
A	cross section	[mm^2]
A_0	initial cross sectional area	[mm^2]
A_1	shift factor	[-]
A_2	shift factor	[-]
B	exponent	[-]
c_1	constant	[-]
c_2	constant	[-]
c_p	heat capacity	[$J \cdot g^{-1} \cdot K^{-1}$]
C	slope of viscosity curve	[-]
C^*	number of active sites	[$mol \cdot g_{cat}^{-1}$]
C_m	monomer concentration	[$kg \cdot m^{-3}$]
d	wall thickness	[mm]
D	reciprocal transition rate	[s]
D_1	constant	[-]
dE	energy	[W]
E	Young's modulus	[$N \cdot mm^{-1}$]
E*	tensile complex modulus	[$N \cdot mm^{-1}$]
E'	tensile storage modulus	[$N \cdot mm^{-1}$]
E''	tensile loss modulus	[$N \cdot mm^{-1}$]
E_a	activation energy	[$kJ \cdot mol^{-1}$]
F	force	[N]
$\hat{F}$	force amplitude	[N]
G_N^0	plateau modulus	[Pa]
G_{FT}	flow transition modulus	[Pa]
G'	shear storage modulus	[Pa]
G''	shear loss modulus	[Pa]
h	height	[mm]
H	gap between the plates	[mm]
$\dot{H}$	heating / cooling rate	[$K \cdot min^{-1}$]
ΔH	enthalpy	[$J \cdot g^{-1}$]
ΔH_m	melting enthalpy	[$J \cdot g^{-1}$]
ΔH_f	melting enthalpy of a perfect crystal	[$J \cdot g^{-1}$]
HWR	height / width-ratio	[$W \cdot g^{-1} \cdot °C^{-1}$]
I	intensity	[-]
J_e^0	equilibrium compliance	[Pa^{-1}]
K	constant	[$Pa \cdot s\ (mol \cdot g^{-1})^a$]
K_1	constant	[-]
K_2	constant	[-]
k_d	deactivation rate constant	[hr^{-1}]

k_p	propagation rate constant	$[m^3 \cdot mol^{-1} \cdot hr^{-1}]$
L	lamella thickness	[mm]
L_m	average lamella thickness	[mm]
L_{max}	maximum lamella thickness	[mm]
L_0	initial gauge length	[mm]
ΔL	displacement	[mm]
m	sample mass	[mg]
M	crystalline mass	[mg]
M_P	monomer concentration	$[mol \cdot L^{-1}]$
M_t	torgue	[N·m]
M_c	critical molecular weight	$[g \cdot mol^{-1}]$
ME	entanglement molecular weight	$[g \cdot mol^{-1}]$
MFR	melt flow rate	$[g \cdot 10^{-1} \cdot min^{-1}]$
MN	number average molecular weight	$[kg \cdot mol^{-1}]$
MW	weight average molecular weight	$[kg \cdot mol^{-1}]$
MWD (=MW/MN)	molecular weight distribution	[-]
MV	viscosity-average molecular weight	$[kg \cdot mol^{-1}]$
n	constant	[-]
p	pressure	[bars]
p_{inj}	injection pressure	[bar]
p_h	holding pressure	[bar]
p_{H2}	partial pressure of hydrogen	[bars]
P	mechanical property	[-]
PD	polydispersity	[-]
$\dot{Q}$	heat flux	$[W \cdot g^{-1}]$
r	radius	[mm]
R	gas constant	$[J \cdot kg^{-1} \cdot K^{-1}]$
R_{out}	outside radius	[mm]
R_p	polymerisation rate	$[kg_{PP} \cdot g_{cat}^{-1} \cdot hr^{-1}]$
$R_{p,0}$	initial polymerisation rate	$[kg_{PP} \cdot g_{cat}^{-1} \cdot hr^{-1}]$
s	displacement	[mm]
$\hat{s}$	displacement amplitude	[mm]
t	time	[s]
t_c	cycle time	[s]
t_{ph}	holding pressure time	[s]
T	temperature	[K]
T_0	reference temperature	[K]
T_c	crystallisation temperature	[°C]
T_{max}	maximum temperature	[°C]
T_m	melting temperature	[°C]
T_m^0	equilibrium melting temperature	[K]
T_{me}	endset melting temperature	[°C]
T_{mt}	melt temperature	[°C]

T_{wz}	mould temperature	[°C]
v_{inj}	injection speed	[mm·min^{-1}]
tan δ	loss factor	[-]
X	molar ratio (H_2/M_p)	[mol·mol^{-1}]
Xa	amount of amorphous fraction	[%]
Xc	crystallinity	[%]
Y	standard format for GPC curve (Y_j^d M_{mj})	[g·mol^{-1}]
α	effective temperature conductivity	[m^2·s^{-1}]
δ	phase angle	[-]
ε	strain	[%]
ε_B	strain at break	[%]
ε_e	engineering strain	[%]
ε_t	true strain	[%]
$\dot{\gamma}$	shear rate	[s^{-1}]
$\dot{\gamma}_{critical}$	critical shear rate	[s^{-1}]
η	viscosity	[Pa·s]
η_0	zero viscosity	[Pa·s]
η_0*	complex zero viscosity	[Pa·s]
φ_e	free surface energy	[J·cm^{-2}]
λ	thermal conductivity	[W·K^{-1}·m^{-1}]
λ’	characteristic retardation time	[s]
ν	frequency	[s^{-1}]
ρ	density	[g·cm^{-3}]
ρ_c	density of crystal phase	[g·cm^{-3}]
σ	stress	[N·mm^{-2}]
σ_e	engineering stress	[N·mm^{-2}]
σ_t	true stress	[N·mm^{-2}]
τ	shear stress	[Pa]
τ*	shear stress at the transition between Newtonian and power law behaviour	[Pa]
$\dot{\nu}$	volume rate	[mm^3·s^{-1}]
ω	angular frequency	[s^{-1}]
Ω	plate velocity	[s^{-1}]
ζ	constant	[-]
aPP	atactic polypropylene	
Au	gold	
B	bimodal	
CM	compression moulding	
CVZD	continuous vibration zone-drawing	
DMA	dynamic mechanical analysis	
DSC	differential scanning calorimetry	
FD	direction of flow	
GP	gas phase	
GPC	gel permeation chromatography	

H_2	hydrogen
iPP	isotactic polypropylene
I	industrial
IM	injection-moulding
LP	liquid pool
M	monomodal
MET	metallocene
$MgCl_2$	magnesium chloride
MLR	multiple linear regression
MPI	moldflow plastic insight
na	not available
PBT	poly(butylene terephthalate)
Pd	palladium
PD	perpendicular to direction of flow
PE	polyethylene
PID	proportional, integral, derivative
POM	polyformaldehyde
PP	polypropylene
RuO_4	ruthenium oxide
sPP	syndiotactic polypropylene
SCORIM	shear-controlled orientation injection moulding
SEM	scanning electron microscopy
TEA	triethyl aluminium
TEM	transmission electron microscopy
$TiCl_4$	titanium chloride
WAXS	wide-angle x-ray scattering
ZN	Ziegler-Natta

SUMMARY

Numerous publications have appeared which focus on the topic ‘structure and end-use properties relationship in PP’. However, none of these research groups has ever tried a holistic approach. A holistic approach based on the “chain of knowledge” aims to determine and understand the end-use properties of parts, based on well-defined polymers. Primarily, the present thesis has followed that idea and studied systematically the influence of the molecular structure on the resultant mechanical properties of injection-moulded polypropylene (PP) parts for the first time. The results found offer exciting and essential new insight into the polymeric structure-properties relationship and provide a more fundamental understanding of isotactic PP.

Isotactic PP with different molecular weights, but very similar polydispersity, was synthesised in gas phase (GP) and liquid pool (LP) processes under defined polymerisation conditions, using a modern Ziegler Natta catalyst. Thus, for the first time, PP powders characterised exactly by their polymerisation kinetics and basic properties have been made available for further material analysis and processing. In consequence, the polymerisation process with appropriate reaction kinetics can be associated with and correlated to a resulting PP powder characterised by its molecular structure, powder morphology, crystallinity, and rheological properties.

Differences between GP and LP polymerisation can be detected in the polymerisation kinetics. The initial polymerisation rate reaches a maximum for LP of approx. 150 $kg_{PP} \cdot g_{cat}^{-1} \cdot hr^{-1}$ in contrast to the initial polymerisation rate for GP, which is only about 45 $kg_{PP} \cdot g_{cat}^{-1} \cdot hr^{-1}$. This difference is caused by the higher monomer concentration within the closest vicinity of the active catalyst sites in the case of liquid propylene polymerisation.

Furthermore, rheological investigations have shown that the zero viscosity of GP-PP is less than that of LP-PP measured at the same molecular weight. The difference can be explained by the various polydispersities (PD) of GP- and LP-PP, which is caused by the different polymerisation process. Additionally, it has been found that the crystalline fraction of all PP samples rises after solidification from the melt. Consequently the folding ability of the polymer chains to crystallites inside the reactor is not as good as in the melt state.

Finally, LP polymerisation results in more homogenous PP material with improved properties, compared to GP polymerisation using the same Ziegler-Natta catalyst and polymerisation conditions.

The well-known PP powders were processed to parts (micro dumbbell specimens) using a newly developed micro-injection moulding technique. Two major reasons argue for the processing technique used; injection moulding is an important melt processing technique in the industry, and micro technology permits the manufacture of testable specimens requiring very small amounts of material. Therefore, by means of micro-injection moulding, micro

dumbbell specimens were obtained under controlled conditions from the freshly produced and well-known PP powders for further characterisation of the new PP polymers in solid state.

Analysis of the solidification behaviour during processing shows that the acting cooling rate is very high, so that polymer crystallisation is almost complete after 1 s. In addition, simulation of the filling behaviour of the micro dumbbell specimens prepared indicate the existence of a high shear rate. The shear rate increases as the molecular weight increases towards a maximum of about $7.5 \cdot 10^5$ s^{-1}. The high shear rates are caused by the very small dimensions of the micro dumbbell specimens and by the low viscosity of the PP samples.

As a result of acting shear stress the macromolecules are oriented, which further is promoted by the fact that the characteristic retardation time, indicating orientation retardation time, depends on the molecular weight and is much higher than cooling time for high molecular weight samples. Consequently, retardation of oriented macromolecules cannot take place.

The micro dumbbell specimens made from LP-PP which are present exhibit extraordinary solid state properties in contrast to commercially-available PP homopolymer. With a tensile strength of up to 100 $N \cdot mm^{-2}$ and an attainable strain at break of more than 30 % the mechanical strength performance is notably higher than the results given by existing literature. The favourable strength and the high deformation ability of the samples studied rise as molecular weight increases, obviously in relation to the shear-induced crystallisation morphology of the samples, which can be schematically explained as the model suggests. Above a molecular weight of 320 $kg \cdot mol^{-1}$ and a critical shear rate of $3 \cdot 10^5$ s^{-1}, so-called shish kebab structures are formed during the injection-moulding process. These highly oriented structures cause an enormous strength capability, which can be documented by TEM analysis. In fact, the number of shish kebabs increases as the molecular weight increases. Also lamellae thickness increases as molecular weight increases from about 10 nm towards a maximum of about 30 nm.

The stiffness of the PP samples studied can be explained in terms of micro mechanics by the existence of an amorphous fraction with a certain molecular mobility. In addition, the strain hardening occurring above yield point during quasi-static tensile tests can be related to the thickness of the lamellae. Furthermore, maximum lamella thickness governs tensile stress, rather than overall crystallinity. The recognised phenomenon that tensile strength and stiffness usually increase in parallel with an increase in crystallinity, is only correct regarding one defined molecular weight.

The oriented morphology (shish kebab structure) inside the micro dumbbell specimens, which are formed as a result of shear-induced crystallisation, is not thermodynamically stable. Annealing of the micro dumbbell specimens prepared causes re-organisation of their morphological structure, mainly of the shish kebab structure.

The aim of this thesis has been successfully achieved by the clarification of the relationship between the influence of molecular structure on the end-use properties. The holistic approach chosen has enabled the chain of knowledge in the PP field to be locked more tightly. This present contribution to a fundamental understanding of polymers in the PP field will further promote the technology of polymer production and processing, and this will facilitate, for instance, the realisation of tailor-made PP with high-strength for special application.

Because of their special properties, the novel LP-PP studied seems to be technically important in particular for applications where very small parts are required. The novel PP has enough potential to replace most other technical polymers in the future.

SAMENVATTING

Verscheidene publicaties zijn verschenen die gericht zijn op het onderwerp ‘struktuur en producteigenschappen relatie in polypropyleen’. Echter, geen enkele onderzoekgroep heeft ooit een holistische aanpak geprobeerd. Een holistische aanpak gebaseerd op de ‘chain of knowledge’ richt zich op het bepalen en begrijpen van de end-use eigenschappen van specimen, gebaseerd op welomschreven polymeren. Dit proefschrift heeft voornamelijk dit idee gevolgd en voor het eerst systematisch de invloed van de moleculaire structuur op de resultatieve mechanische eigenschappen van spuitgegoten polypropyleen (PP) specimen bestudeerd. Het gevonden resultaat biedt een enerverend en nieuw inzicht in de struktuur-eigenschappen relatie van polymeren en biedt een beter fundamenteel begrip van isotactisch polypropyleen.

Isotactisch PP met verschillend moleculair gewicht maar met gelijke polydispersiteit, werd gesynthetiseerd in gasfase (GP) en vloeibaar propyleen (LP) processen onder gedefinieerde polymerisatie condities, met een moderne Ziegler Natta katalysator. Dus, voor het eerst zijn PP poeders, precies gekarakteriseerd door hun polymerisatiekinetiek en basiseigenschappen, geschikt gemaakt voor verdere materiaalanalyse en verwerking. Als gevolg hiervan kon het polymerisatieproces met geschikte reactiekinetiek geassocieerd worden met en gecorreleerd worden aan resulterend PP poeder gekarakteriseerd door moleculaire structuur, poeder morfologie, kristalliniteit en rheologische eigenschappen.

Verschillen tussen GP en LP polymerisatie kunnen gevonden worden in de polymerisatiekinetiek. De aanvankelijke polymerisatiesnelheid bereikt een maximum voor LP van 150 $kg_{PP} \cdot g_{cat}^{-1} \cdot hr^{-1}$ in tegenstelling tot de initiële polymerisatiesnelheid voor GP, die slechts 45 $kg_{PP} \cdot g_{cat}^{-1} \cdot hr^{-1}$ is. Dit verschil wordt veroorzaakt door de hogere monomeerconcentratie in de dichtste nabijheid van de actieve katalysator centra in het geval van vloeibaar propyleenpolymerisatie.

Verder hebben rheologische onderzoeken uitgewezen dat de nul viscositeit van GP-PP minder is dan dat van LP-PP, gemeten in hetzelfde moleculaire gewicht. Het verschil kan verklaard worden door de verschillende polydispersiteiten (PD) van GP- an LP-PP, die veroorzaakt zijn door de verschillende polymerisatieprocessen. Bovendien is gevonden dat de kristallijne fractie van alle PP monsters toeneemt na afkoeling van de smelt. Hieruit blijkt dat de buigzaamheid van de polymeerketen tot kristallen in de reactor niet zo goed is als in gesmolten staat. Tenslotte, LP polymerisatie resulteert in meer homogeen PP materiaal met verbeterde eigenschappen, in vergelijking met GP polymerisatie als gebruik wordt gemaakt van dezelfde Ziegler-Natta katalysator en polymerisatiecondities.

De bekende PP poeders werden verwerkt in specimen (micro dumbbell exemplaren) gebruikmakend van een nieuw ontwikkeld micro-injection moulding (or micro-spuitgiet) techniek. Twee belangrijke redenen pleiten voor de gebruikte procestechniek; spuitgieten is

een belangrijke procestechniek in de industrie, en microtechnologie staat de vervaardiging van testexemplaren toe die zeer kleine hoeveelheden materiaal vereisen. Daarom werden door middel van micro-spuitgieten micro dumbbell exemplaren verkregen onder gecontroleerde omstandigheden uit zuiver geproduceerde en bekende PP poeders voor verdere karakterisering van de nieuwe PP polymeren in vaste vorm.

Analyse van de stollingseigenschap gedurende het proces laat zien dat de opgetreden afkoelingssnelheid erg hoog is, zodat het polymeer bijna volledig binnen 1 seconde kristalliseert. Bovendien laat simulatie van de vuleigenschap van de bereide micro dumbbell exemplaren het bestaan zien van een hoge 'shear' snelheid. De shear snelheid neemt toe met toenemend moleculair gewicht tot een maximum van ongeveer $7.5 \cdot 10^5$ s^{-1}. De hoge shear snelheden worden veroorzaakt door de zeer kleine omvang van de micro dumbbell exemplaren en door de lage viscositeit van de PP monsters.

Als gevolg van de shear spanning oriënteren de macromoleculen zich wat verder bevorderd wordt door het feit dat de karakteristieke retardatie tijd, de oriënterende retardatie tijd, afhangt van het moleculaire gewicht en is veel langer dan de afkoelingstijd voor hoog moleculair gewicht monsters. Als gevolg daarvan kan retardatie van georiënteerde macromoleculen niet plaatsvinden.

De micro dumbbell exemplaren gemaakt van LP-PP die aanwezig zijn, vertonen buitengewoon vaste vorm eigenschappen in tegenstelling tot het commercieel beschikbare PP homopolymeer. Met een treksterkte tot 100 $N \cdot mm^{-2}$ en een haalbare breekspanning van meer dan 30 %, is de mechanische sterkteprestatie opmerkelijk hoger dan de resultaten weergegeven in de bestaande literatuur. De gunstige sterkte en de hoge deformatiecapaciteit van de bestudeerde monsters nemen toe met toenemend moleculair gewicht, kennelijk in relatie tot de shear veroorzaakte kristallisatie morfologie van de monsters, wat schematisch kan worden weergegeven, zoals het model suggereert. Boven een moleculair gewicht van 320 $kg \cdot mol^{-1}$ en een kritieke shear snelheid van $3 \cdot 10^5$ s^{-1}, worden de zogenaamde shish kebab structuren gevormd gedurende het spuitgietproces. Deze sterk gerichte structuren veroorzaken een enorm sterktevermogen, wat gedocumenteerd kan worden door TEM analyse. In feite neemt het aantal shish kebabs toe als het moleculaire gewicht toeneemt.

Ook de lamellendikte neemt toe als het moleculaire gewicht toeneemt vanaf ongeveer 10 nm tot een maximum van ongeveer 30 nm.

De stijfheid van de bestudeerde PP monsters kan verklaard worden in termen van micromechanica door de aanwezigheid van een amorfe fractie met een zekere moleculaire beweeglijkheid. Daarnaast kan de spanningverharding die boven het 'yield punt' voorkomt gedurende quasi-statische trekproeven gerelateerd worden aan de dikte van de lamellen. Bovendien, de maximale lamellendikte controleert de trekspanning eerder dan de algehele kristalliniteit. Het verschijnsel dat de treksterkte en stijheid parallel toenemen met toenemende kristalliniteit, is correct mits het een gedefinieerd moleculair gewicht betreft.

De georiënteerde morfologie (shish kebab structuur) in de micro dumbbell exemplaren, die zich gevormd hebben als gevolg van kristallisatie door shear is thermodynamisch niet stabiel. Temperatuur behandeling (annealing) van de bereide micro dumbbell exemplaren veroorzaakt reorganisatie van hun morfologische structuur, voornamelijk de shish kebab structuur.

Het doel van dit proefschrift is succesvol tot stand gebracht door de opheldering van de relatie tussen de invloed van de moleculaire structuur en de producteigenschappen. De gekozen holistische aanpak heeft de keten van kennis (or ‘chain of knowledge’ see first allinea) op het gebied van PP nauwer gesloten. Deze huidige bijdrage aan fundamenteel begrip van polymeren op het gebied van PP zal de technologie van de polymeerproductie en processen bevorderen en dit zal, bijvoorbeeld, de realisatie van ‘tailor-made PP’ met ‘high-strength’ voor speciale doeleinden vergemakkelijken.

Vanwege de speciale eigenschappen, blijken de bestudeerde nieuwe LP-PP technisch belangrijk in het bijzonder voor toepassingen waar zeer kleine deeltjes vereist zijn. De nieuwe PP heeft genoeg potentieel om de meeste andere technisch hoogwaardige polymeren in de toekomst te vervangen.

1 INTRODUCTION

Within the wide range of polymers, polyolefins constitute the largest segment of a market with a capacity of about 70 million tons worldwide. One current type of this commodity is essentially isotactic polypropylene (PP). Although it was developed in the early 1950s by Ziegler and Natta and has been manufactured commercially since the mid-1960s, PP still shows an average growth rate of 6% due to its wide range of properties and good cost/performance ratio.[1] The economical success of iPP is based especially on its processability and wide applicability.[2-4] Applications of iPP can be found in specific fields, such as packaging, and the automotive and electronics industries.

Constant expansion, new markets and innovative processing techniques require more than ever universally adaptable product properties. This demand explains the continued intensive research on PP in order to make its synthesis and processing more efficient and to improve product performance. For example, a break-through was achieved some years ago using metallocene catalysts to polymerise propylene. Due to the unique composition of metallocene, tailor-made PP can be synthesised with very low polydispersity (PD) and improved impact strength. Not only the catalyst, but also reactor technique and polymerisation conditions, as well as the actual melt-processing conditions, demonstrate crucial influences on the properties of PP parts.

In order to achieve purposeful changes in final product performance, information as to how these influences affect properties is required; in addition to this, the actual influences have to be described, defined and preferentially understood. However, such understanding is best achieved by following the chain of knowledge.

By „chain of knowledge“, we mean scientific and technical knowledge of the genesis of a particular polymer part, starting with the synthesis of the basic polymer, through processing the polymer into parts, including possible treatments (such as annealing), up to the final applications with the required end-use properties.

However, the influence of structure on final properties is far-reaching and very complex. Many influencing factors can act either synergistically or contrarily. Thus the relationship between structures and properties in solid state can be defined seriously and successfully only if the governing factors are classified and steps in the chain of knowledge are studied separately.

Many researchers have addressed the structure-properties relationship, but the danger exists that such research results include a complex mixture of unknown influencing factors, with the result that the actual relationships are concealed. Furthermore, a fundamental understanding of the structure-properties relationship becomes difficult and is probably in several cases incorrect.

1.1 Influence of molecular weight on properties of PP – A LITERATURE REVIEW

The molecular weight (MW), molecular weight distribution (MWD) and tacticity of the macromolecule are mainly influenced by the catalyst system used, the prevailing polymerisation conditions and the hydrogen content.[5-22] For example, the tacticity of the macromolecule is virtually determined by the external donor when modern Ziegler-Natta catalysts are used for polymerisation. Nowadays, the catalyst systems are of such high quality that they guarantee a high isotacticity within a certain range and thus the influence of the tacticity on the final properties of PP plays a minor role. Naturally, the influence of end groups is small, since the molecular weight of PP used for processing is high enough that the relation of end group to the residual macromolecule becomes negligible. Therefore, in practice, one of the most important factors which governs the quality of PP is molecular weight and its distribution, which can control various properties of PP, such as stiffness, strength, temperature resistance, etc.

As it is not possible to cover the influence of molecular weight on morphology and properties in a review of this extent, only the basic features, which are essential to the study of the relationship between molecular structure and end-use properties, are reviewed. Moreover, this chapter attempts to point out the necessity of following the chain of knowledge for a fundamental understanding of the structure-property-relationship.

The origin and many aspects of synthesis, processing, and properties of PP are covered in the Polypropylene Handbook edited by Moore.[23] Recently published articles also provide and overview of developments and studies in the area of the science of polyolefins, such as polymerisation kinetics, catalyst upgrading, rheology, crystallisation kinetics, processing, structure and morphology, deformation behaviour etc.[24-29]

One of the first attempts to clarify the relationship between molecular weight and mechanical properties was presented by Flory[30] as early as 1945. He proposed an empirical, mathematical formula for a correlation of molecular weight and mechanical properties, as described in eq. 1.1.

$$P = c_1 + \frac{c_2}{MW} \qquad (1.1)$$

where P is the mechanical property, MW is the molecular weight, and c_1 and c_2 are constants.

Earlier, this equation by Flory was applied mainly for polystyrene. Ogawa[31] revealed that Flory's mathematical correlation held very well for the fitting of the flexural strength and the elastic tensile modulus, depending on the molecular weight. However, when using eq. 1.1 it was not possible to correlate the tensile strength and strain at break to the molecular weight.

In the case of PP, he supposed that the history of preparing the samples might be influencing the result.

Finally, this simple mathematical model (eq. 1.1) can be used to describe roughly and to estimate the mechanical properties, depending on the molecular weight. However, in reality, the relationship between the molecular structure and the final properties is more complex than is assumed here; this is the case in particular when no freshly produced polymer is used. Therefore, this equation is too simple and ultimately of little use in describing the structure-property relationship.

Some years later, Osawa[31] attempted to describe the relation between the properties, morphological structure and processing by means of a more complex mathematical model. His approach was based on the statistical method of multiple linear regression (MLR). In a case of forging PP, he found, using his model, a good correlation between the structure and the tensile strength and modulus. In principle, the mathematical model established by Osawa[31] fits the basic requirements, but only for the polymer system referred to. Nevertheless, the results found by Albano et al.[32] confirm Osawa's findings. They also developed a model for analysing the relation between thermal history, mechanical properties, and molecular weight of PP. Therefore, a multivariable analysis was carried out and a model for correlating the relation of molecular weight, crystallinity and mechanical properties (i.e. tensile strength, Young's modulus, impact strength) was established. The algorithm used was a combination of Gauss-Newton and Levenberg-Marquardt methods. Based on multivariable analysis, they estimated the mechanical behaviour of PP with regard to its molecular weight. They found that crystallinity increases as molecular weight decreases and thus tensile strength increases. However, it should be noted that their studies on the influence of molecular weight and processing conditions on mechanical properties were performed under solidification conditions which were not industrially appropiate. (The existing cooling rates for preparing their samples were much too low.) All samples for their analysis were processed by dynamic cooling of the molten polymer at low cooling rates of between 2.5 and 20 $K \cdot min^{-1}$, using a moulding press. Usually, in practice, cooling rates of several thousands of Kelvins per minute are in use. As a result of the much faster solidification process, different morphological structures are formed in industrial parts, as compared with the structures Albano et al. were using in their research work.

In general, existing efforts are not sufficient for modelling and mathematical prediction of the relationship between molecular weight and final properties. The reason for this is the complexity of the structure-property-relationship and the fact that an understanding is still lacking of the effect of molecular weight on processing, the solidification process at defined cooling conditions and on the resulting morphology, all of which ultimately govern the final properties of polymer parts. This continues to be the case even though this is an area of polymer science which has been subject to intensive study in recent decades.[31-72]

Kantz et al.[34] found as early as 1972 that molecular structure and processing conditions influence the skin-core morphology of injection-moulded PP samples. The molecular properties, such as MW and MWD (degree of isotacticity remaining constant) and the melt

temperature preferably affect crystallite orientation, which is the principal parameter governing tensile strength, impact strength, and shrinkage. Altendorfer and Seitl[35] confirmed these observations and stated that commercial PP with varying MW and MWD showed a differently oriented morphology of injection-moulded parts. The skin-core morphology along the flow path varies, depending on the molecular characteristics. Low molecular weight PP with narrow MWD exhibits less orientation coupled with a thin skin layer. In contrast to this, high molecular weight PP with broad MWD shows highly oriented structures. Furthermore, in the case of low molecular weight PP only one intermediate layer can be observed, whereas high molecular weight PP showed two intermediate layers. In addition, Philips et al. found that the chain axis orientation decreases as the distance from the gate increases and the melt temperature at a fixed location increases. In the case of PP, Jay et al.[36] observed an increase in orientation as the molecular weight increases. The reason for this is the enhancement of the nucleation and the growth rate as a function of the molecular weight.

Although Philips et al.[37] also observed changes in crystallite orientation as a function of the materials variables (i.e., MW, MWD, tacticity), they could not find significant differences in the crystallinity and stiffness of PP samples, depending on the molecular weight. Similar results have been demonstrated by Incarnato et al.[38], who have compared the resulting mechanical properties of a series of films made from recycled PP using cast technology. While the rheological behaviour (mainly zero viscosity and shear thinning) and thus the processability varied as a function of the molecular weight, the mechanical properties, such as Young's modulus, tensile strength and break point were constant for all injection-moulded PP samples.

While studies by several independent researchers confirm the finding of Philips et al. and Incarnato et al., there have also been numerous investigations that have yielded contradictory results. For example, the results of Fujiyama and Wakino[39] clearly showed different mechanical and thermal properties of injection-moulded samples when homopolymer PP's with different molecular weights were used. They studied the properties of flexural test specimens made from six different PP's with molecular weights from 186 to 639 $kg \cdot mol^{-1}$ using also different cylinder temperatures (200 to 320°C) during melt processing. The results found show that the stiffness and strength of the specimen become higher as the molecular weight and the cylinder temperature become higher, because of increasing crystallinity. In addition, the thickness of skin layer and, in consequence, impact strength becomes higher as the molecular weight and cylinder temperatures become lower. Furthermore, the a*-axis oriented component fraction of the crystalline PP increases as molecular weight and cylinder temperature increase. The reason for the variation in skin-core morphology and orientation along the flow direction was explained from the viewpoint of the growth of recoverable shear strain at the gate and the relaxation of the PP melt in the cavity, depending on the molecular weight. The higher-order structures are inhomogeneous in the flow and thickness directions, which strongly influence the properties of the product.

In general, parts with a thick skin layer show improved impact strength in association with poor dimensional stability. In contrast, highly crystalline samples possess high stiffness and strength, but tend to be brittle. The reason for this is the different formation of lamellae as

a function of molecular weight. Gahleitner et al.[40] observed higher crystallisation temperatures for lower molecular weight samples and as a result lamellae structure varies as molecular weight varies. This also has been demonstrated by Michler[41], who has observed for HDPE an increase in thickness of lamellae as molecular weight increases. As a consequence of the changed morphology, the final properties are different. In 1974, Young[42] was already stating that the thickness of lamellae is the main determining factor of yield stress; the thicker the lamellae, the higher the yield stress. Moreover, Schrauwen et al.[43] revealed that lamella thickness is the determining factor influencing strain hardening of semi-crystalline polymers. They observed an increased strain hardening, when thicker lamellae exist. Furthermore, the thickness of lamellae plays an important role in the total energy absorbed during impact fracture, as attributed by van der Meer.[44]

Exciting findings of the influence of molecular weight on the mechanical properties were presented by Prox and Ehrenstein.[45] They reported a pronounced increase in stiffness and tensile strength of injection-moulded PP samples as a function of molecular weight. Moreover, they observed the highest tensile strength of 80 $N \cdot mm^{-2}$ and stiffness of approx. 3 800 $N \cdot mm^{-2}$ in association with low deformability and low strain at break of 32 %, for the injection-moulded PP sample with an average molecular weight of 470 $kg \cdot mol^{-1}$. These values in mechanical properties are 2.5 times higher when compared to those usually observed for injection-moulded samples made from PP. The reason for these extraordinary mechanical properties is assumed to be caused by self-reinforcement as a result of an oriented and anisotropic morphology inside the PP sample. The phenomenon of increasing tensile strength as a result of high orientation is already known from studies on cold drawn fibres. Highly drawn fibres obtain strength and stiffness even in the range of GPa, but this is also coupled with low deformability. Candia et al.[46] explained this low deformability by the drastic reduction of the molecular mobility in the amorphous component during drawing.

However, Fujiyama and Wakino[39] have ascertained that the reason for the improved mechanical properties of injection-moulded samples (presented by Prox and Ehrenstein) is a formation of the so-called shish kebab supramolecular structure. They identified in injection-moulded PP samples oriented structures with main skeleton structures, whose axis is parallel to machine direction, piled epitaxially with a*-axis oriented imperfect lamellar structures by means of wide-angle X-ray scattering (WAXS). In addition, they found a higher density of shish kebab in the intermediate layer, between the skin layer and the core, which results in a pronounced increase in tensile strength. The tensile yield stress in machine direction of the skin layer was about 1.5 times higher than that of the core layer.

The first description of the shish kebab supramolecular structure is credited to Pennings and Kiel[47], but Keller et al.[48-50] were among the first to assign the formation of row nucleated columnar structures (i.e. shish kebab) to crystallising melt under high shear stresses. Kalay and Bevis[51,52] even took advantage of this kind of shear-induced crystallisation in order to improve the final properties of plastic products. They reported that the impact strength and Young's modulus of moulded parts, using a special shear-controlled orientation injection moulding (SCORIM) processing technique, increased up to four times more than parts made by a conventional injection-moulding process. These observations were attributed

to shish kebab morphology developed by the action of shearing on the solidifying melt. In addition, Kalay and Bevis[52] found that the tensile strength of parts made from PP using SCORIM and a conventional injection-moulding process increases as the molecular weight increases. In contrast, Young's modulus of the conventional PP samples increases slightly as the molecular weight increases, but clearly decreases in the case of the SCORIM samples.

To make matters more complex, also the processing technique and conditions determine the final properties. In general, it is known that low cooling rates at crystallisation lead to higher crystallinity and, in consequence, to the higher stiffness of samples. In contrast, higher cooling rates cause an oriented and thick skin layer with high impact strength.

Researchers who have processed PP with the same molecular weight and in different processing conditions have discovered variations in the morphology and properties.[37-40,53-57] For example, Isayev et al.[53,54] indicated for iPP with a molecular weight of 351 $kg \cdot mol^{-1}$ a dependence of the formation of morphology on the shear rate. They found an increasing thickness of shear-induced skin layer as the flow rate (in correspondence with the shear rate) and the distance from the die entrance of single-screw extruder increased. In addition, they observed a limiting shear rate depending on temperature, below which no shear-induced crystallisation could occur. Similarly, the data of Zhu and Edwards[55] demonstrate the effect of thickness of injection-moulded isotactic PP plates on shear-induced morphology and morphological distribution through the depth direction of the plates. The preferential orientation of crystalline lamellae along the flow direction strongly depends on the thickness of the plate. Shish kebab structure is found roughly 100 µm from the surface of plates, regardless of the thickness of plates. Moreover, Seki et al.[56] found that crystallisation was accelerated after the cessation of shearing, while the quiescent crystallisation kinetics were not affected by the molecular weight and molecular weight distribution. They found a critical value of 0.12 $N \cdot mm^{-2}$ for the wall shear stress above which shear-induced crystallisation occurs. The long chains greatly enhance the formation of threadlike precursors, but only mildly enhance the formation of pointlike precursors. These results are confirmed by Gahleitner et al.[40], who have investigated injection-moulded PP samples of different molecular weight.

However, of particular importance are other findings of Gahleitner et al., published in 1996.[40] They studied several PP grades, which are synthesised in the pilot plant Spheripol process using a 4th generation Ziegler-Natta catalyst. The molecular weight of some PP samples was varied by peroxide-controlled degradation from 766 to 135 $kg \cdot mol^{-1}$. They noticed that the influence of mechanical properties (i.e., impact strength, tensile strength, stiffness, etc.) on molecular weight depends strongly on the PP grades used. Changes in the molecular weight of commercial PP grades have almost no influence on the stiffness, whereas the stiffness of peroxide-controlled PP types increases clearly as molecular weight increases. Moreover, they recognised that a heterogeneous nucleation effect is strongly dependent on the molecular weight of the materials. The crystallisation temperature (used to judge the

efficiency of nucleation agents) of nucleated and non-nucleated PP samples of rising molecular weight shows that the nucleation effect increases first and then decreases again with falling molecular weight.

Furthermore, Gahleitner et al.[58] observed a linear correlation between molecular weight and spherulitic growth rate for PP - the higher the molecular weight the lower the spherulitic growth rate. Besides this, the flexural modulus is dominated by the tacticity and the polymerisation conditions (mainly the type of catalyst system) and less by the molecular weight. For impact strength molecular weight is the primary defining factor. Furthermore, Gahleitner and his co-workers have compared the resulting crystallisation behaviour, final morphology and mechanical properties for a series of homopolymer PP's made from conventional Ziegler-Natta catalyst systems and novel metallocene (MET) catalysts. The comparison of crystallisation behaviour shows a higher growth rate in the metallocene-based PP's, because of their lower tacticity. Furthermore, the morphology of MET- and ZN-based PP's are different, since the MWD is different (lower in case of MET-based PP's) and is the determining factor for the skin layer formation. Besides this, the MET-based PP's do not follow the normal correlation between tacticity and modulus for ZN-products.

A similar pronounced difference in the properties of MET- and ZN-based PP was observed by Fujiyama and Inata.[59,60] They studied the rheological properties and the melting and crystallisation behaviour of a PP they had synthesised in a molecular weight range of 205 to 434 $kg \cdot mol^{-1}$, polymerised on the one hand using a metallocene catalyst and on the other hand using a Ziegler-Natta catalyst system. The results found showed that the zero viscosity, die swell, shear storage modulus G', melt tension and the critical shear rate at which a melt fracture occurs for a MET-based PP are lower when compared to a ZN-based PP. This is attributed to the difference in specific rheological properties such as MWD. The MWD of a MET-based PP is much narrower than that of a ZN-based PP. In addition, the melting and crystallisation temperature of a MET-PP is lower than that of a ZN-PP. This is assumed to be due to the uniform intermolecular distribution of defects such as stereo-irregular bond for a MET-PP.

Viville et al.[61] even determined a difference in the melting and crystallisation behaviour of PP, using identical heterogeneous Ziegler-Natta catalyst, but different polymerisation conditions. The inter-chain tacticity distributions of the PP are affected by the change of the polymerisation conditions, which, in turn, modifies the rigidity properties of the polymer. In consequence, the crystallisation and melting behaviour of the PP's are different. However, all the PP samples, synthesised in different polymerisation conditions, showed that the melting temperature remained constant with increasing molecular weight and the crystallinity and crystallisation temperature were the highest for PP with a molecular weight of 100 $kg \cdot mol^{-1}$.

In the results obtained on PP synthesised by themselves, Gahleitner et al.[40,58], Fujiyama et al.[59,60] and Viville et al.[61] reveal that polymerisation history also influences the behaviour and properties of polyolefins. Nevertheless, the studies in material sciences covering the influence of molecular structure on morphology and resultant properties hardly ever consider the origin (polymerisation history) of their investigated polymer, as briefly

summarised in Table 1. This seems to be the reason, why many results are still difficult to compare and in some cases even differ substantially. For example, the effect of molecular weight on mechanical properties is still a matter of some controversy, despite the fact that numerous studies have been carried out on this topic in the past.

Therefore, it is of great importance to study the influence of molecular weight on the melt and solid state properties of PP in a holistic approach (including polymerisation and processing history) in order to achieve a basic and thorough understanding.

This is a major target of the present work.

Table 1.1: A brief summary of previous studies on the relation between molecular structure and properties of PP

Author	*Year*	*Synthesis*	*MW* [kg·mol^{-1}]	*Process-ing*	*Influence of*	*on morphology and properties*			*Ref.*
						morphology, Xc, orientation	*melt properties*	*solid state properties*	
Stern	2005	LP, ZN	101-1600	IM	MW	X	X	X	62,63
Schrauwen	2004	-	260-500	CM	MW, cool.	X	-	X	43,63
Zhu	2004	-	fractions	IM	MW, proc.	X	-	-	55
Elmouni	2003	-	171-350	-	MW	X	X	-	65
Yamada	2003	-	51-605	-	MW, cryst.	X	-	-	66
Tiemblo	2002	-	MV=40-180	-	MW, oxi.	X	-	X	67
Fujiyama	2002	ZN, MET	205-434	extrusion	MW, cat	X	X	-	59,60
Fujiyama	2002	ZN	170-630	IM	MW, proc.	X	-	X	57
Loos	2002	Solution, slurry, GP, bulk, MET	up to 1200	-	MW, polym.	X	-	-	68
Seki	2001	-	186-923	-	MW, shear	X	-	-	56
Albano	2001	-	210-800	CM	MW, cool.	X	-	X	33
Marigo	2001	ZN	MV=7-53	-	MW, cat	-	X	-	69
Jay	1999	-	208-377	-	MW, shear	X	-	-	36
Guo	1999	-	4 different MW	IM	MW, proc.	X	-	-	70
Gahleitner	1999	Spheripol, ZN	135-766	-	MW	X	-	X	58
Ibhadon	1998	-	10^5 - 10^6	-	MW, cryst.	X	-	X	71
Kalay	1997	-	197-460	SCORIM	MW, proc.	X	-	X	51,52
Gahleitner	1996	Spheripol, ZN	135-766	-	MW, nucl.	X	-	X	40
Phillips	1994	-	290-690	CM	MW, proc.	X	-	X	37
Osawa	1992	-	160-235	IM	MW	-	-	X	32
Fujiyama	1991	-	186-630	IM	MW, proc.	X	-	-	39
Prox	1991	-	240-653	IM	MW, proc.	X	-	X	45
Sadiku	1990	-	229-690	film	MW	X	-	-	72

ZN = Ziegler-Natta catalyst, MET = metallocene catalyst, LP = liquid pool, GP = gas phase, MW = weight-average molecular weight, MV = viscosity-average molecular weight, MFR = melt flow rate, cat. = catalyst, IM = injection moulding, CM = compression moulding, polym. = polymerisation conditions, proc. = processing conditions, cool. = cooling rate, cryst. = crystallisation conditions, nucl. = nucleation, oxi. = thermooxidation

1.2 Aim of the thesis

The aim of this thesis is to study the influence of the molecular structure on the solid state properties of newly synthesised PP by taking a holistic approach and, thus, to gain a fundamental understanding of the original relationship between the molecular structure and the end-use properties. However, this task can only be achieved successfully by following systematically and finally closing the “chain of knowledge. The so-called “chain of knowledge” involves the polymerisation process, the properties of the synthesised polymer, the melt processing and the resulting end-use properties of the parts.

For this purpose, polypropylene in a wide molecular weight range has to be precisely synthesised in a reactor under defined polymerisation conditions and afterwards processed into parts under defined, industrial-like conditions, using a modern melt processing technique. Thorough analysis of the polymerisation kinetics, the molecular, rheological and thermal properties of the synthesised PP powders, as well as the flowing and solidification behaviour of the polymer during processing and the resulting morphology with the specific mechanical properties, enable the essential single chain elements - synthesis, processing and end-use properties - to be studied and understood. In consequence, the knowledge attained leads to the linking together of the individual chain elements and, as a result, the chain of knowledge can be closed for the first time.

Therefore, this thesis focuses on an improved insight into fundamental polymer science and makes a very exciting contribution to modern material progress.

2 ON THE STRUCTURE AND DEFORMATION BEHAVIOUR OF POLYPROPYLENE

2.1 Structure and morphology of polypropylene

Polypropylene (PP) is a linear macromolecule produced by dissociating double bonds between two carbon atoms of asymmetrical propylene monomer. The primary chain characteristic is determined by the type of polymerisation technique, polymerisation conditions, and mainly by the catalyst system used. The types of catalysts, as well as the support of the catalyst and the external and internal donors, affect the composition and, even more, the configuration of the macromolecule. In the case of PP, different configurations (tacticity) of the methyl groups along the main chain skeleton are possible due to asymmetric propylene monomer. PP is termed isotactic PP (iPP), when the methyl groups are arranged equilaterally. PP (sPP) is syndiotactic, when the methyl groups are arranged alternately, and when no order is present, we speak of atactic PP (aPP), as shown in Figure 2.1. All three stereoisomeric PP's are in use, but they differ clearly in their properties. Most common applications involve iPP.

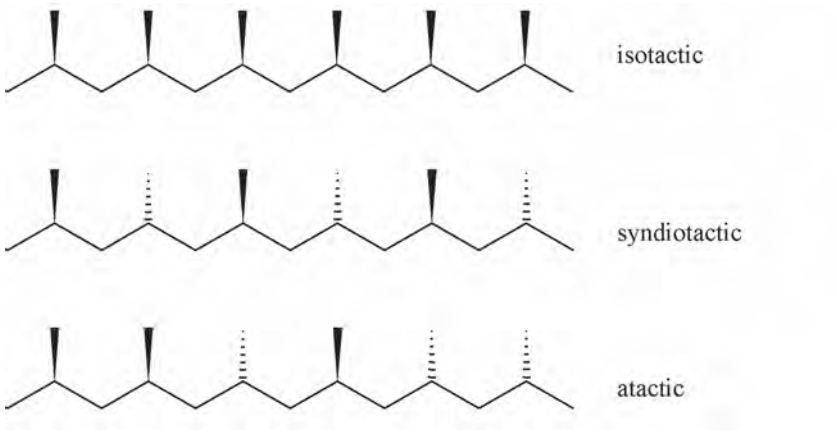

Figure 2.1: Schematic illustration of existing stereochemical configurations of PP (a. isotactic, b. syndiotactic, c. atactic)

In a crystalline state, the macromolecules of PP usually take the shape of a helix as shown in Figure 2.2, due to a thermodynamic tendency and, taking the side group into consideration, a tendency to take a spatial conformation with the lowest intermolecular energy.

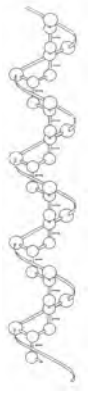

Figure 2.2: Helical configuration of isotactic polypropylene in the crystalline state.[23]

During crystallisation of the quiescent melt, these helical macromolecules fold into lamellae as shown in Figure 2.3. The starting point of crystallisation are nuclei in the supercooled amorphous melt. The lamellae consist of a three-dimensional folded configuration of polymer chains fixed in a crystalline order. Lamellae thickness and lamellae thickness distribution are essentially governed by the length of the macromolecule, crystallisation temperature, and degree of supercooling.[73,74] The higher the crystallisation temperature and the longer the molecule chains, the longer the fold length. Within the lamellae the individual macromolecules lie folded parallel to crystallites; conversely the macromolecules in the interfacial layer are amorphous. The amorphous portion involves chain ends, molecule loops, entanglements, and chain bridges between two crystallites (tie molecules). Linkages between the lamellae are governed by the number of entanglements and tie molecules. Nevertheless, the amorphous phase is often the weak link in the polymer.

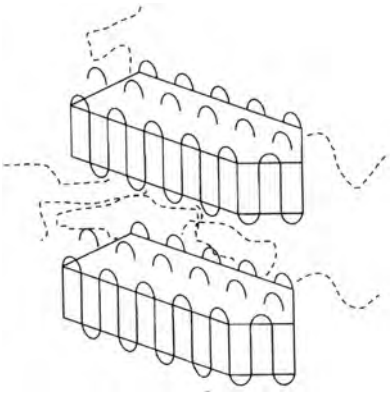

Figure 2.3: Schematic illustration of lamellae

Isothermal crystallisation of a quiescent melt

During crystallisation of quiescent molten polymer usually a spherulitic superstructure is formed.[73,74] A spherulite grows by the branching of the lamellae. Packages of lamellae lie behind each other in radial direction. Thereby, lamellae fibrils are formed that are typical for spherulites. During isothermal crystallisation of a quiescent melt, the spherulites grow isotropically in spatial directions, so that a radially symmetrical structure develops, as shown in Figure 2.4. The polymer chains inside the lamellae are oriented perpendicular to the radius of the spherulite. The lamellae do not fill out the entire space in the spherulites; they are separated from each other by amorphous polymer. Therefore, a polymer is always semi-crystalline. The semi-crystalline state is defined by its crystallinity, which indicates the ratio of the amount of single crystals to overall structure. The diameter of a spherulite is usually between 0.1 and 1 mm.[75]

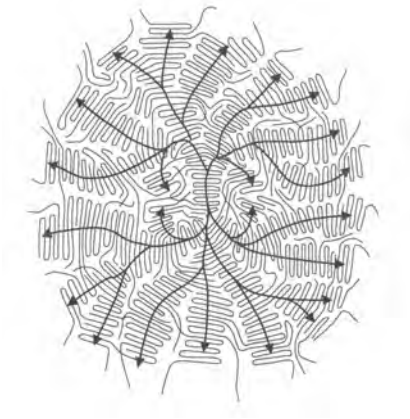

Figure 2.4: Schematic illustration of a spherulite

There are various crystalline modifications of PP, i.e., the chains of the macromolecules fold into lamellae in different ways. In the case of isotactic PP, three different modifications are known: the α-modification with a monoclinic unit cell; the β-modification with a trigonal unit cell; and the tricline γ-modification. However, the γ-modification can be observed only sporadically, in particular, only when low molecular weight iPP crystallises under high pressure.[76] The α- and β-modifications of isotactic PP differ (apart from other properties) by their different birefringence, which can be observed under a light microscope between cross-polarisation, and by their different growth rates.[77,78]

Figure 2.5 shows typical spherulitic structures of the α modification from an iPP in polarised light, crystallised from quiescent plastic melt. Between two crossed polarisers the spherulites of α-modification of PP show the characteristic “spherulite cross” (Maltese cross). This ‘Maltese’ cross is caused by the central symmetrical arrangement of the lamellae. No such light deflections can be observed when sheave-like spherulites are formed, as in the case of β-modification of PP.

The formation of either α- or β-modification can be supported by the type of catalyst used; adding specific nucleating agents, however, can preferably cause the formation of either of these modifications. These methods are commonly used for the specific altering of the properties of PP. For instance, β-modification of PP exhibits improved impact strength. In contrast, the heat resistance of α-modification of PP is approx. 10°C higher than for β-modification of PP, since the melting temperature of typically 165°C for the α-form is reduced to 155°C for β-form PP.[79,80]

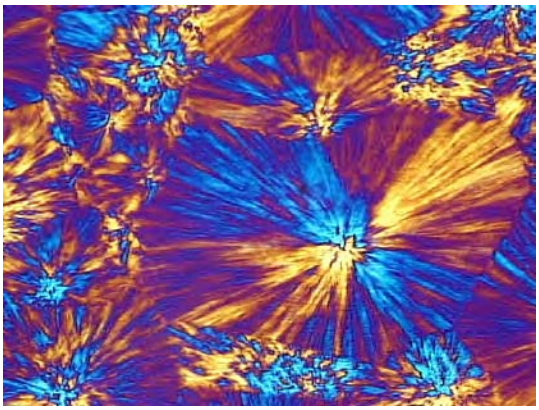

Figure 2.5: α-modification of iPP investigated in cross-polarised light

Non-isothermal crystallisation of a quiescent melt

The morphology of a polymer is essentially determined by the acting crystallisation conditions.[81-83] For instance crystallisation kinetics is affected by the degree of supercooling of the melt. When the cooling rate is high, the crystallisation temperature is lowered. Thus nuclei formation is promoted by thermodynamic inertia of the molecules and results in a higher number of smaller spherulites. When molten polymer is cooled fast (quenched) till below its glass transition temperature, crystallisation is prevented entirely, and virtually amorphous solidification is obtained. In contrast, a higher degree of crystallisation is achieved by slow cooling. During the melt processing of plastic, the cooling rate can be affected by the melt and mould temperature.

Non-isothermal crystallisation of a sheared melt

Melt processing of polymers in industrial conditions exerts a high level of shearing and elongation flow on the melt.[50-60] During the filling of molten polymer into a cavity, macromolecule orientation and stretching occur, depending on the flow rate. In addition, the polymers are exposed to high temperature gradients and, where close to the wall, to high cooling rates as hot melt comes in direct contact with the cooled mould. Therefore, in the layer close to the surface the orientated macromolecules freeze suddenly. Both conditions – flowing melt and high cooling rates – influence crystallisation behaviour and result in the formation of anisotropic and non-homogenous structures that are different from morphologies formed after crystallising under isothermal and quiescent conditions.

The presence of so-called skin-core morphology is well-known for injection-moulded samples of semi-crystalline polymers, as schematically shown in Figure 2.6 according to model by Woodward.[84] Three different layers are represented in the paper, although Matsumoto et al.[85] observed at least six layers in injection-moulded polypropylene, using a polarising microscope.

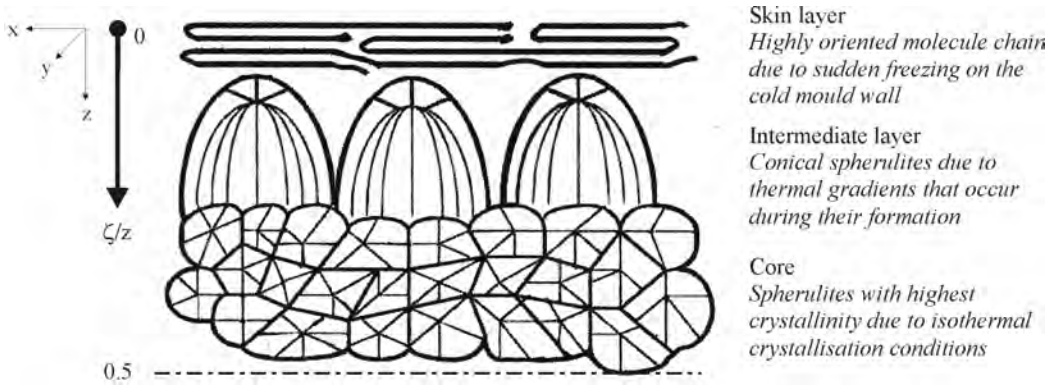

Figure 2.6: Schematic representation of the skin-core morphology of an injection-moulded specimen

In fact, the skin layer usually consists of highly oriented chains and is typically non-spherulitic. In contrast, the core is usually spherulitic and exhibits the highest crystallinity. For some samples, the spherulites in a region between the skin and the core have conical shapes due to thermal gradients that occur during their formation.

The thicknesses of the several layers are governed mainly by polymer melt properties and the actual processing conditions (flow rate, melt and mould temperatures).[34,35] The structure also varies across and along the part due to different flow and temperature conditions.[39,43] The homogeneity of the morphology also governs properties of the part such as stiffness, strength, heat resistance, chemical resistance, and dimensional stability.

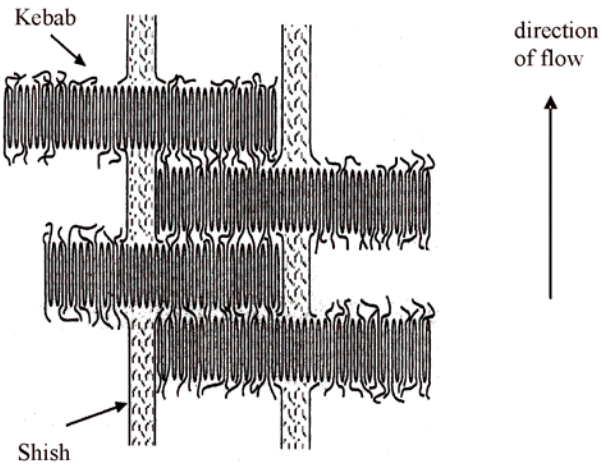

Figure 2.7: Schematic illustration of a shish kebab structure

Under special crystallisation conditions, the formation of unusual structures can be promoted further. One known morphological structure is the so-called shish kebab structure. Figure 2.7 shows a schematic illustration of the shish kebab structure. Here, extended macromolecules (shish) lie parallel to each other and lamellae (kebab) are formed in circles around them.

This type of morphology is unique due to the nature of its structure, coupled with extraordinary properties, such as high strength and stiffness. These highly oriented shish kebabs grow preferentially during crystallisation in solution and when shear stress on the melt is high.[36,39,48-50] Shish kebabs can also be formed during the cold drawing of films or fibres. During the drawing procedure, the spherulites break and orient themselves to extended structures, such as shish kebab.

2.2 Deformation behaviour of polypropylene in solid state

Polymers are viscoelastic materials with an expressed time- and temperature dependency of their mechanical properties and thus show non-linear deformation behaviour. This special viscoelastic behaviour of polymers is caused by the macromolecules, which do not respond spontaneously to an applied load, rather the individual molecule chains, which are anxious to diminish the applied load to an equilibrium value by rearrangement.[86] This phenomenon is called either strain or stress relaxation, depending on the type of load, which can be either stress or strain controlled. The duration of the relaxation process determines the relaxation time.

The speed of molecular rearrangement depends on the load level and on the mobility of the macromolecules, which again is governed by the physical and chemical structure and arrangement of the molecules (i.e., side group, bonding, etc.). Temperature also accelerates the rearrangement of the macromolecules as a result of increasing mobility, coupled with a higher free volume.

In addition to the specific structural properties of the polymer (i.e. molecular weight, degree of branching) and the environmental conditions (i.e. temperature, humidity, etc.), also the thermal-mechanical history of the samples affects the deformation behaviour. For example, molecular orientation and degree of crystallisation influence strongly the long-term properties. For that reason and, thus, for technical use, the time- and temperature-dependent deformation behaviour of polymeric parts is of particular importance.

If the loading time is short in comparison with the duration of the molecular rearrangement, the polymer's behaviour is stiff and brittle, but, if the molecule chains have sufficient time to relax the polymer becomes soft and tough (Figure 2.8).

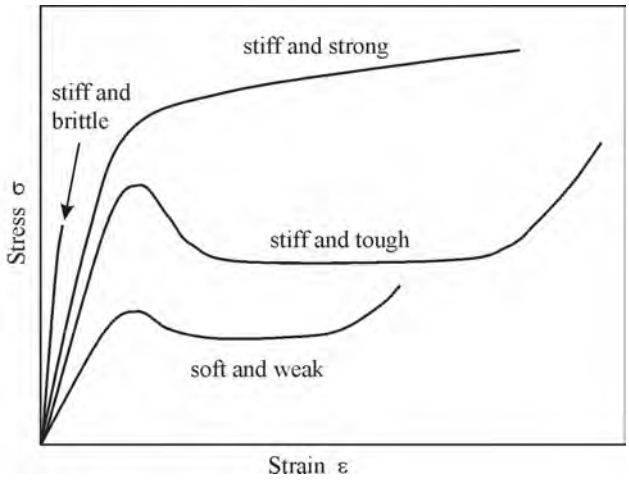

Figure 2.8: Stress-strain diagram of polymers with different deformation behaviour

Depending on the initial molecular structure of the semi-crystalline polymer the ductile failure, coupled with a plastic deformation is caused by the existing morphological structure (spherulites, lamellae) and the amorphous fraction. The plastic deformation of the spherulites at different strain is demonstrated in Figure 2.9.[87]

After reaching the yield point, necking of the samples occurs associated with an extension of the spherulites. Thereby the spherulitic structure is deformed but not changed. As the deformation level increases, the strain within the deformation zone increases as a result of the ongoing extension of the spherulites or the conversion to a new structure. In addition, the width of the deformation zone is extended through the inclusion of new material from the borders of the deformation zone.

The deformation of the spherulites does not take place homogeneously. A substantial influence is exhibited by the orientation of the lamellae within the spherulites relative to the direction of deformation.

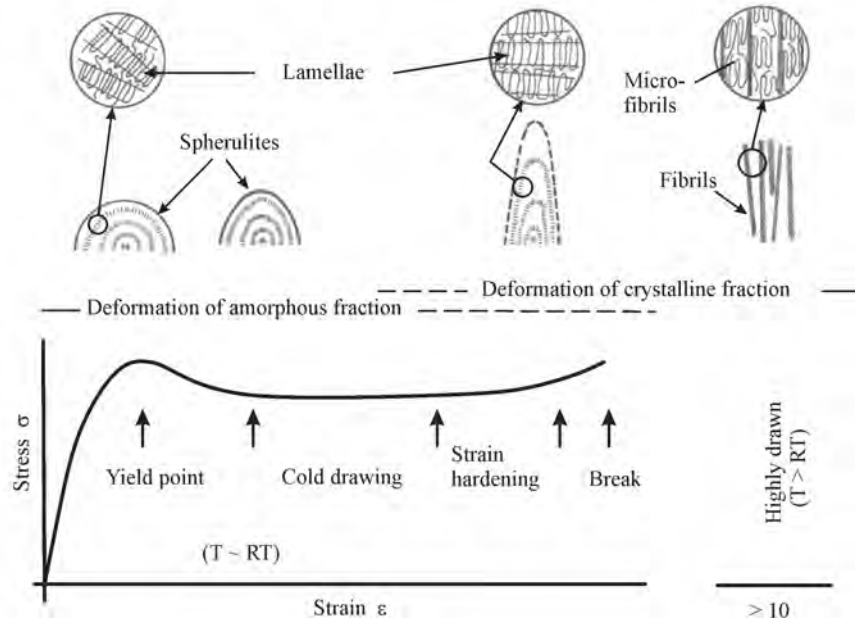

Figure 2.9: Deformation of spherulites as function of the strain[87]

In order to describe the deformation behaviour of polymers, several models and mechanisms exist, which are presented in numerous papers.[88-93] The most well-known deformation mechanism is attributed to Peterlin.[91-93]

Generally, three different cases are observed for the deformation of the lamellae, which are shown schematically in Figure 2.10.

a. The radial lamellae lie parallel to the direction of deformation
   Tensile forces act in the direction of the crystallographic a-axis. Samuels[94] postulated that these cause separation of the lamellae into microblocks and a small stretching of the amorphous fraction. Based on Peterlin's[95] theory, the lamellae become compressed as a result of the acting load and, in addition, the height of the crystallites is reduced because of tilting and shearing. The separation of the lamellae into microblocks also occurs.

b. The radial lamellae lie at 45° to the direction of deformation
   Shear forces act on the lamellae. According to Samuels, the lamellae align themselves perpendicularly to the loading direction by breaking into small blocks and by tilting and gliding processes. In contrast to Samuels's findings, Peterlin observed a rotation of the lamellae parallel lying diagonally to the loading direction and afterwards the same deformation process as described in a. takes place. In a destruction zone the lamellae are finally reorganised in microfibrils.[93] These microfibrils are interconnected by tie molecules. When the reorganisation of the lamellar structure to a fibrillar structure is completed, the microfibrils are finally deformed homogeneously up to their rupture.

c. The radial lamellae lie perpendicular to the direction of deformation
   Tensile forces act in the direction of the crystallographic c-axis, i.e., in the direction of the molecule chain. Peterlin and Samuels concluded from their research that here only the distance of the lamellae increases; hence, only the amorphous fraction is changed.

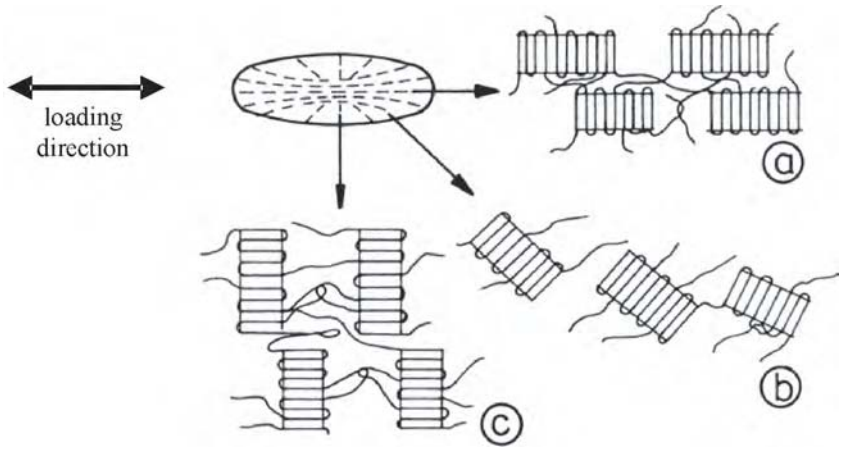

Figure 2.10: Deformation mechanism of lamellae, depending on direction of deformation[87]

Kestenbach and Petermann[96] interpret the plastic deformation behaviour at high strain as a “de-crystallisation” process where stress-induced re-crystallisation takes places after the breaking of the lamellae. The microfibrils are considered as a crystalline fraction of stretched chains.[97]

Müller[98] and Jäckel[99] explain the morphological and structural reorganisation processes by adiabatic heating as a result of friction over the melting temperature and thus by local flowing processes. However, Vincent[100] is of the opinion that the cold drawing, which occurs at low strain rates, cannot be explained by means of adiabatic heating due to friction. He proposes that the stress applied reduces the stiffness of the material. The decreasing stiffness results from the separation of lamellae and tie molecules, induced by deformation. This theory is supported by the fact that areas of lesser stiffness show higher strain and thus lead to local flowing processes.

Stretching of lamellae at lesser strain leads to the creation of crazes, as observed by Michler[87] using TEM. Crazing should be understood as the creation of voids due to stretching of the amorphous fraction. In cases of semi-crystalline polymers the crazing process is coupled with reorganisation of the lamellae to microfibrils. The borders of the crazes are formed by the lamellae and are stretched in between macromolecules, which are combined to fibrils. In contrast to cracks, crazes can partially transfer the mechanical load, since fibrils are oriented parallel to the direction of deformation. In the case of PP crazing already occurs at a relatively low strain of 2.5 to 3 % and above 10 % cold drawing and strain hardening appears.[101,102] Generally, necking takes place in association with a reduction of the cross-section, and the material is stretched significantly at the same time. The stiffness and strength increase as a result of strain hardening.

In contrast to the deformation mechanisms of spherulitic PP different processes affect the stress-strain behaviour of hard-elastic fibres and films. First, a high strain recovery of 80 to 100 % can be observed after drawing the material, even to a strain of 100 % or more compared to the low maximum strain recovery of 50 % for spherulitic PP.[103] Admittedly, tests were always carried out in the direction of flow and/or drawing. Therefore, the mechanism of deformation extends also only in tensile direction and, thus, perpendicular to the oriented lamellae.

Göritz and Müller[104] suggest a three-step deformation process. In the first step, at a strain of approx. 5 %, the hard fibre is deformed purely elastic. Here, the stress-strain curve in the corresponding stress-strain diagram is linear (Figure 2.8). In the second step, when the strain is above the yield point, the amorphous fraction between the crystallites is expanded and oriented (decrease of entropy). The stress-strain curve shows a plateau. In the third step, at a strain of above 60 %, the lamellae are sheared and chains are pulled out from the lamellae. This is expressed in the stress-strain diagram by a pronounced rise. Cayrol and Petermann[105] confirmed these findings by means of TEM investigations. They observed sheared lamellae on drawn PE films (ε = 50 %).

3 EXPERIMENTAL METHODS

3.1 Polymerisation

The polymerisation of propylene in GP and LP was carried out in a 5-litre stainless steel autoclave reactor, as seen in Figure 3.1. This reactor was equipped with a PID temperature control system for maintaining quasi-isothermal conditions. Experimentally, the reaction rate of LP polymerisation was measured using a calorimetric principle, developed at the University of Twente and described by Samson et al.[13,14] and Pater et al.[15,16] in more detail. Under isothermal bulk conditions and assuring a constant heat transfer coefficient from reactor to jacket, the temperature difference between reactor and jacket is a measure of the reaction rate.

For gas phase polymerisation the reaction rate can be estimated by continuously measuring the pressure inside the reactor and neglecting non-sorption of the monomer in the amorphous part of the polymer.[17]

In addition, the experimental set-up and data analysis for liquid pool and gas phase polymerisation have been described in detail by Al-haj Ali et al.[106] and van Putten.[107]

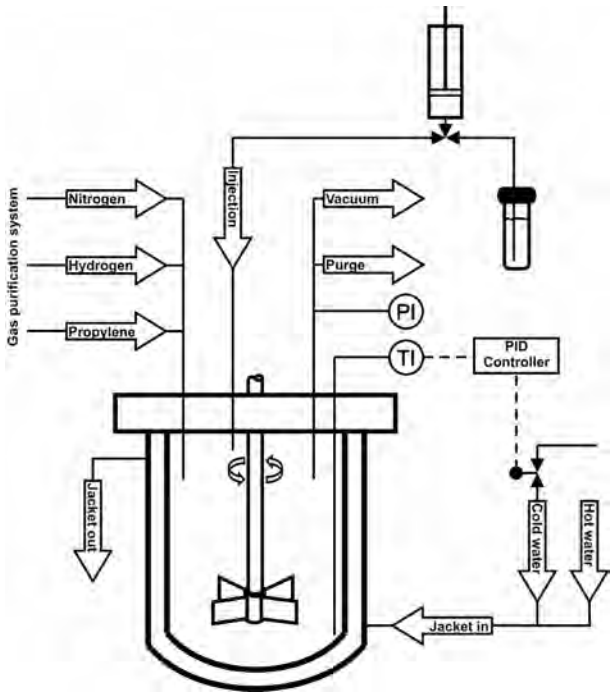

Figure 3.1: Schematic drawing of the polymerisation set-up

3.1.1 Catalyst preparation

The modern catalyst used for propylene polymerisation was an $MgCl_2/TiCl_4$ catalyst in conjunction with triethyl aluminium (TEA) as co-catalyst, an internal phthalate donor, and an external silane donor, which is suitable for GP and LP propylene polymerisation. In a glove box in a nitrogen atmosphere the catalyst was activated with a small amount of co-catalyst. The external silane donor, the TEA, and hexane were mixed together in a vial. The components contact time of 30 minutes led to complexation of the silane and the TEA at room temperature. In a second vial the catalyst was diluted in hexane. 10 minutes later, the mixture of external donor and TEA as well as the diluted catalyst were injected.

3.1.2 Polymerisation procedure

3.1.2.1 Liquid pool polymerisation

For liquid pool polymerisation, the reactor was first filled with liquid propylene at room temperature, reaching a pressure of about 35 bar. Before adding hydrogen, the reactor was successively heated up to a polymerisation temperature of 70°C while counteracting the rising pressure by purging the system, always ensuring that the reactor was completely filled with liquid propylene. After this, the reactor was enriched with the required hydrogen to a total maximum pressure of 60 bar. The polymerisation conditions are shown in Table 3.1.

Then the polymerisation reaction was started by injecting the scavenger (TEA) and the catalyst in succession. Between approx. 30 and 60 minutes the polymerisation reaction was terminated by injecting methanol. The reactor was vented, cooled down and afterwards purged several times with nitrogen to remove the monomer. Finally, the powder was taken from the reactor and dried for 4 hours in a vacuum oven at a temperature of 50°C.

Table 3.1: Polymerisation conditions for synthesising PP in liquid pool

Sample	*T* [°C]	T_{max} [°C]	*p* [bar]	H_2 [mg]	H_2 [mole%]
PP-L1600	70	70.6	35	0	0
PP-L1120	70	71.9	52	25	0.02
PP-L833	70	72.5	51	50	0.05
PP-L462	70	72.8	50	150	0.15
PP-L361	70	72.9	43	150	0.15
PP-L320	70	73.8	48	250	0.26
PP-L244	70	71.5	51	500	0.51
PP-L153	70	71.9	48	1 000	0.99
PP-L101	70	74.8	48	1 500	1.56

3.1.2.2 Gas phase polymerisation

The gas phase experiments were performed in a sequence of pre-polymerisation to prevent thermal runaway of the growing particle in the initial stage and gas phase main polymerisation. First pre-polymerisation was performed at a moderate temperature of 40°C and started by injecting scavenger (TEA) and catalyst. The scavenger was injected 5 minutes prior to the catalyst. After successful pre-polymerisation (about 20 g pre-polymer has be prepared), propylene was evaporated by opening the purge and after rinsing the reaction continued in the gas phase. The reactor was heated up to 70°C and filled with gaseous propylene and subsequently hydrogen. During the gas phase polymerisation process, the pressure was kept constant at 25 bar by adding gaseous propylene through an automated mass-flow controller. The most essential polymerisation conditions are shown in Table 3.2. To end the experiment, the reactor was flashed off and the powder was taken from the reactor and dried for 4 hours in a vacuum oven at 50°C.

Table 3.2: Polymerisation conditions for synthesising PP in gas phase

Sample	*T* *[°C]*	*p* *[bar]*	*H_2* *[mg]*	*H_2* *[mole%]*
PP-G1120	70	25	0	0
PP-G1150	70	25	25	0.18
PP-G877	70	25	50	0.37
PP-G444	70	25	100	0.73
PP-G417	70	25	150	1.09
PP-G157	70	25	1 500	9.92

3.2 Melt processing

Micro dumbbell specimens were manufactured from the liquid pool polymerised PP powder under industrial conditions using a newly developed injection-moulding process. Afterwards, some micro dumbbell specimens were annealed in a convection oven (Heraeus) for 1 hour at temperatures of 100°C and 140°C for improving the perfection of the crystalline structure.

3.2.1 Injection moulding machine

An Arburg 220 S Allrounder 150-30 injection moulding machine was used to produce the specimens. This injection moulding machine was specially equipped with a newly developed 12 mm flat cut screw, which enables a gentle processing of polymers to micro parts under practical conditions. Only a few grams (30 grams min.) were required to manufacture enough parts of homogeneous quality for further investigations. This means a considerable advantage for processing polymers synthesised in laboratories in particular, where often only a few grams to a maximum of approx. 100 g can be polymerised. No other industrially relevant processing technique is capable of producing parts from such small amounts of resin.

The injection moulding machine is equipped with a two-cavity mould. A Kistler pressure sensor is mounted inside one cavity for measuring cavity pressure continuously. A temperature control system is used to control mould temperature and keep it constant at moderate temperatures of 60°C during processing.

3.2.2 Micro dumbbell specimen

The overall dimensions of the micro dumbbell specimens produced are shown in Figure 3.2. In addition, Figure 3.3 shows a photograph of a micro dumbbell specimen beside a match, in order to compare its size. The length of the micro dumbbell specimens is 25 mm and the cross-section of the small, parallel zone is 1.25 x 0.5 mm^2. The total mass of one micro dumbbell specimen produced is 10 mg.

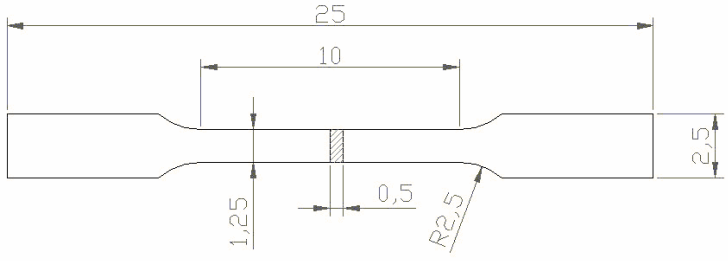

Figure 3.2: Dimensions of the micro dumbbell specimen

Figure 3.3: Juxtaposition of a micro dumbbell specimen and a match

3.2.3 Processing procedure

For manufacturing micro dumbbell specimens from synthesized PP powders with different molecular weights, the most significant injection-moulding processing conditions were kept constant. The processing conditions are shown in Table 3.3. The melt temperature was altered from 210°C to 250°C, due to the pronounced difference in viscosity of the samples. The higher molecular weight samples could only be processed at a relatively high melt temperature of 250°C. For better comparison, samples with lower molecular weights were also produced at this melt temperature. Holding pressure was set almost equal to injection pressure, which of course varies due to variations in the flow behaviour of the samples, depending on molecular weight.

The total volume (two micro dumbbell specimen + gate) of one shot amounted to 400mg and the residence time was less than 5 min.

Table 3.3: Processing conditions for manufacturing micro dumbbell specimens

Sample	T_{mt} *[°C]*	T_{wz} *[°C]*	v_{inj} *[mm·min^{-1}]*	p_{inj} *[bar]*	p_h *[bar]*	t_{ph} *[s]*	t_c *[s]*
PP-L1600	250	60	10	1 950	2 000	4	15.4
PP-L1120	250	60	10	1 400	1 000	4	15.4
PP-L833	210	60	10	1 600	1 600	4	15.4
PP-L462	210	60	10	1 540	1 500	4	15.4
PP-L361	250	60	10	1 000	1 000	4	15.4
PP-L320	210	60	10	520	500	4	15.4
PP-L244	250	60	10	900	1 000	4	15.4
PP-L153	250	60	10	1 050	1 000	4	15.4
PP-L101	210	60	10	355	300	4	15.4
PP-M256	250	60	10	650	600	4	15.4
PP-L445	250	60	10	500	500	4	15.4

T_{mt} = melt temperature, T_{wz} = mould temperature, v_{inj} = injection speed, p_{inj} = injection pressure, p_h = holding pressure, t_{ph} = holding pressure time, and t_c = cycle time

3.3 Molecular structure and morphology

3.3.1 Gel permeation chromatography

The structural data (average molecular weight (MW) and molecular weight distribution (MWD)) were analysed by GPC. The GPC measurements were performed with a Waters Alliance GPCV 2000 with 3 TSK GMHXL-HT Columns. The detector used was a differential refractive detector, and data acquisition was performed by the software package Waters Millenium 4.00 with GPCV option. The measurements were carried out at a temperature of 155°C with 1,2,4-trichlorobenzene (TCB) as solvent and narrow MWD polystyrene standard as reference.

3.3.2 Differential scanning calorimetry

The thermal properties of the samples (powder and micro dumbbell specimen) were measured by means of differential scanning calorimetry (DSC).[108]

DSC detects the absorbed or lubricated energy of samples, caused by chemical or physical transitions of the materials. For example, during melting the polymer absorbs energy ΔH (endothermal transformation) or discharges energy while crystallising (exothermal transformation). Those calorimetrical changes are measured as a function of temperature or time (eq. 3.1).

$$\Delta H = \int c_p \cdot dT \qquad (3.1)$$

The difference in temperature dT between the sample and a reference is determined, while both pass through a defined temperature-time program. The temperature difference corresponds to the flowing heat flux $\dot{Q}$ and, thus, the heat capacity c_p can be described as follows.

$$c_p = \frac{\dot{Q}}{m \cdot \dot{H}} \qquad (3.2)$$

where m is sample mass and $\dot{H}$ is heating or cooling rate.

Finally, the heat flux is plotted as a function of the reference temperature for presenting the measured calorimetrical behaviour of the sample.

The DSC investigations were carried out at a temperature range of 30 to 280°C, using a Mettler-Toledo DSC type 821^e. A sample mass of (5.6 ± 0.1) mg of PP powder was placed in a 20 µl aluminium crucible and measured in a nitrogen atmosphere at a heating and cooling rate of 20 $K \cdot min^{-1}$.

In crystallinity calculations, the melt peak was integrated in the temperature range from 90°C to 190°C and a melting enthalpy of 209 $J \cdot g^{-1}$ was used for 100 % crystalline material.[109,110]

3.3.3 Polarisation microscopy

Polarisation microscopy is widely employed in the assessment of spherulitic crystalline polymers and in the analysis of morphology and orientations in solid state plastics. Polarisation microscopes always have two polarisation filters. When both polarisation filters are placed at 90° angels, light polarised by the first filter and oscillating in one plane is screened out completely by the 2nd filter. However, by placing a birefringent sample between the filters, the oscillation plane given by the 1st filter can be distorted in such a way that the light component no longer oscillating in that plane can pass through the 2nd filter. Thereby, structures become recognisable in polarised light.

The analysis of samples under a light microscope is performed mainly on microtomed sections with a thickness of approx. 10 to 15 µm. Following a rule of thumb, the thickness of the sections should be half the diameter of the expected spherulites.

For morphological investigation, the dumbbell specimens were sectioned using a Leica RM 2165 automatic rotary cryo-microtome. Thin, 10 micron sections were cut at -100°C to prevent artefacts caused by deformation of the samples during cutting. Since the morphology inside the injection-moulded micro dumbbell is inhomogeneous across and along the specimen, all sections were taken from the same position for best comparison between the separate samples. Here, the sections were taken on the shoulder near the gate and across the specimen thickness as shown schematically in Figure 3.4. A Zeiss Axioplan 2 light microscope (inserting a λ-plate) was used to observe the morphology in polarised light.

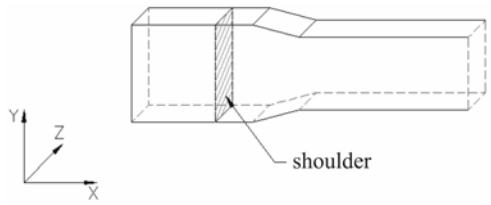

Figure 3.4: Position of the samples taken for investigation in cross-polarised light

3.3.4 Scanning electron microscopy

The scanning electron microscope (SEM) allows the study of surface structure at high magnification and with excellent depth of field.[111] The SEM generates a beam of electrons in a vacuum. That beam is collimated by electromagnetic condenser lenses, focussed by an objective lens, and scanned across the surface of the sample by electromagnetic deflection coils. The secondary electrons (electrons released by the samples) are detected and amplified by a photomultiplier tube. By correlating the sample scan position with the resulting signal, an image can be formed, which shows the surface topography of the sample.

In order to study the morphology of semi-crystalline polymers, the amorphous fraction has to be dissolved with an appropriate solvent and, thus, the crystalline fraction only remains. Additionally, to avoid electrical charging of the non-conducting plastic sample, it has to be given a conductive vapour-coating.

The SEM used for observing the shape and geometry of the PP powders was a LEO Gemini operated at an acceleration voltage of 10 kV. Samples were pre-treated by sputtering the surface with Au/Pd.

The analysis of the microstructure of the micro dumbbell specimens was carried out at the University of Halle; a JEOL 6300 was used with an acceleration voltage of 15 kV for analysing. Before testing, samples were cut from the shoulder and the centre of the parallel zone of the specimen (Figure 3.5) and afterwards etched with a mixture of potassium permanganate, concentrated sulphuric acid and water for 20 min at room temperature, following a modified procedure proposed by Olley et al.[112] After cleaning and drying the samples, their surface was coated with 12nm Au.

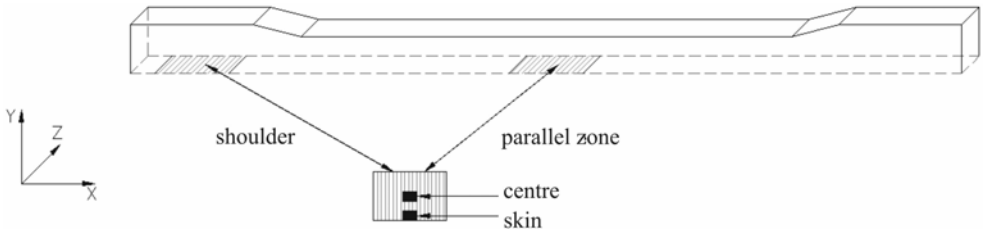

Figure 3.5: Positions of the samples taken for investigation in scanning electron microscopy

3.3.5 Transmission electron microscopy

The principal of the transmission electron microscope (TEM) is yery similar to the SEM principle, but in contrast to SEM, a beam of electrons is projected through the sample. Therefore, TEM requires the preparation of ultra-thin sections with a thickness of only a few nanometres. Additionally, plastics samples have to be contrasted for better resolution.[111]

The TEM investigations were carried out at the University of Halle. Samples were taken from the centre of the parallel zone, as shown in Figure 3.6. Ultra-thin sections, with a thickness of approx. 80 nm, were cut from the centre of the parallel zone (LEICA Ultracut, DIATOME diamond knife) and subsequently stained with ruthenium tetroxide. Afterwards, the sections were analysed at an accelerating voltage of 200 kV using a JEOL JEM 2010.

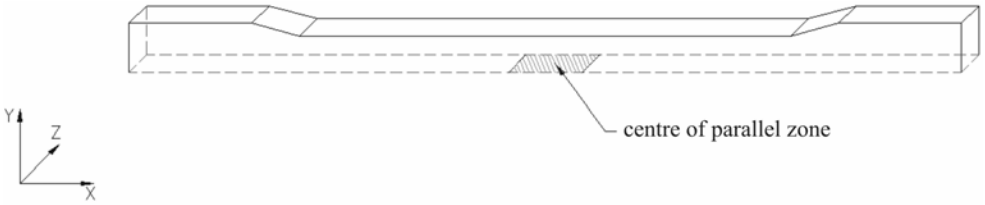

Figure 3.6: Position of the samples taken for investigation in transmission electron microscopy

3.3.6 Wide-angle x-ray scattering

The orientation of the crystalline structure in solid state PP can be analysed by means of wide-angle x-ray scattering (WAXS). Radiated X-rays reflect on atoms and crystal lattice. The angle of those reflections varies according to the order of the structure. By analysing and evaluating these reflections, the crystalline structure, the orientation of the crystalline fraction and its quantity can be determined.[113]

For WAXS experiments on the PP powders, the Rigaku Geigerflex was used to measure diffraction intensity versus 2Θ. The measurements were performed within a diffraction angle range of between 10° and 40°. The WAXS measurements on micro dumbbell specimens were performed at the Consejo Superior de Investigaxiones Scientificas institute (CSIC), Madrid, Spain. There the orientation in the parallel zone and shoulder of the micro dumbbell specimens was investigated.

3.4 Properties

3.4.1 Rheometry

The flow behaviour (viscosity) can be analysed by means of a plate-plate rheometer. For that purpose, the molten sample is deformed at a given velocity, and the torque required for deforming is measured.[114] The shear rate $\dot{\gamma}$ is calculated from the velocity applied, taking apparatus dimensions into consideration, as described in eq. 3.3 for Newtonian liquid.

$$\dot{\gamma}(r) = r\frac{\Omega}{H} \tag{3.3}$$

where Ω is the plate velocity, r is the radius of the plate and H is the gap between the plates.

The corresponding stress τ is determined by the torque measured and is presented in eq. 3.4.

$$\tau(r) = r\frac{2\,M_t}{\pi\,R_{out}{}^4} \tag{3.4}$$

where R_{out} is the outside radius and M_t is the torque.

Finally, the viscosity η as a function of shear rate is described as follows.

$$\eta = \frac{\tau}{\dot{\gamma}} \tag{3.5}$$

The viscoelastic properties of molten polymer are measured similarly to the rheological properties. Instead of deforming the molten polymer only in rotation, oscillation deformation is applied (eq. 3.6).

$$\dot{\gamma} = \hat{\dot{\gamma}}\sin(\omega t) \tag{3.6}$$

where $\hat{\dot{\gamma}}$ is the amplitude, ω is the angular frequency and t is time.

The amplitude and phase angle of the sample response (eq. 3.7) is evaluated in order to analyse the viscoelastic behaviour of the samples.

$$\tau = \hat{\tau}\sin(\omega t + \delta) \tag{3.7}$$

where δ is phase angle.

All rheological investigations were carried out using a Bohlin Instruments Gemini 200 plate-plate rheometer. The shear-dependent viscosity (shear thinning behaviour) was analysed in rotation at 200°C, whereby the shear rate was logarithmically varied from 0.001 to 100 s^{-1}. The shear modulus of polymer melt and its dependency on angular frequency was obtained by oscillation measurements. At a temperature of 200°C, a sinusoidal strain with a constant amplitude of 1 % was applied and the angular frequency was subsequently varied from 0.01 to 100 s^{-1}. For both methods in rheological testing, the gap between both plates was 0.5 mm, and the measuring system was purged with nitrogen to avoid any sample degradation.

3.4.2 Tensile test

The tensile test is one of the most important test methods for determining mechanical properties in a quasi-static loading direction. This test is usually performed by continuously monitoring the force that develops as the sample is elongated at a constant rate of extension.

Primarily, engineering stress σ_e and engineering strain ε_e is obtained by dividing the elongation by the reduced gauge length (eq. 3.8) and the measured load on the sample by the initial cross-sectional area (eq. 3.9). However, in order to consider the change of the cross-section of the samples during elongation, the true stress and true strain has to be calculated. The calculation of the true stress-strain curve is based on the assumption that the volume of the dumbbell specimen is constant and not influenced during polymer deformation. True stress and true strain can be found in eq. 3.10 and 3.11.

$$\varepsilon_e = \frac{\Delta L}{L_0} \tag{3.8}$$

$$\sigma_e = \frac{F}{A_0} \tag{3.9}$$

$$\varepsilon_t = \int_{L_0}^{L_i} \frac{dL}{L} = \ln \frac{L_i}{L_0} = \ln \frac{L_0 + \Delta L}{L_0} = \ln(1+\varepsilon) \tag{3.10}$$

$$\sigma_t = \frac{F}{A_0}(1+\varepsilon) = \sigma(1+\varepsilon) \tag{3.11}$$

where ε_e is engineering strain, ε_t is true strain, σ_e is engineering stress, σ_t is true stress, L_0 is initial gauge length, ΔL is the measured displacement, F is measured load, and A_0 is initial cross sectional area.

As a result, the true stress-strain curve of plastics materials can be obtained and, therefore, specific mechanical properties, such as stiffness and tensile strength, can be determined.

Uniaxial tensile tests were performed with a Gabo Qualimeter Eplexor 150 N in quasi-static mode. The micro dumbbell specimens were mounted between two clamping jaws at a distance of 15 mm with a contact force of 1 N. Measurements were performed at 25°C with a strain rate of $3 \cdot 10^{-4}$ s^{-1}.

3.4.3 Dynamic mechanical analysis

By means of dynamic mechanical analysis (DMA), the viscoelastic properties of polymers in solid state can be determined depending on temperature and frequency.[115] A periodical force is applied to the measured sample (eq. 3.12), and the responding amplitude and phase are determined (3.13).

$$F(t) = \hat{F} \sin \omega t \qquad (3.12)$$

$$s(t) = \hat{s} \sin(\omega t - \delta) \qquad (3.13)$$

where F is force, s is displacement, t is time, δ is phase angle, and ω is angular frequency.

By measuring the viscoelastic response of the sample, the complex modulus E*, storage modulus E', loss modulus E'' and the loss factor tan δ can be determined. Generally, in dynamic measurements the elastic modulus is treated as a complex entity:

$$E^* = E' + i\,E'' \qquad (3.14)$$

The viscoelastic properties were analysed in tensile mode using a Gabo Qualimeter Eplexor 150 N dynamic mechanical analyser. The temperature dependence of the storage modulus E', loss modulus E'' and the loss tangent tan δ were analysed from -50 to 150°C at a heating rate of 5 $K \cdot min^{-1}$ where the frequency was varied stepwise from 0.5 to 50 s^{-1}. A contact force of 1 N was applied and the oscillation amplitude of 0.2 % strain was kept constant, whereas the static strain was set at 0.5 %. Subsequent to measurement, the temperature-time superposition equation according to WLF (eq. 3.15) was applied for generating a master curve.

$$\log a_T = -\frac{c_1 (T - T_0)}{c_2 + (T - T_0)} \qquad (3.15)$$

where a_T is shift factor, c_1 and c_2 are constants, T is temperature, and T_0 is reference temperature.

4 MATERIALS

The semi-crystalline PP mainly used in this study was produced in the high-pressure laboratory at the University of Twente as described in detail in Chapter 3.1.

To the PP powders obtained, CIBA IRGANOX B215 stabiliser (1 % for stabilising polymers against oxidative and thermally induced degradation during melt processing) was added to avoid any degradation of the polymer during the tests.

Additionally, commercially-available industrial samples were studied for comparison with the laboratory synthesised PP samples. These industrial PP samples are synthesised, using a different reactor and different Ziegler-Natta catalysts. Sample PP-I395 is produced in gas phase and samples PP-M256 and PP-B445 are made in a liquid phase polymerisation process. Furthermore, sample PP-M256 is produced in one stage (it is monomodal), whereas, product PP-LB445 is made in at least two stages (it is bimodal), with a significant difference in MW between the two stages.

The PP samples polymerised in the laboratory were in powder form, as opposed to the industrial samples, which are generally available in pellet form. This means the PP samples from the industry passed through an additional process step. It should also be mentioned that the industrial samples might include unknown additives.

The characteristics of all polymer samples used in this study are shown in Table 4.1.

Table 4.1: Molecular characteristics of investigated PP

Type		*Sample*	*MW* [kg·mol^{-1}]	*PD* [-]
lab grade	gas phase	PP-G1120	1 120	9.4
		PP-G1150	1 150	8.0
		PP-G877	877	7.9
		PP-G444	444	7.1
		PP-G417	417	7.4
		PP-G157	157	9.1
industrial grade		PP-I395	395	4.9
lab grade	liquid pool	PP-L1600	1 600*	na
		PP-L1120	1 120	6.4
		PP-L833	833	6.6
		PP-L462	462	7.2
		PP-L361	361	6.8
		PP-L320	320	6.8
		PP-L244	244	7.3
		PP-L153	153	7.3
		PP-L101	101*	na
industrial grade		PP-M256	256	5.7
		PP-B445	445	6.9

* evaluated from rheological data, na = not available, B = bimodal molecular weight distribution, G = gas phase PP, I = industrial gas phase, L = liquid pool PP, M = monomodal molecular weight distribution, MW = weight average molecular weight, and PD = polydispersity

5 SYNTHESIS – GAS PHASE AND LIQUID POOL POLYMERISATION

Polypropylenes are commercially produced using various polymerisation processes; the main ones are the gas phase (GP) processes, most often using a fluidised bed reactor, or liquid bulk processes, with a bulk loop reactor.[23,24,116] In leading polymerisation technologies, such as Spheripol and Spherizone (both Basell), Unipol (Dow), Innovene (BP) and Borstar (Borealis), both methods come into use and, in some cases, are even coupled. However, the liquid pool process is gaining in relative importance. Here it should be noted that the so-called slurry process is in a liquid phase as well, but in this process the liquid propylene is dissolved and polymerised in a diluent (e.g. hexane or heptane). By contrast, the liquid pool process uses pure liquid propylene monomer itself as a reaction medium. In comparison with the gas phase process, this results in two advantages: a higher polymerisation rate due to higher monomer concentration and more homogenous distribution of added components. This tends to reduce operating costs and thus leads to more efficient production of polypropylene.

In the past, continuous efforts have been made to improve reactor operability and to better control polymer properties. In particular, this research has been based on many kinetic and morphological analyses, as evidenced by numerous publications.[5-20,117-124] Furthermore, there are many articles discussing the final properties of plastic parts influenced by structural changes and processing conditions.[125-129] However, these papers contain hardly any information on the "kinetic history" of synthesized polymers and, moreover, there are no studies comparing the PP quality obtained from experiments carried out in gaseous and liquid propylene while using identical, modern Ziegler-Natta (ZN) catalysts.

Furthermore, knowing how polymerisation technique affects polymerisation kinetics and the characteristics of synthesized polymer is very important for a fundamental understanding of the relationship between catalyst behaviour, polymerisation process, chain structure, processing behaviour, and end-use properties. Gahleitner[130] has termed such sophistication, reaching from the production of polymers to their final properties, the 'chain of knowledge'. It is an important tool for speeding up market-oriented product development.

This philosophy guides the way this chapter focuses on a comparison of the structure and characteristic properties of PP synthesised by gas phase and liquid pool polymerisation processes with identical highly active Ziegler-Natta (ZN) catalyst, taking polymerisation kinetics into consideration.

5.1 Polymerisation Kinetics

The kinetics of GP and LP polymerisation with heterogeneous catalysts is described using a kinetic model of the first order, which is based on the following assumptions:[13,14]

- Reaction rate is proportional to the total concentration of active centres in catalysts
- Activation is completed during pre-contacting
- Deactivation is of the first-order
- Use of an average reactivity for the multi-site catalysts

For isothermal conditions the reaction rate R_P can be described as a function of time according to the following equation:

$$R_p = R_{P,0}\, e^{-k_d t} \qquad (5.1)$$

with

$$k_d = k_{d,0}\, e^{\frac{-E_{a,d}}{RT}} \qquad (5.2)$$

Here $R_{p,0}$ is the initial reaction rate, k_d is the deactivation constant, $E_{a,d}$ is the activation energy for the lumped deactivation reaction, and T stands for temperature.

In order to compare the polymerisation kinetics of GP and LP polymerisation processes, the initial reaction rate $R_{p,0}$ was mathematically calculated by linearising the reaction rate - time (R_p-t) curve to the maximum reaction rate and subsequent extrapolation to t = 0. Figure 5.1 shows the measured reaction rate - time (R_p-t) curve for PP-L833 (dashed line indicates the fitted and extrapolated R_p-t curve) as an example.

Figure 5.2 shows the measured reaction rate as a function of time for the LP experiments. An obvious rise in the polymerisation rate is visible at the beginning of the reaction. This effect is caused by the kinetic measurement method and is invalid due to the assumption of quasi steady state. After the reaction rate peaks, deactivation of the catalyst is recognizable by a continuous decay in the reaction rate after a polymerisation time of about 10 minutes.

The deactivation process of the active sites on the catalyst depends strongly on the initial activity. For example, the activity of PP-L244 drops to approx. 60 % from a maximum activity of $R_{p,10}$ = 120 $kg_{PP} \cdot g_{cat}^{-1} \cdot hr^{-}$ to an activity of $R_{p,60}$ = 70 $kg_{PP} \cdot g_{cat}^{-1} \cdot hr^{-1}$ within 50 minutes, contrary to the almost constant activity of 20 $kg_{PP} \cdot g_{cat}^{-1} \cdot hr^{-1}$ in the case of PP-L1600.

In fact, the time-dependent reaction rate profile (measured at the University of Twente for the first time in 1996) reflects characteristically the polymerisation run for each experiment and can, therefore, be considered as a kinetic fingerprint for the respective polymer produced.

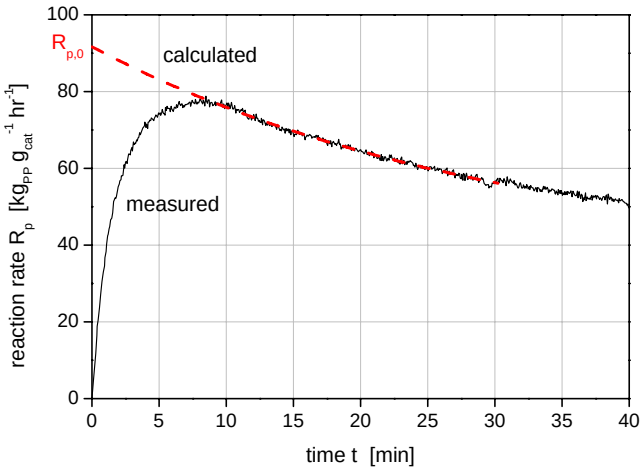

Figure 5.1: Measured and calculated reaction rate - time curve as example for PP-L833

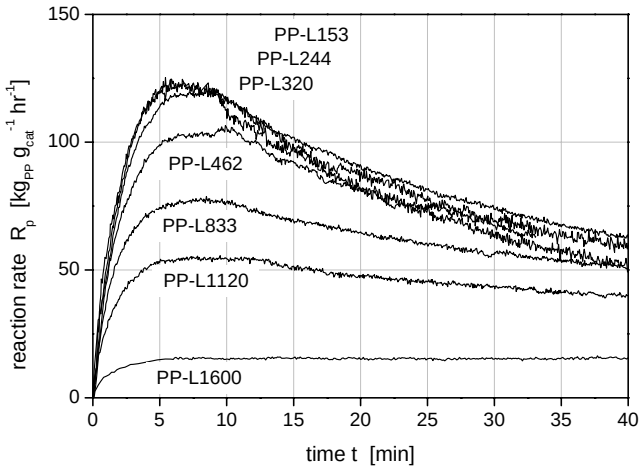

Figure 5.2: Time-dependent reaction rate for liquid pool experiments

Figure 5.3 shows the calculated initial reaction rate as a function of hydrogen concentration for GP and LP polymerisation. As mentioned above, the presence of hydrogen increases the initial polymerisation rate significantly. It is well known that hydrogen influences the activity of catalysts, but the mechanism of the activation process by hydrogen is still the subject of controversy.[13-20,119-123] Although various theories exist, the majority opinion is that the so-called dormant or sleeping sides, caused by irregular 2,1 insertion of the monomer, are reactivated by hydrogen, thus increasing the overall catalyst activity.

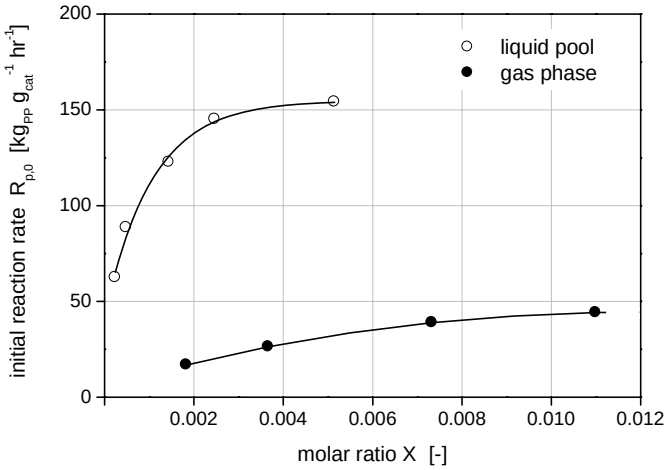

Figure 5.3: Initial reaction rate in gas phase and liquid pool polymerisation as a function of the molar ratio X (hydrogen concentration in proportion to the monomer concentration)

For LP the initial polymerisation rate peaks at approx. 150 $kg_{PP} \cdot g_{cat}^{-1} \cdot hr^{-1}$ and at approx. 45 $kg_{PP} \cdot g_{cat}^{-1} \cdot hr^{-1}$ in GP. This significant difference between maximum initial polymerisation rates can be explained by higher monomer concentration near the active centre in LP polymerisation, as reported by Meier.[17]

Natta et al.[18] (1959) were the first to study hydrogen response on the molecular weight of olefin polymerisation using α-$TiCl_3$ catalysts. They found that the experimental data fitted well using eq. 5.3, where the reciprocal molecular weight is a root function of partial hydrogen pressure.

$$\frac{1}{MW} = K_1 + K_2\sqrt{p_{H_2}} \qquad (5.3)$$

When using molar ratio instead of pressure, eq. 5.3 can be rewritten as follows:

$$p_{H_2} \sim \frac{H_2}{M_p} = X$$

$$\frac{1}{MW} = K_1 + K_2\sqrt{X} \qquad (5.4)$$

where K_1 and K_2 are structural constants and X the molar ratio (hydrogen concentration (H_2) in proportion to monomer concentration (M_p)).

Transforming eq. 5.3 to eq. 5.4, this function can be easily used for comparing hydrogen response in GP and LP polymerisation. Figure 5.4 shows that the measurement points for both GP and LP fit well using eq. 5.4, particularly at high hydrogen concentrations. In contrast, substantial deviation from linearity exists at low hydrogen concentrations. Nevertheless, molecular weight decreases as hydrogen amount increases due to an increase in the chain transfer reaction by hydrogen. This result is in good agreement with the first results of Natta et al. and numerous other investigations using modern ZN catalysts.[13-20,119-123]

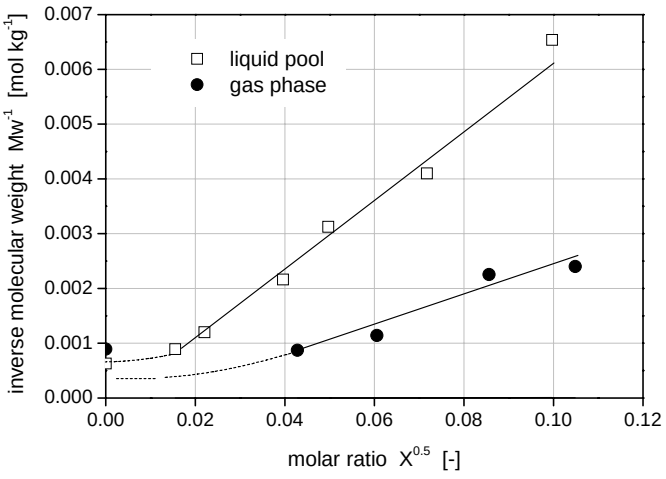

Figure 5.4: Inverse average molecular weight as a function of mole fraction hydrogen for gas phase and liquid pool polymerisation

By contrast, hydrogen does not influence the polydispersity (PD) calculated from the molecular weight distribution (MWD) significantly. Only negligible changes occur using different amounts of hydrogen for propylene polymerisation. The monomodale PD measured by GPC varies for LP-PP between 6.4 and 7.3. By contrast, the PP produced in GP yields a noticeably broader MWD of approx. 8. These are typical values for PP polymerised with a multi-site fourth-generation ZN catalyst. In the meantime, modern ZN catalysts are capable of producing PP with a PD of approx. 3. With single-site catalysts (e.g. metallocene) it is even possible to obtain polymers with a considerably narrower MWD of PD ~ 2.

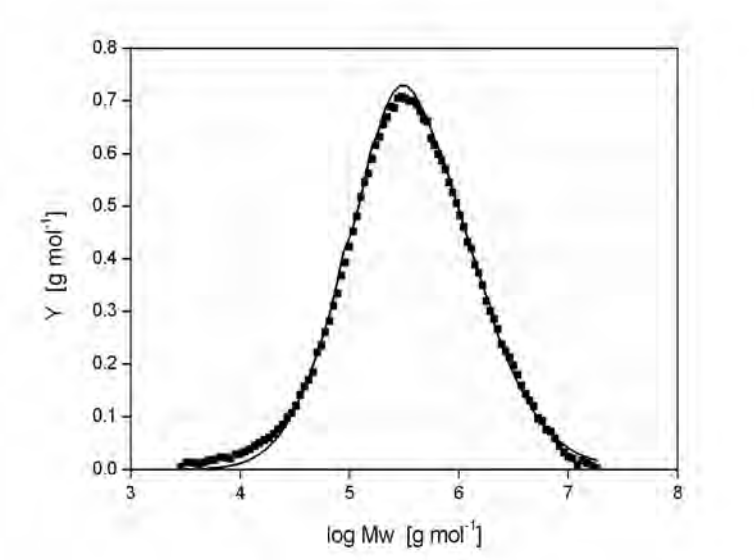

Figure 5.5: Experimental GPC curve fitted with a modelled MWD for PP-L833[131]

The MWD can be modelled based on the measured polymerisation kinetics. Weickert[131] presents a four-site model which permits the prediction of MWD for LP-PP. Figure 5.5, for example, shows an experimental GPC curve fitted with a modelled MWD for PP-L833 (solid line indicates the model). The model and the measured GPC results show that the PD is not fundamentally influenced by hydrogen. The PD is small, but not significantly affected by the polymerisation technique used. The PD of GP PP is slightly higher than that of LP-PP due to the pre-polymer/main polymer mixture, in the case of two-step GP polymerisation.

5.2 Characterisation of PP powder

5.2.1 Rheological properties

Using rheological measurements, it is possible to analyse shear-dependent flow behaviour and, therefore, to characterise the pseudo plasticity, i.e., shear thinning behaviour, of polymer melts and their zero viscosity. As a result, the flow behaviour of GP and LP-PP can be comparatively discussed.

Figure 5.6 shows the shear thinning behaviour of LP-PP with various average molecular weights corresponding to the concentration of hydrogen during polymerisation.

It is obvious that the viscosity of PP polymers drops as shear rate increases. At low shear rates, which characterise the Newtonian plateau, zero viscosity depends on molecular weight and decreases conversely to hydrogen concentration and, therefore, as average molecular weight decreases. At a higher shear rate, the slope of the viscosity curve, representing pseudo plasticity, varies, depending on average molecular weight. The slope becomes flatter with higher hydrogen concentration (i.e. with lower average molecular weight).

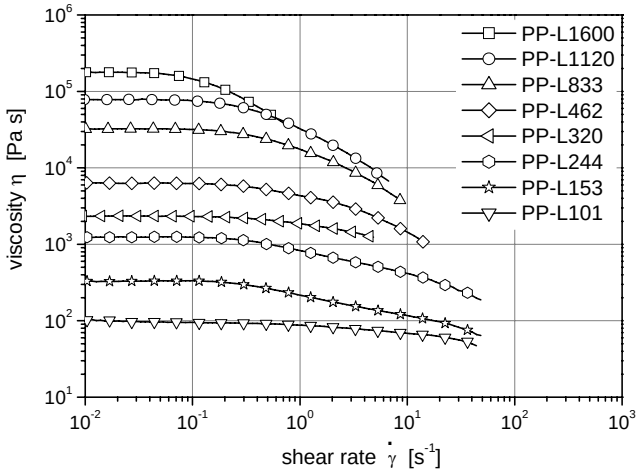

Figure 5.6: Shear thinning behaviour of liquid pool PP series

At low shear rates, molten polymers have a constant viscosity, the so-called Newtonian plateau, which is equivalent to zero viscosity η_0 and strongly affected by the molecular weight of the sample. It is well known, that above a critical molecular weight Mc, zero viscosity η_0 relates to the average molecular weight MW according to eq. 5.5.

$$\eta_0 \approx K\, MW^a \qquad (5.5)$$

The zero viscosity of linear polymers with narrow molecular weight distribution varies with average molecular weight exhibiting a power of approx. 3.4. In the case of PP, power values from 2.9 to 3.8 are mentioned in the literature.[38,114,115,130,132,133] However, no details are provided with regard to polymer synthesis (catalysts, polymerisation technique, polymerisation temperature, etc.) or additives, such as anti-oxidants or lubricants, which may influence these results.

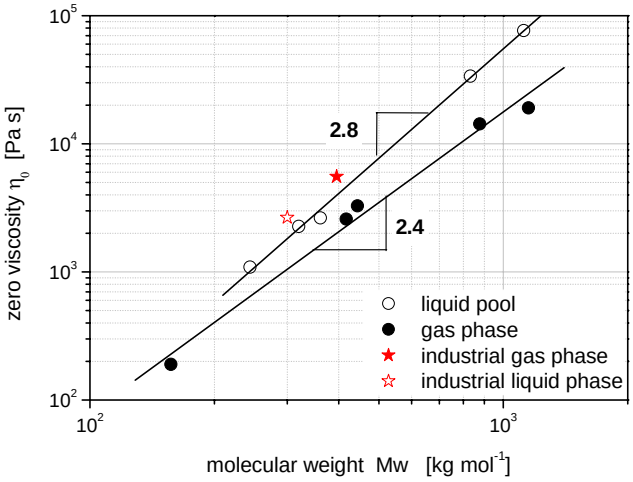

Figure 5.7: Zero viscosity versus average molecular weight of gas phase and liquid pool PP

Here, the zero viscosity was determined by fitting the measured viscosity curve, using the Carreau viscosity model.

$$\eta_{(\dot{\gamma})} = \frac{\eta_0}{\left(1 + (D\dot{\gamma})^2\right)^C} \qquad (5.6)$$

where D is the reciprocal transition rate, C is the slope of the viscosity curve in the shear thinning area, and $\dot{\gamma}$ is the shear rate. This viscosity model has been shown to have enough flexibility to fit several experimental viscosity curves.[134] The data determined for the LP-PP powders are presented in Table 5.1.

The relationship between zero viscosity and the average molecular weight of GP- and LP-PP is shown in Figure 5.7. LP-PP shows a linear double logarithmic relation with a slope of 2.8 for the mathematical fit of the logarithmic curve. As opposed to experiments in LP, a slope of 2.4 on logarithmic coordinates is found for GP-PP. The industrial PP, synthesised in gas and liquid phase, respectively, shows almost the same values as LP-PP.

Based on this linear double logarithmic relationship, the average molecular weight for two LP-PP samples (PP-L1600 and PP-L101) can be estimated as 1 600 kg·mol^{-1} for

PP-L1600 and 101 kg·mol^{-1} for PP-L101. The high molecular weight sample PP-L1600 could not be analysed by GPC due to a lower solubility in TCB. Therefore, the investigation of zero viscosity is an advantage, especially for extremely high molecular weight samples, in order to determine the average molecular weight of these chromatographically undetectable PP samples.

Moreover, comparison of GP- and LP-PP shows lower zero viscosity for GP-PP at the same average molecular weight. This is due to different molecular weight distribution. In the case of broad molecular weight distribution, a countable fraction of short polymer chains exists; these act as lubricants and may improve the flow behaviour of long polymer chains. Consequently, the broader molecular weight distribution of the GP-PP of about PD = 8 leads to lower zero viscosity in comparison to LP-PP, which has an average PD of 6.8. Note that the PD of the industrial GP sample is notably narrower than the PD of the GP-PP samples, which were polymerised in the laboratory.

Table 5.1: Zero viscosity η_0, reciprocal transition rate D, and slope of viscosity curve C, determined by fitting the viscosity curve of liquid pool synthesised PP series, using the Carreau model

Sample	η_0 *[Pa·s]*	*D [s]*	*C [-]*
PP-L1600	195 700	7.65	0.438
PP-L1120	76 640	3.70	0.284
PP-L833	33 730	3.37	0.182
PP-L462	6 280	4.20	0.008
PP-L361	2 640	3.60	0.002
PP-L320	2 260	3.24	0.004
PP-L244	1 090	3.75	0.012
PP-L153	290	4.10	0.012
PP-L101	90	1.12	0.003

Additionally, evaluation of the loss and storage modulus is helpful in gaining useful molecular information. A graph of the storage and loss modulus of the LP-PP versus frequency for three different LP-PP samples (varying average molecular weight) is shown in Figure 5.8. In all cases at low frequency the loss modulus G'' (characterising plastic behaviour) is higher than the storage modulus G' (characterising elastic behaviour). The polymer chains have sufficient time for molecular displacement; this is why they follow the oscillating excitation by rheometer. At higher frequencies the relaxation time of the polymer chains becomes too small in comparison to the input frequency; therefore, the molecular chains lack mobility and flow with lessening viscosity. In consequence, the storage modulus becomes higher than the loss modulus.

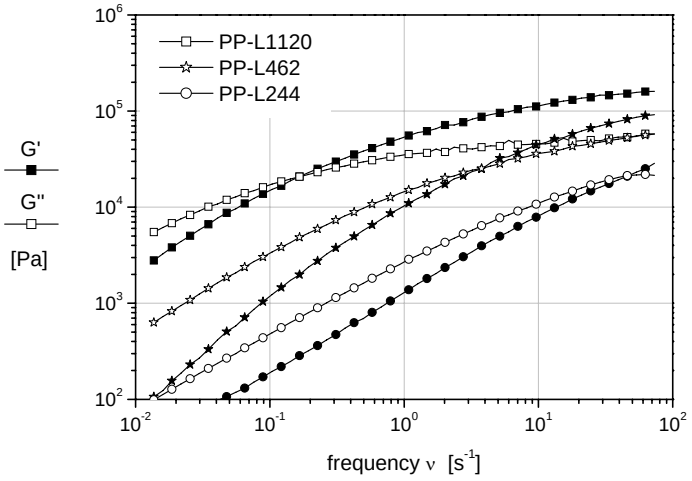

Figure 5.8: Storage and loss modulus versus frequency of liquid pool PP (T = 200°C)

The frequency at which the storage modulus G' crosses the loss modulus G'' is the so-called crossover frequency. This point depends strongly on the average molecular weight and the molecular weight distribution as shown in Figure 5.9.

The slight difference in slope between the GP and LP-PP, as well as the values of the industrial PP samples, can be explained by the different molecular weight distribution, as mentioned above, and is also reported by other authors.[115,135]

Furthermore, the effect of the molecular weight distribution on the viscoelastic behaviour of polymer melt can be characterised using a log G' – log G'' plot, as shown in Figure 5.10. It was found[136-138] that such a plot is sensitive to the structural state of polymer and can by used to evaluate the relative intensity of elasticity to viscosity. Harrell and Nakajima[138] established that G' at a constant G'' is higher for ethylene-propylene copolymer samples with broader molecular weight distribution. Fujiyama et al.[57] verified these results for homopolymer PP samples.

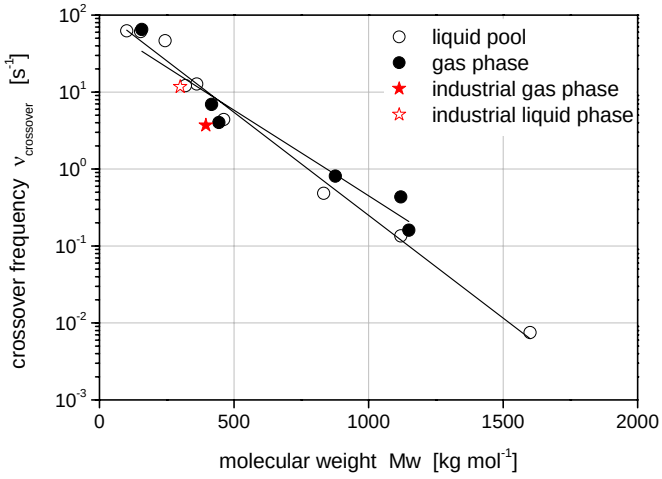

Figure 5.9: Crossover frequency, measured by rheometer versus average molecular weight of gas phase and liquid pool PP (T = 200°C)

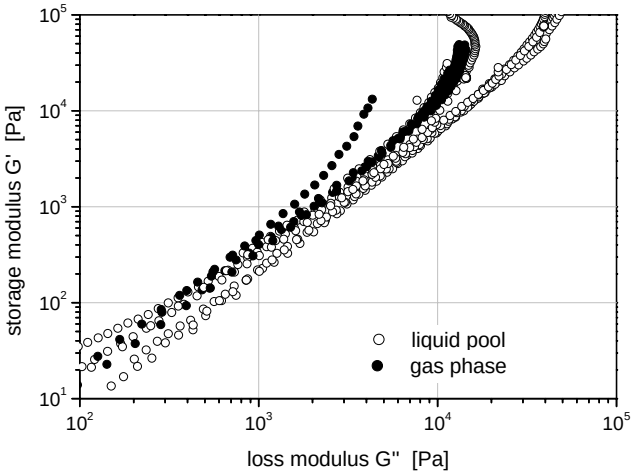

Figure 5.10: Storage modulus G' versus loss modulus G'', measured by rheometer on gas phase and liquid pool PP samples (T = 200°C)

Figure 5.10 shows the log G' – log G'' plot for GP-PP and LP-PP. The measured data of all samples of both polymerisation experiments are scattered around a straight line. However, comparison of the storage modulus at the same loss modulus of GP and LP shows a higher storage modulus for the GP-PP samples. Therefore, GP-PP behaves more elastically than LP-PP. This can be attributed to the narrow molecular weight distribution in the case of LP-PP and is in full agreement with the results of Fujiyama et al.[57]

5.2.2 Crystallinity and crystallite size distribution

DSC measurements were carried out on different PP materials to study the melt enthalpy, representing the crystallinity of each sample, and its crystallite size distributions. The first heating scans for the series of LP experiments are shown in Figure 5.11. The dashed line serves to highlight the variation in the peak maximum location of the melting range with molecular weight. The melting peak of the lower molecular weight PP samples (adding high hydrogen concentration during polymerisation) shifts to a lower temperature, except for the melting peak of the PP sample PP-L1600 where no hydrogen was added during its LP polymerisation. This sample takes a special position, although it is scattered around the maximum peak temperature of 165°C as well as are the other samples. The melting point of 165°C is typical for endothermic melting of the α-phase.[139-143]

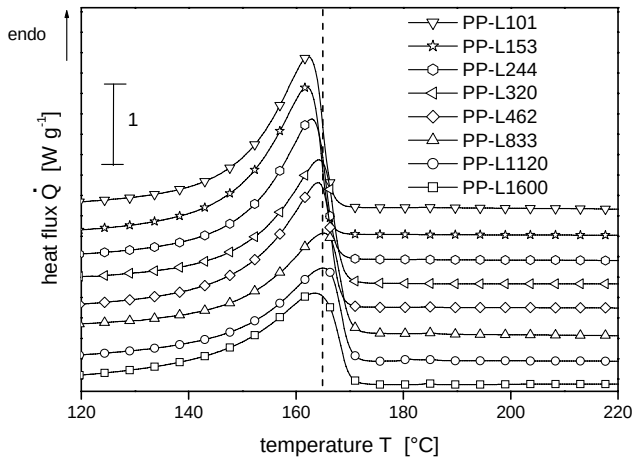

Figure 5.11: DSC scan for various liquid pool PP powders (1st heating, heating rate: 20 K/min, N_2 atmosphere)

Moreover, it is remarkable that the melting endotherms of the lower molecular weight PP samples become higher and narrower compared to higher molecular weight materials. This result will be discussed separately in connection with Figure 5.13.

Figure 5.12 shows the measured melting enthalpy against the average molecular weight from the first and second heating scan of GP and LP-PP samples. The melting enthalpy was integrated in the temperature range from 90 to 190°C using a linear baseline. As expected and as shown in Figure 5.12, the melting enthalpy decreases as the average molecular weight increases to a minimum melting enthalpy in the first heating scan of about 70 $J \cdot g^{-1}$ for both gas and LP-PP. This effect occurs because the higher molecular weight polymer hinders the crystallisation process, which leads to lower crystalline fraction.

Furthermore, it is apparent that the melting enthalpy of all PP samples at the second heating is higher than at the first heating. However, the PP powders were degassed after polymerisation and annealed during the drying procedure; this should usually increase the crystallinity. Obviously the folding of the polymer chains to crystallites inside the reactor is not as good as in the melt state.

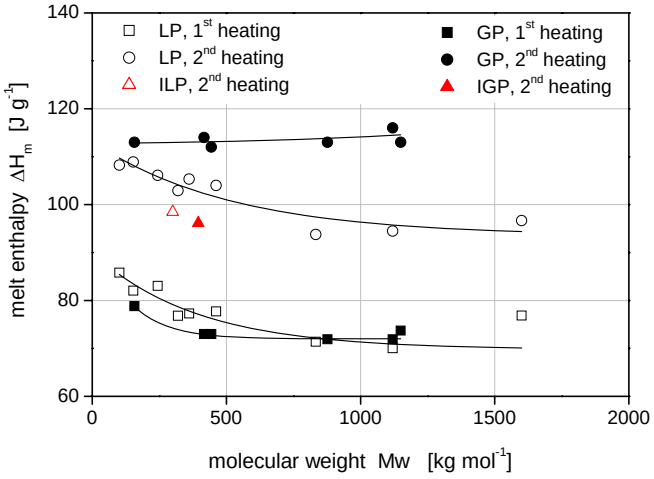

Figure 5.12: Melting enthalpy versus molecular weight of gas phase and liquid pool PP, determined by DSC

Moreover, the melting enthalpy from the second heating scan is higher in the case of the GP-PP series than that of the LP-PP. This result can be explained in reference to the rheological analysis. It was found that the GP-PP shows lower zero viscosity in comparison to LP samples. Consequently, the higher flowability of the GP-PP polymers leads to improved crystallisation capability.

From the industrial PP samples (gas and liquid phase PP samples) only the melting enthalpy of the second heating is demonstrated in Figure 5.12, since these samples contain unknown additives, which can affect their behaviour. Additionally, the samples were melt processed after their polymerisation, which altered their thermal history. For these reasons, only the second heating can be discussed with the other PP samples. The melting enthalpy analysed in the second heating of the industrial PP samples is slightly lower than that of the PP samples polymerised in the laboratory.

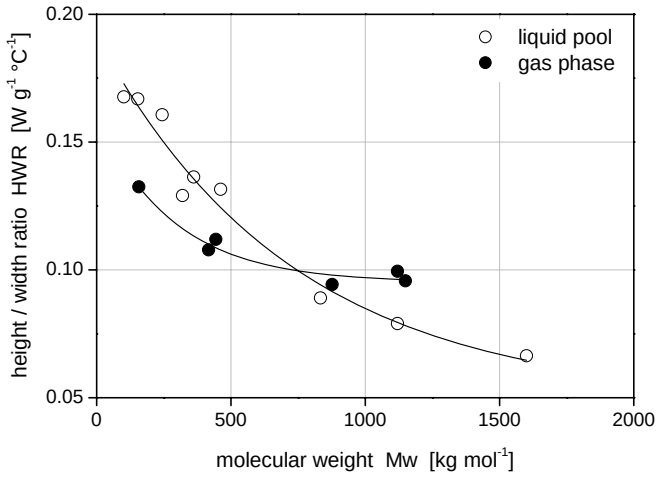

Figure 5.13: Height/width ratio of melting peak, measured by DSC versus average molecular weight of gas phase and liquid pool PP (1st heating, heating rate: 20 K/min, N_2 atmosphere)

Figure 5.13 shows the height/width ratio of the melting peak as a function of average molecular weight for both GP and LP-PP samples. The height/width ratio describes the crystallite size distribution of a semi-crystalline material; the higher ratio exhibits narrow crystallite size distribution and, therefore, more homogenous crystallinity.

The LP-PP samples show a considerable decrease in height/width ratio as the average molecular weight increases. Therefore, the crystallite size distribution becomes broader as the average molecular weight increases. In the case of GP-PP, the trend between the structural properties and the average molecular weight is also visible, but not so distinctive. This is presumably caused by the relatively broad molecular weight distribution of the GP samples; PD is about 8 for GP-PP samples and less than 7.3 for LP-PP samples.

5.2.3 Particle morphology

5.2.3.1 Crystal structure

The WAXS diagram (intensity versus 2Θ) of PP-L1600, PP-L1120 and PP-L101 is shown in Figure 5.14. As expected from the DSC results, the α-phase of crystallinity exists for the majority. Additionally, a small diffraction peak at about 20° 2Θ can be noticed for the PP-L101 sample, which Marigo et al.[69] and de Rosa et al.[144] have found for the reflex of the existence of a γ-polymorphous structure in iPP. Consequently this observed (117) peak identifies the γ-modification of the crystalline structure, although it could not be analysed by DSC due to limited resolution of such calorimetric measurements. Campbell et al.[76] have reported that the γ-phase is developed preferably in PP samples with low molecular weight and high pressure during the solidification process. Therefore, it seems the γ-modification of crystalline structure occurs in the case of the low molecular weight PP sample PP-L101 due to the existing high polymerisation rate, which results in high local pressure at the active sides of the catalyst.

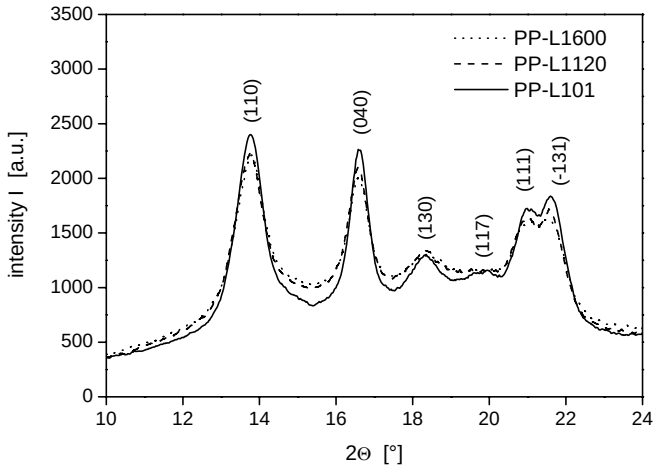

Figure 5.14: WAXS scans of liquid pool PP samples

5.2.3.2 Particle shape

Figure 5.15 shows the shape of PP particles obtained after polymerisation in GP and LP, which were detected by the SEM investigation. Representative of both polymerisation processes are particles shown which were polymerised without hydrogen and with 50 mg and 1 500 mg of hydrogen. As expected, the images show the typical dented-but-smooth surface morphology for particles polymerised with Ziegler-Natta catalysts. It was proved that the polymer tends to replicate the shape and texture of the catalyst.[145,146] When polymerisation starts, the support material ($MgCl_2$ here) begins to fragment, and the polymer grows to a particle around each fragment.

In spite of the different polymerisation processes, no significant differences in morphology can be recognised between GP and LP particles. This could be a result of the two-step polymerisation in the GP process. The morphological structure which is formed during the pre-polymerisation process in LP dominates for the final GP particle structure.

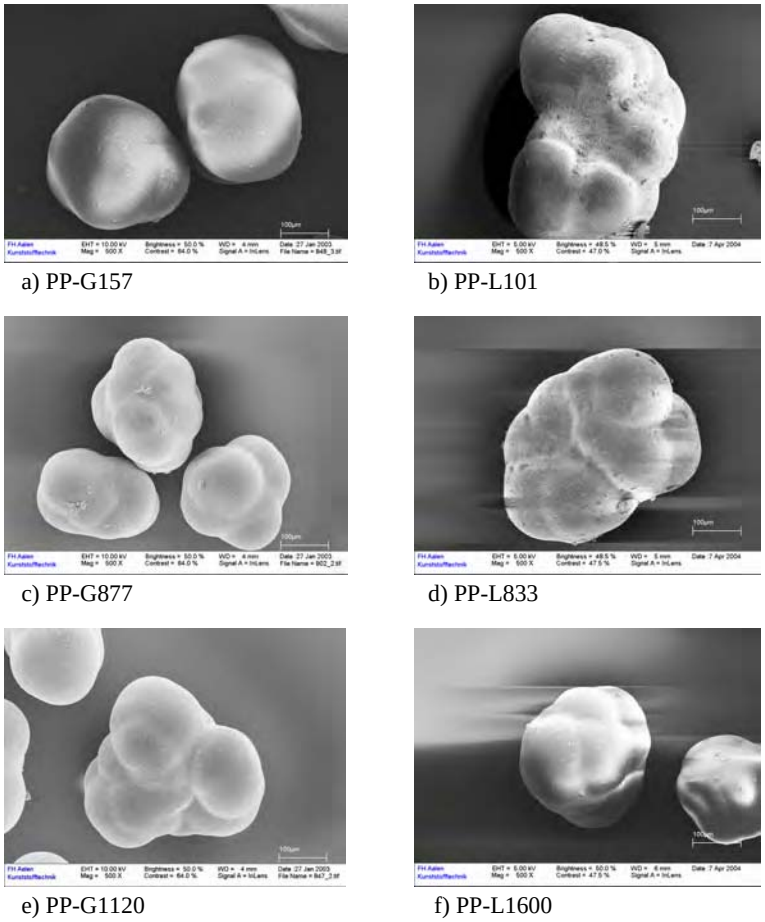

a) PP-G157 b) PP-L101

c) PP-G877 d) PP-L833

e) PP-G1120 f) PP-L1600

Figure 5.15: Particle geometry of gas phase and liquid pool polymerised PP powder observed by SEM

Figure 5.16 shows the cross-section of particles from LP experiments. As a result, different porosity of the particles can be observed. All samples exhibit lower porosity than PP-L101. Strong porosity with large pores is obtained only for the particle polymerised at a high polymerisation rate.[15]

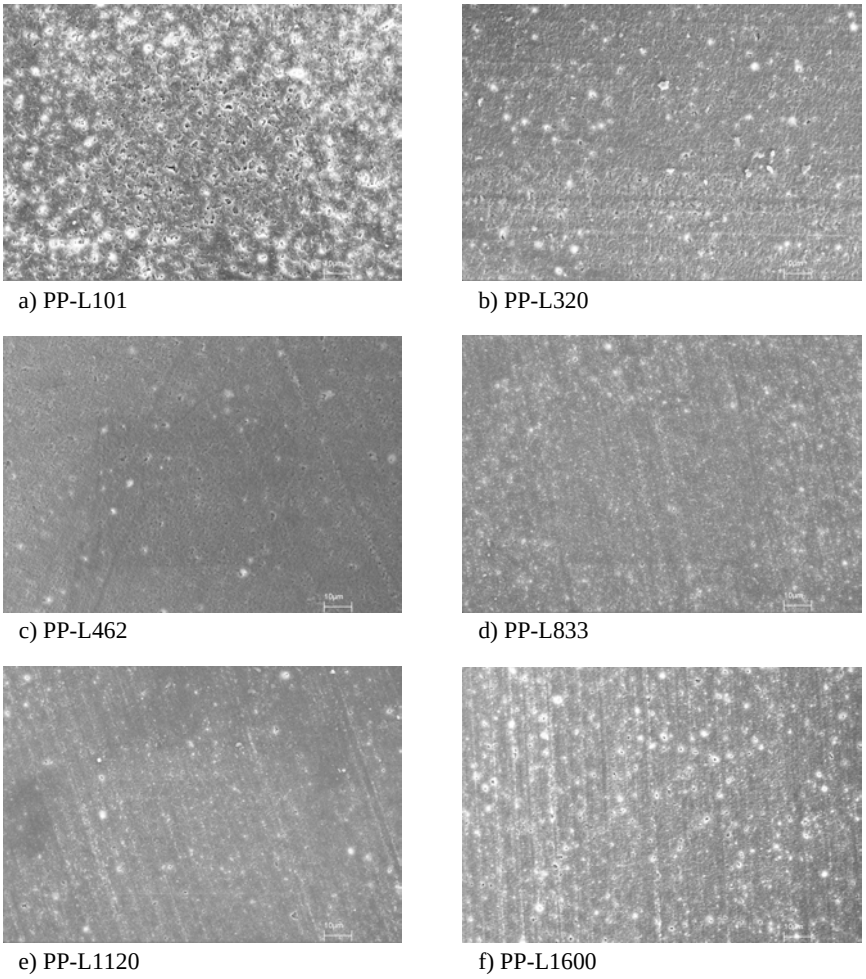

a) PP-L101 b) PP-L320

c) PP-L462 d) PP-L833

e) PP-L1120 f) PP-L1600

Figure 5.16: Cross-section morphology of liquid pool particles observed by SEM

5.3 Conclusion

The quality of polymers achieved from the main polymer polymerisation processes for PP synthesis (a GP and LP polymerisation technique) was compared taking the known kinetic fingerprint into consideration. In particular, the effect of hydrogen on polymerisation kinetics and subsequently on structural, rheological, thermal and morphological properties of polypropylene was investigated.

A series of PP samples with different average molecular weights of up to 1 600 $kg \cdot mol^{-1}$ in GP and LP were synthesised using hydrogen as the molecular weight modifier.

Differences between GP and LP polymerisation could be detected in the polymerisation kinetics, as well as in rheological and thermal properties. For example, the initial polymerisation rate for LP peaks at approx. 150 $kg_{PP} \cdot g_{cat}^{-1} \cdot hr^{-1}$ in contrast to the initial polymerisation rate for GP, which is only about 45 $kg_{PP} \cdot g_{cat}^{-1} \cdot hr^{-1}$. This difference is caused by the higher monomer concentration on the catalysts' active sides in the case of liquid propylene polymerisation.

Furthermore, rheological investigations have shown that the zero viscosity of GP-PP is lower than that of LP-PP measured at the same molecular weight. The difference could be explained by different PDs of GP- and LP-PP. This also seems to be the reason for the higher elasticity of GP-PP.

Studies on thermal properties have imposed the effect of polymerisation technique on crystallite distribution. LP-PP with low molecular weights have shown narrow crystallite size distribution; particularly the PP sample PP-L101 shows considerable and highly homogenous crystallinity. Additionally, it has been found that the crystalline fraction of all PP samples rises after solidification from the melt. Consequently the folding ability of the polymer chains to crystallites inside the reactor is not as good as in the melt state.

From morphological investigations it could be recognised that besides the highly prevailing α-form majority, a small fraction of γ-modification in the crystalline structure exists in PP with low molecular weight.

In fact, the industrial PP samples polymerised in gas and liquid phase show properties similar to the PP samples synthesised in the laboratory.

Finally, LP polymerisation results in more homogenous PP material with improved properties, compared to GP polymerisation using the same Ziegler-Natta catalyst and polymerisation conditions.

6 PROCESSING

Injection moulding is one of the most commercially important fabrication processes for moulding a broad spectrum of thermoplastics. The big advantage of injection moulding is the manufacture of final parts with complex geometries in a very short time without any additional post-treatment. Millions of parts can be produced of exactly the same quality.[147-149] This is also the reason for the increasing significance of injection moulding in the production of complex and multifunctional parts with high load-bearing capacity. The latest strong trend on the market is toward miniaturised parts with a high utilisation factor. A suitable processing technology is required to ensure that such innovative products are feasible and competitive. Micro-injection moulding is a processing technology which can provide the solution for such requirements.

Micro-injection moulding makes it possible to process micro parts with innovative characteristics using only several hundred grams of polymer. The main advantage lies in the fact that the reactor technique used for synthesising novel PP is limited to 500 g polymer powder. Thus, micro-injection moulding can be used to manufacture parts under industrial conditions even from such a small amount of PP. This is of great importance when studying end-use properties of polymers after melt processing, since the processing conditions have a strong influence. It is well-known that final properties are affected by variations in the processing conditions. A polymer exhibits different morphologies and resultant properties depending on the applied pressures (injection pressure, holding pressures), temperatures (melt and mould temperatures), and cooling conditions, as well as on acting shearing, even when a polymer with the same molecular characteristics is used.[51-58]

Nowadays, in particular the analysis of the influence of the flow on the morphology and properties of semi-crystalline polymers is a motive for extensive studies.[36,55,56,73,81,150-158] Several techniques are in use in order to understand the mechanisms of shear-induced crystallisation. The basic idea of the current studies is to separate shearing and cooling, which affect the nucleation and the creation of shear-induced structures, and consequently to clarify the following basic questions on the mechanism of shear-induced crystallisation:[158]

(i) Is there a critical shear rate, at which the shear-induced crystallisation is caused?
(ii) What effect does the duration of shearing have on the shear-induced crystallisation?
(iii) How is the origin of the formation of shear-induced structure dependent upon the shear rate and shear time?
(iv) How does thermodynamics influence the shear-induced crystallisation?

The laboratory techniques used are:

(i) Moving plates – the shear can be either applied parallel, coaxial, rotational or biconical
(ii) Fibre pull-out – a glass fibre is placed in the polymer melt between two plates and pulled out from the isothermal melt with a defined shear stress
(iii) Die extrusion – the polymer melt is pushed through a nozzle with a defined load

These methods are suitable to study in-situ (during crystallisation of the molten polymer) the origin of nucleation and creation of structures, caused by shearing. However, most of the experiments presented in the current study do not conform to the conditions in industrial processes. In fact, the solidification process under shearing is more complex in industrial process (e.g. injection moulding), where the polymer melt is sheared and crystallised at the same time. Moreover, temperature and shear profiles are present in the mould. Hence, non-isothermal conditions exist during shearing.

Differences between laboratory experiments and real industrial processes also exist in the manner of shear applied. In case of laboratory experiments, the shear is applied on a quiescent melt by pulling out a fibre. In contrast, in the injection-moulding process the flowing melt shears along the quiescent wall of a mould and/or along an already frozen skin layer.

In the case of injection moulding, shear-induced crystallisation occurs not in isobaric conditions, but at melt pressures of up to 2 000 bar. In 1967 van der Vegt and Smit[159] stated that the pressure affects the crystallisation behaviour. They found that the melting and crystallisation temperatures increase as the pressure increases. Fasano et al.[160] confirmed this phenomenon and formulated a mathematical description for the solidification process of a polymer sample under a prescribed pressure, taking into account the shrinking flow induced by thermal contraction and crystal growth.

Furthermore, the laboratory experiments are limited to a maximum shear rate of 100 s^{-1}, which is clearly lower than the shear rate acting in an industrial melt process. In injection moulding, shear rates of between 10^2 and 10^4 s^{-1} are present, in some cases shear rates of 10^5 s^{-1} or even more can be obtained.[161] Besides this, the cooling rate under industrial conditions during injection moulding can reach several thousands of Kelvins per minute.

To this end, this chapter studies the influence of the molecular weight on processability of novel PP under industrial conditions. Major foci are the analyses of acting shearing during filling and solidification behaviour. Both parameters strongly influence morphology and the resulting properties. Previous research on the PP powders obtained has been made use of.

6.1 Analysis of injection-moulding process

Injection-moulding is the process of forcing molten plastic into a shaping cavity. First, the plastic is compressed there during cooling, and subsequently, it is ejected from the mould used. There are three major steps in the injection-moulding process, which are shown schematically in Figure 6.1:

1. Injection

   During the injection phase, plastic material, in the form of powder or pellets, is loaded into a hopper on top of the injection unit. The pellets are fed into the cylinder where they are heated by convection (heat transfer from heated cylinder to the material) and by friction (generated by a rotating screw). Within the heating cylinder there is a driven screw that mixes the molten pellets and forces them to the tip of the screw. As soon as enough material has accumulated in front of the screw, the injection process begins. The molten plastic is inserted into the mould through a sprue, while the pressure and speed are controlled by the screw motion.

2. Cooling

   After the mould is volumetrically filled, holding pressure is applied until complete solidification to prevent volume shrinkage and, in addition, the plastic is allowed to cool to its solid form within the mould.

3. Ejection

   The clamping unit is opened, which separates the two halves of the mould. Afterwards an ejecting rod and plate eject the finished part from the mould. The unused sprues and runners are automatically cut by opening the mould.

This procedure is repeated periodically.

Hereby, the injection and cooling process have a key influence on the development of the structure, and thus they affect the final properties of the part. For this reason, the filling and solidification process will be discussed in more detail.

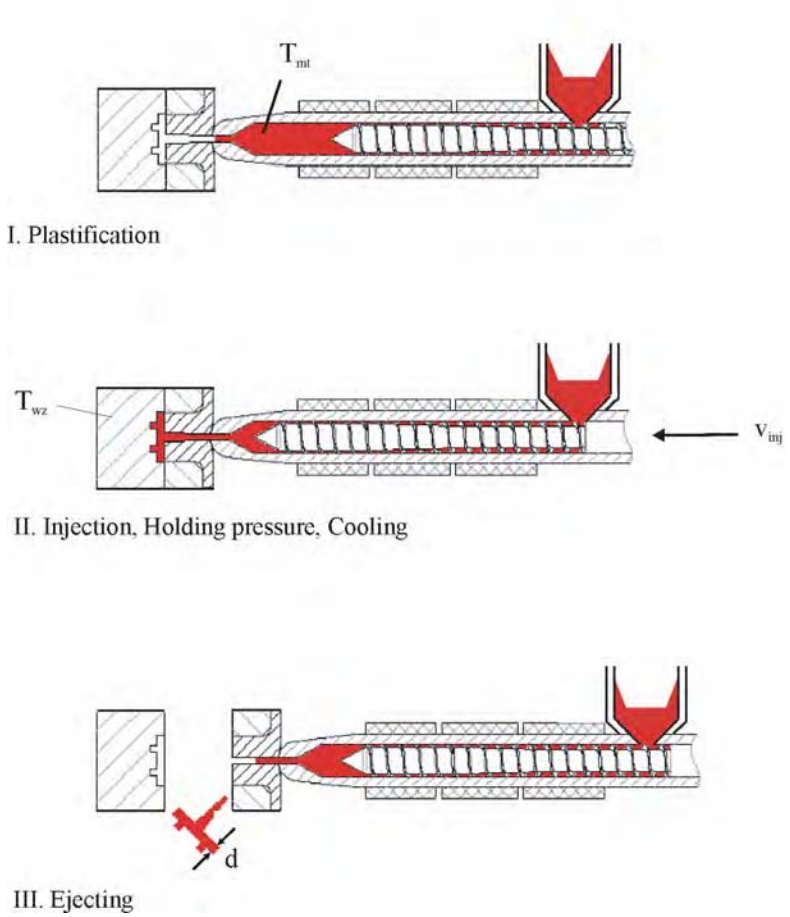

Figure 6.1: Steps of the injection-moulding process

The filling process frequently imposes a high level of mechanical and thermal stress on the melt. The main parameters affecting the filling process are:

- wall thickness of the part (d)
- injection speed ($v_{inj.}$)
- melt temperature (T_{mt})
- mould temperature (T_{wz})

Moreover, the acting shear during melt flow leads to internal friction processes and thus to local temperature increase. Figure 6.2 shows a typical temperature, velocity, and shear profiles of a flowing plastic melt in a cooled injection mould.

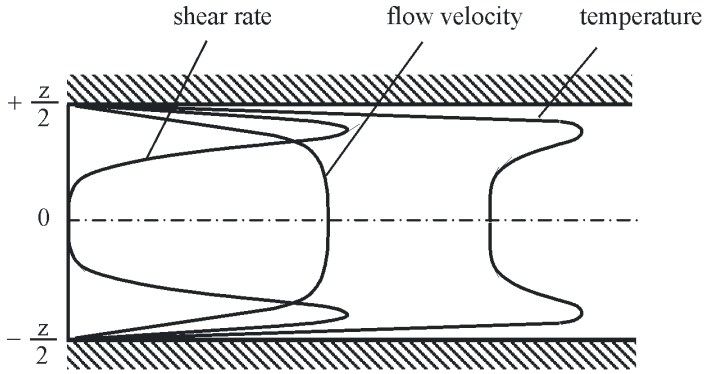

Figure 6.2: Temperature, velocity and shear rate profiles in a flowing plastic melt

During filling, the flow front moves forward at a given flow velocity. Due to wall adhesion and/or adhesion between the melt and the frozen layer, a velocity profile develops in the flow channel with the largest gradient close to the frozen layer. The highest flow velocity is reached at the centre of the cavity; the difference in velocity between the layers is usually very small. In addition, the cooling rates are very low at the centre.

Since the flow velocity is highest at the centre of the flow channel, the melt is rearranged across the part on the flow front (extensional flow), as shown schematically in Figure 6.3. As a result the melt front, being highly viscous because of its contact with “cool” air, is stretched and it freezes suddenly on contact with the cool mould wall. Thus extensional flow leads to deformation and orientation of the macromolecules. As a result, the layers directly on the part surface are highly oriented. As the skin layer thickens, the flow channel becomes narrower and the effective flow velocity increases, also resulting in a higher shear rate. Consequently, orientation increases continuously until the mould is filled completely.

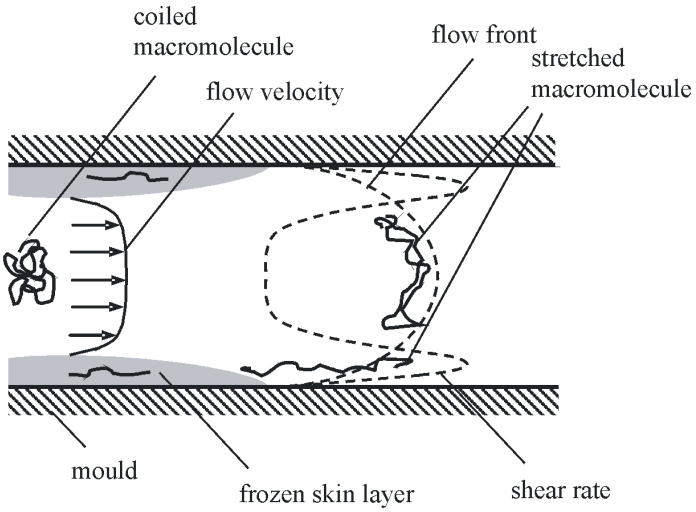

Figure 6.3: Deformation of macromolecules in flowing melt

However, the formation of orientation is superimposed by the relaxation process due to the viscoelastic behaviour of a thermoplastic polymer. These relaxation processes are even more important when the flowing melt stagnates before solidifying, whereby the induced orientation can relax during crystallisation. Once the polymer solidifies, orientation relaxes more slowly and even stops below glass transition.

6.1.1 Simulation of the filling process

The commercial flow analysis software program Moldflow Plastic Insight (MPI) was used to simulate the filling process. Thermal and rheological properties of the LP-PP samples (as reported in Chapter 5) were implemented into the database. A Cross-WLF viscosity model (eq. 6.1 and 6.2) was used to characterise the temperature and shear rate dependence of viscosity.

$$\eta = \frac{\eta_0}{1 + \left(\frac{\eta_0 \dot{\gamma}}{\tau^*} \right)^{(1-n)}} \tag{6.1}$$

with

$$\eta_0 = D_1 \, e^{\left[\frac{-A_1 (T - T_r)}{A_2 + [T - T_r]} \right]} \tag{6.2}$$

where η is the viscosity, η_0 is the zero viscosity, $\dot{\gamma}$ is the shear rate, n is a constant, τ^* is the shear stress at the transition between Newtonian and power law behaviour, D_1 is a constant, T is the temperature, T_r is the reference temperature, and A_1 and A_2 are shift factors.

Table 6.1: Data for simulation of the filling behaviour by MPI

Sample	*n* [-]	*τ** [Pa]	*D_1* [Pa·s]	*T_r* [K]	*A_1* [-]	*A_2* [K]	*c_p* [J·kg^{-1}·K^{-1}]	*k* [W·m^{-1}·K^{-1}]
PP-L1600	0.001	40 081	$3.5 \cdot 10^{34}$	263.15	84.5	51.6	2 940	0.155
PP-L1120	0.01	58 368	$1.6 \cdot 10^{21}$	263.15	49.4	51.6	2 940	0.155
PP-L833	0.01	38 378	$4.8 \cdot 10^{27}$	263.15	67.5	51.6	2 940	0.155
PP-L462	0.139	16 209	$7.3 \cdot 10^{18}$	263.15	45.1	51.6	2 940	0.155
PP-L320	0.148	11 484	$2.6 \cdot 10^{25}$	263.15	63.8	51.6	2 940	0.155
PP-L101	0.523	5 402	$1.9 \cdot 10^{6}$	263.15	13.1	51.6	2 940	0.155

n = constant, τ^* = shear stress at the transition between Newtonian and power law behaviour, D_1 = constant, T_r = reference temperature, A_1 = shift factor, A_2 = shift factor, c_p = specific heat capacity, and k = thermal conductivity

Table 6.1 presents the data implemented in MPI for simulating the filling process. The micro injection-moulding processing conditions used were: mould temperature 60°C, injection speed 10 mm·min^{-1}, and melt temperature 210°C for PP samples with low viscosity (PP-L101, PP-L320, and PP-L462), but 250°C for PP-L1120 and PP-L1600 samples.

Figure 6.4 shows the shear rate at filling as a function of length of the micro dumbbell specimen from a representative selection of PP samples.

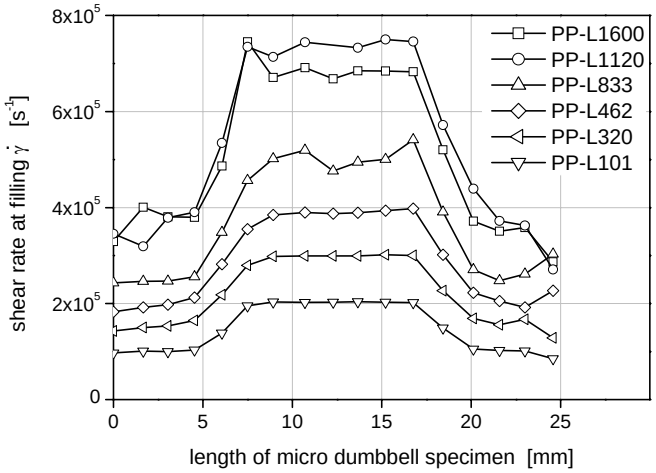

Figure 6.4: Shear rate at filling versus the length of the dumbbell specimen for a representative selection of the liquid pool PP series

The shear rate $\dot{\gamma}$ describes the flow rate in the flow direction relative to part thickness and is proportional to the shear stress τ according to eq. 6.3.

$$\tau = \eta \cdot \dot{\gamma} \qquad (6.3)$$

with η standing for viscosity.

In Figure 6.4, it is obvious that the shear rate rises precipitously after approx. 5 mm length of the micro dumbbell specimen. There the dumbbell specimen tapers to a parallel zone before amplifying again to the second shoulder of the specimen. In the parallel zone, the cross section is halved from 2.5 x 0.5 mm^2 at the shoulder to 1.25 x 0.5 mm^2. Furthermore, the shear rate varies at different points of the dumbbell specimen, as can be seen even better in Figures 6.5 and 6.6.

Moreover, the shear rate increases as the molecular weight increases from about $2 \cdot 10^5$ s^{-1} towards a maximum of about $7.5 \cdot 10^5$ s^{-1}. Here, the shear rates are high due to the small geometry of the micro dumbbell specimen. The shear rate of a Newtonian liquid on the cavity wall is related to the cross-section of the flow channel (= cross-section of the micro dumbbell specimen) according to eq. 6.4.

$$\dot{\gamma} = \frac{6\,\dot{v}}{A\,h} \qquad (6.4)$$

where $\dot{v}$ is the volume rate (~ injection speed $v_{inj.}$), h is the height, and A is the cross-section of the flow channel.

Therefore, the shear rate is reciprocally proportional to the height and cross-section of the micro dumbbell specimen. When comparing the shear rate at filling for a micro dumbbell specimen with that of a larger dumbbell specimen using the same material, the shear will be much lower for the latter specimen. Figure 6.7 shows the shear rate at filling for the eight times larger "standard" dumbbell specimen with a wall thickness of 4 mm, a width of 10 mm in the parallel zone, and an overall length of 150 mm. Simulation was carried out using the basic properties of the high molecular weight samples PP-L1600 and the same injection-moulding processing conditions (T_{mt} = 250°C, T_{wz} = 60°C, $v_{inj.}$ = 10 mm·min^{-1}). In comparison of the maximum shear rate value of the larger "standard" dumbbell specimen with the micro dumbbell specimens, a maximum shear rate of only $1 \cdot 10^3$ s^{-1} can be found which is, consequently, 750 times lower. As a result, substantially higher orientation of the materials inside the micro dumbbell specimen, probably mostly in the parallel zone and close to the wall, is expected

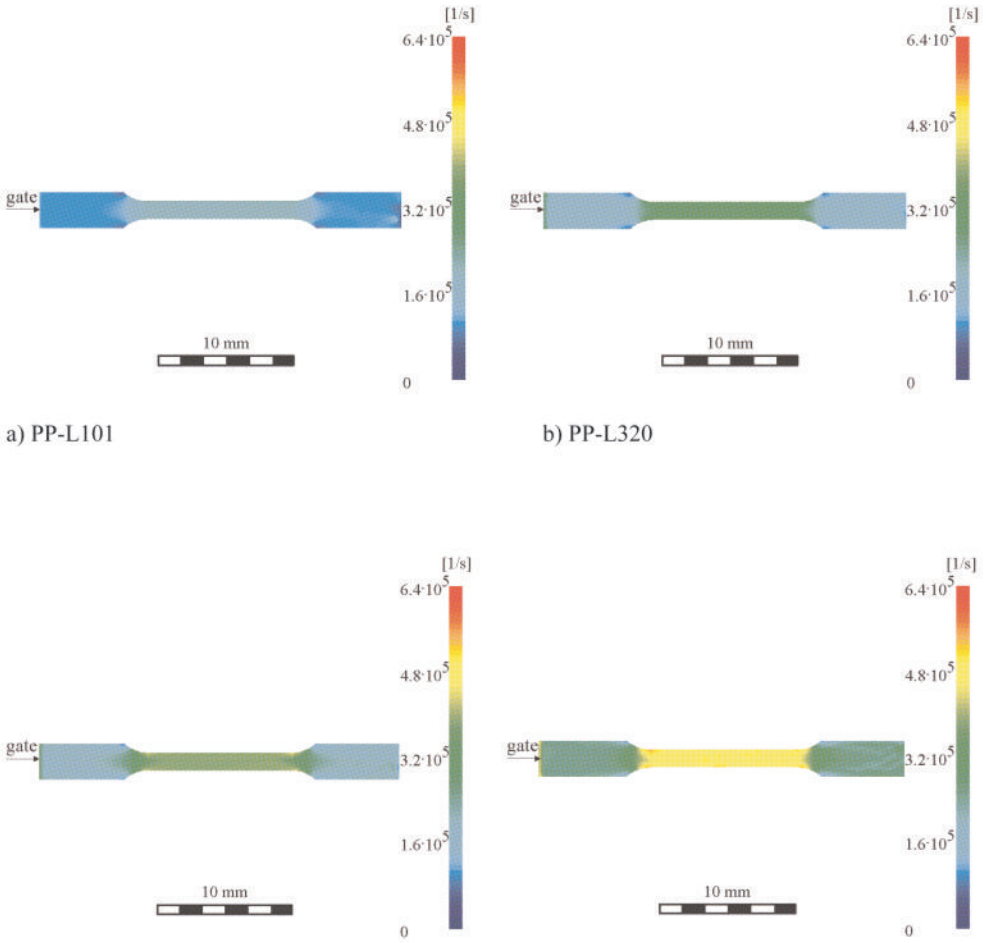

Figure 6.5: Simulation of shear rate at filling of the micro dumbbell specimen for a selection of LP-PP samples, using MOLDFLOW (T_{mt} = 210°C, T_{wz} = 60°C, $v_{inj.}$ = 10 mm·min^{-1})

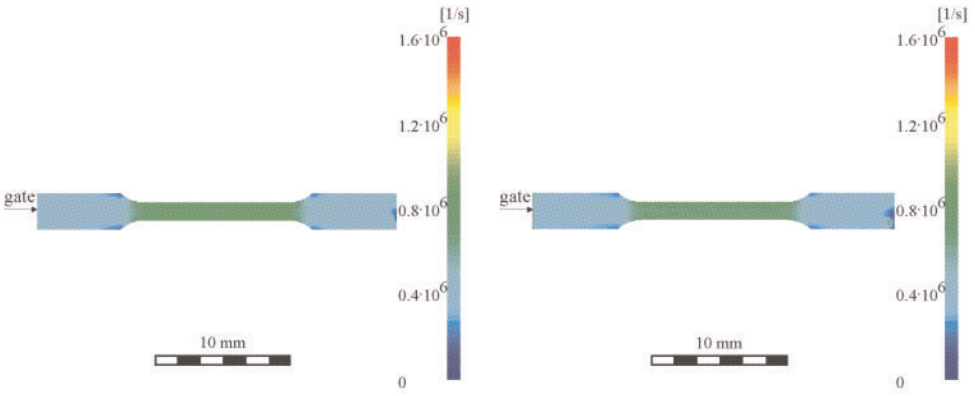

a) PP-L1120 b) PP-L1600

Figure 6.6: Simulation of shear rate at filling of the micro dumbbell specimen for a selection of LP-PP samples, using MOLDFLOW (T_{mt} = 250°C, T_{wz} = 60°C, $v_{inj.}$ = 10 mm·min^{-1})

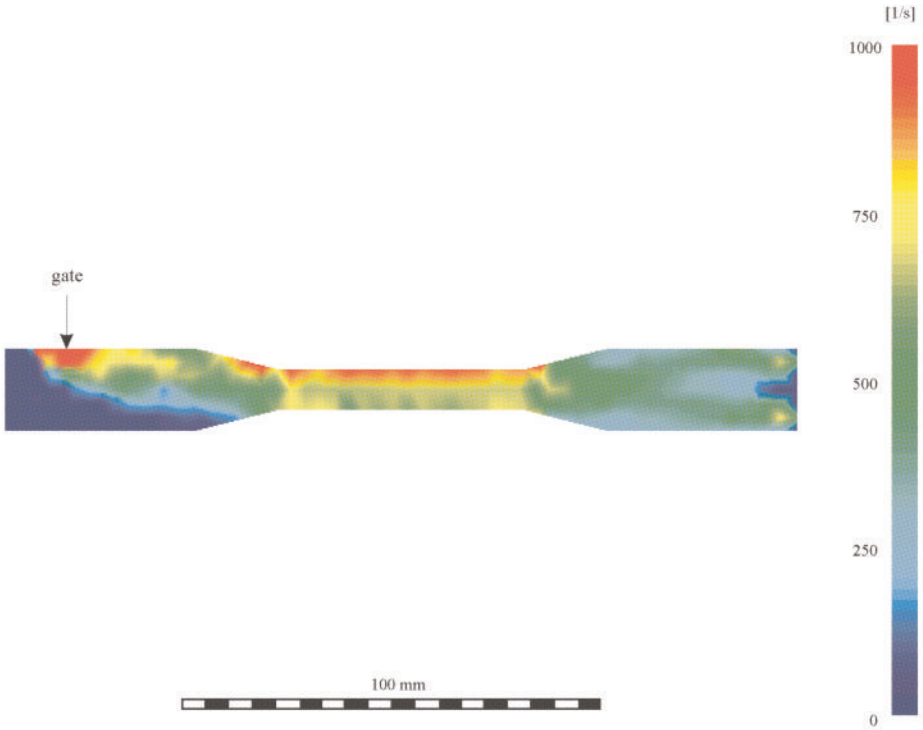

Figure 6.7: Simulation of shear rate at filling of a "standard" dumbbell specimen for high-viscous PP samples PP-L1160, using MOLDFLOW (T_{mt} = 250°C, T_{wz} = 60°C, $v_{inj.}$ = 10 mm·min^{-1})

6.1.2 Investigation of the solidification process

Investigations and calculations of crystallisation kinetics in the past usually referred to analysis of the crystallisation process of quiescent polymer melts. Recent investigations have tried to study the influence of shear on crystallisation.[150-158] For example, Eder and Janeschitz-Kriegl[155] tried to find out how long the orientations last subsequent to the flow process and how they influence shear-induced crystallisation. This effect has to be taken into consideration especially for the extrusion of polymer melts, in order to understand the extrusion process. However, during the injection-moulding process, several layers freeze at the point of highest orientation.

The cooling process essentially depends on the acting temperature gradient inside the mould. Assuming a quiescent melt and a part thickness much lower than the part length or width, the part can be considered as an infinite extended plate with thickness d. Based on this assumption, temperature distribution over the cross section can be calculated simply, since temperature distribution is reduced from a three-dimensional to a one-dimensional problem.[162]

In order to be able to indicate the spatiotemporal temperature distribution of the cooling process, a thermal conductivity equation (eq. 6.5) has to be solved

$$\frac{\partial^2 T}{\partial x^2} - \alpha \frac{\partial T}{\partial t} = 0 \qquad (6.5)$$

with

$$\alpha = \frac{c_p \rho}{\lambda} \qquad (6.6)$$

where α is effective temperature conductivity, c_p is specific heat capacity, λ is thermal conductivity, and ρ is density,

under the initial condition t = 0.

$$T(x, t = 0) = T_{wz} + (T_{mt} - T_{wz})\,\mathrm{rect}\left(\frac{d}{2}\right) \qquad (6.7)$$

Applying the Laplace transform to the thermal conductivity equation (6.5) yields

$$\frac{\partial^2 T(x,s)}{\partial x^2} - \alpha s T(x,s) + \alpha T(x,0^+) = 0 \qquad (6.8)$$

A formal solution is

$$T(x,s) = c_1(s)\, e^{\sqrt{\alpha s}x} + c_2(s)\, e^{-\sqrt{\alpha s}x} \qquad (6.9)$$

The coefficients $c_1(s)$ and $c_2(s)$ are determined from the initial conditions:

1. heat flow density $j(x = 0, s) = 0$
2. boundary temperature

The solution of eq. 6.8 in the transform domain results in

$$T(x,s) = T\left(\frac{d}{2}, s\right) \frac{\cosh\left(\sqrt{\alpha s}\, x\right)}{\cosh\left(\sqrt{\alpha s}\, \frac{d}{2}\right)} \qquad (6.10)$$

Equation (6.10) can be understood as a product of the perturbation $T\left(\frac{d}{2}, s\right)$ and the Green function

$$G(x,s) = \frac{\cosh\left(\sqrt{\alpha s}\, x\right)}{\cosh\left(\sqrt{\alpha s}\, \frac{d}{2}\right)} \qquad (6.11)$$

In order to apply the convolution theorem, multiplication of two factors in Laplace space corresponds to the convolution integral of the inverse transformation in time space.

Due to the initial conditions the inverse transformation of the perturbation $T\left(\frac{d}{2}, s\right)$ is known as

$$T\left(\frac{d}{2}, t\right) = T_{wz} + \left(T_{mt} - T_{wz}\right)\, \Theta(t) \qquad (6.12)$$

$\Theta(t)$ being the unit step function

The inverse transformation of the Green function G(x,s) by means of the residue theorem yields eq. 6.13.

$$G(x,t) = \frac{4\pi}{\alpha d^2} \sum_{n=0}^{\infty} (2n+1)(-1)^n \cos\left((2n+1)\pi \frac{x}{d}\right) e^{-\frac{(2n+1)^2 \pi^2}{\alpha d^2} t} \qquad (6.13)$$

The convolution of perturbation $T\left(\frac{d}{2}, s\right)$ with the Green function G(x,s) results in a spatiotemporal temperature profile during cooling of a infinitely expanded plate with thickness d.

$$T(x,t) = T_{wz} + \left(T_{mt} - T_{wz}\right) \frac{4}{\pi} \sum_{n=0}^{\infty} \frac{(-1)^n}{2n+1} \cos\left((2n+1)\pi \frac{x}{d}\right) e^{-\frac{(2n+1)^2 \pi^2}{\alpha d^2} t} \qquad (6.14)$$

Figures 6.8 and 6.9 show the temperature distribution at different times, using mould temperature T_{wz} = 60°C and melt temperatures T_{mt} = 210°C (Figure 6.8) or T_{mt} = 250°C (Figures 6.9).

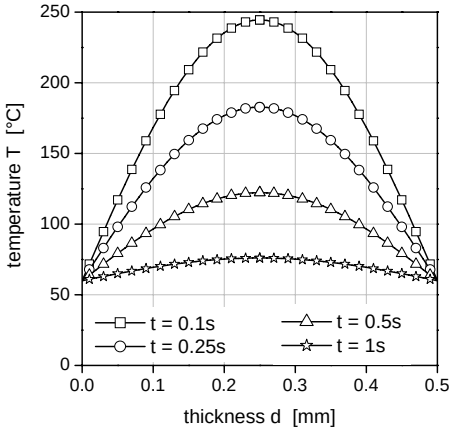

Figure 6.8: Temperature profile for several cooling times (T_{wz} = 60°C, T_{mt} = 210°C)

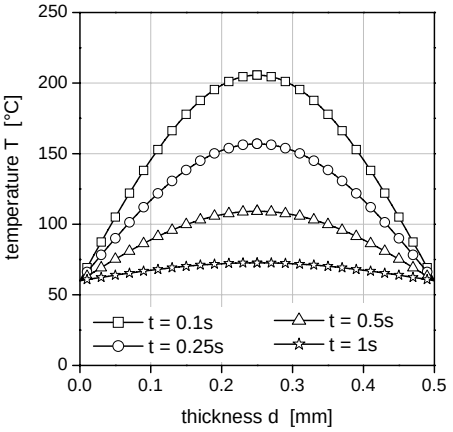

Figure 6.9: Temperature profile for several cooling times (T_{wz} = 60°C, T_{mt} = 250°C)

From eq. 6.14 it follows that the temporal temperature drop is different at each point of the plate. However, an average temperature $\overline{T}(t)$ can be described under the above boundary conditions:

$$\overline{T}(t) = \frac{1}{d}\int_0^d T(x,t)\,dx \qquad (6.15)$$

$$\overline{T}(t) = T_{wz} + (T_{mt} - T_{wz})\ \frac{8}{\pi^2}\ \sum_{n=0}^{\infty} \frac{(-1)^{2n}}{(2n+1)^2}\ e^{-\frac{(2n+1)^2\pi^2}{\alpha d^2}t} \qquad (6.16)$$

The average temperature can be used as the integral temperature change in a part with thickness d.

Figure 6.10 shows the average temperature as a function of time across the micro dumbbell specimen, using two different initial conditions – T_{mt} = 210°C und T_{mt} = 250°C.

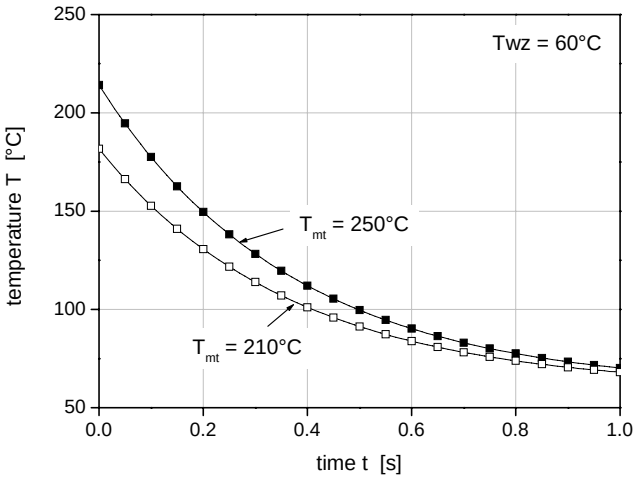

Figure 6.10: Calculated cooling behaviour of PP

It is obvious, that solidification occurs quickly in both cases. The average cooling rate varies from approx. 3 000 $K \cdot min^{-1}$ to 8 000 $K \cdot min^{-1}$. After approx. 0.4 s, the crystallisation temperature is reached, as determined by DSC. Of course, it has to be considered that the crystallisation temperature T_c depends on the cooling rate. Eder and Janeschitz-Kriegl[163] found that the crystallisation temperature decreases as the cooling rate increases, in fact in a linear manner. However, according to this study, the crystallisation temperature would be 0°C when a cooling rate of about 270 $K \cdot min^{-1}$ is acting. This means that in our case, crystallisation cannot occur and thus formation of crystalline structures is not possible for almost all injection-moulding processes when the recommended mould temperature of 60°C is used and cooling rates of more than 300 $K \cdot min^{-1}$ exist. However, the crystalline structures in PP can be easily observed in polarised light for almost all injection-moulded parts. Obviously, Eder and Janeschitz-Kriegl did not consider shear-induced nucleation and crystallisation during injection-moulding processes in connection with the higher crystallisation rates.

Assuming that crystallisation occurs at a temperature of at least 60°C (mould temperature), then solidification should theoretically be finished after 1 s. Hence, cooling time ranges between a minimum of 0.4 s and a maximum of 1 s, according to calculations, for manufacturing micro dumbbell specimens from PP. Note that no shear-induced local temperature increase is considered.

The solidification process during injection moulding can also be observed by means of an implemented cavity pressure sensor, which continuously measures surface pressure on the part close to the gate. Figures 6.11 and 6.12 show representative cavity pressure curves for a selection of PP samples manufactured at two different melt temperatures (T_{mt} = 210°C, T_{mt} = 250°C).

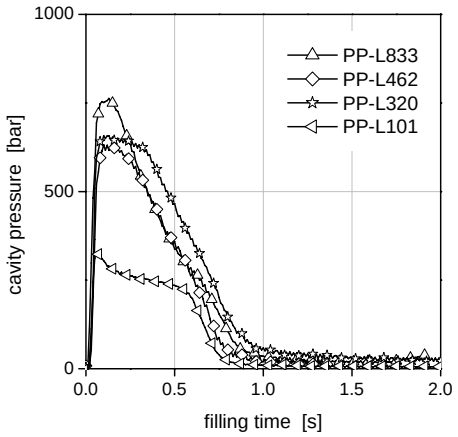

Figure 6.11: Cavity pressure of the PP samples PP-L833, PP-L462, PP-L320, and PP-L101 (T_{mt} = 210°C, T_{wz} = 60°C, $v_{inj.}$ = 10 mm·min^{-1})

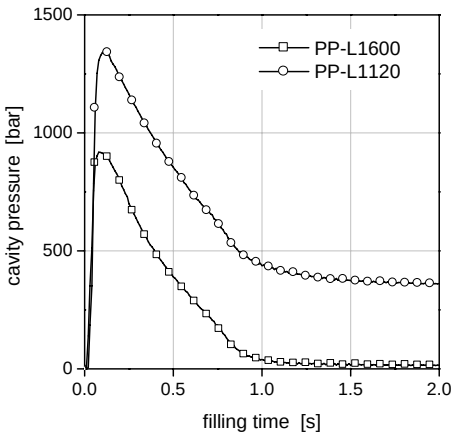

Figure 6.12: Cavity pressure of the PP samples PP-L1600, and PP-L1120 (T_{mt} = 250°C, T_{wz} = 60°C, $v_{inj.}$ = 10 mm·min^{-1})

When filling starts, an obvious rise in cavity pressure is visible. This effect is caused by volumetric filling of the cavity, whereby injection pressure increases. Subsequently, injection pressure is switched over to holding pressure. The volume contraction due to melt cooling is compensated by additional pressing of the melt into the cavity. The cavity pressure curve drops more or less sharply, depending on the existing holding pressure. After freeze-in the gate (no more melt can be pressed into the cavity), the cavity pressure drops to an ambient pressure. Thereafter, the part shrinks continuously, due to thermal contraction and slow crystallisation.

Cavity pressure increases as molecular weight increases. Higher viscosity materials require more pressure to fill the cavity and prevent volume contraction. In the case of PP-L1600, the maximum available injection pressure from the injection moulding machine is too low even to fill the cavity completely and, as a result, the cavity pressure is lower. In contrast, PP-L1120 exhibits a cavity pressure of 1 400 bar, which does not drop to an ambient pressure. Even after complete solidification, about 400 bar pressure is measurable because of deformation of the mould plate. Samples PP-L833, PP-L320, PP-L153, and PP-L101 distinctively show that the holding pressure can act longer at lower molecular weight. The time between the pressure peak and pressure drop becomes longer as molecular weight increases. The holding pressure was set equal to the injection pressure during injection moulding of the PP samples. Hence, also here we see that crystallisation has finished after 1 s.

As already mentioned above, the macromolecules are exposed to extreme shear rates in the direction of flow during cavity filling. As a result of the acting shear stress the macromolecules are oriented, but unloading the material leads to retardation of the orientation attributable to equilibrium conformation (e.g. coils or other energetically favourable molecular arrangements) and to a re-shearing. The ratio of the reversible shearing and the acting shear stress is defined as elastic compliance. The constant limit value at very low shear rates of compliance corresponds to the equilibrium compliance J_e^0.

By dividing the equilibrium compliance by the zero viscosity, the characteristic retardation time λ' is calculated according to eq. 6.17.

$$\lambda' = \eta_0 \, J_e^0 \tag{6.17}$$

with

$$J_e^0 = \lim_{\omega \to 0} \frac{G'}{G''^2} \tag{6.18}$$

The characteristic retardation time indicates the time for reducing elastic deformations. The characteristic retardation times of the PP samples are calculated based on the measured viscoelastic properties (see Chapter 5.2, Figure 5.8) at a temperature of 200°C. From Table 6.2, it is obvious that the characteristic retardation time of 19.3 s for the high molecular weight samples PP-L1600 is much higher than the characteristic retardation time of 0.3 s for the low molecular weight samples PP-L101. Therefore, in the case of PP-L1600, retardation of molecule orientation is about 60 times slower than in the case of PP-L101. Hence, it is to be expected for high molecular weight samples that preferred oriented structures, such as shish kebab, exist in the direction of flow.

Table 6.2: Characteristic retardation time of the synthesised PP series (T = 200°C)

Sample	J_e^0 *[Pa^{-1}]*	*η_0* [Pa·s]*	*λ' [s]*
PP-L1600	$2.98 \cdot 10^{-5}$	785 600	19.3
PP-L1120	$7.23 \cdot 10^{-5}$	123 370	6.6
PP-L833	$1.38 \cdot 10^{-4}$	35 030	4.5
PP-L462	$2.65 \cdot 10^{-4}$	7 470	1.7
PP-L361	$6.20 \cdot 10^{-4}$	2 580	1.5
PP-L320	$4.16 \cdot 10^{-4}$	2 690	1.2
PP-L244	$4.14 \cdot 10^{-4}$	1 080	0.4
PP-L153	$1.79 \cdot 10^{-3}$	190	0.3
PP-L101	$3.14 \cdot 10^{-3}$	110	0.3

J_e^0 = equilibrium compliance, η_0* = complex zero viscosity, and λ' = characteristic retardation time

6.2 Evaluation of injection-moulding process

The analysis of viscosity is valuable for classifying the influence of processing on possible polymer degradation. As already mentioned, the polymer is strongly mechanically and thermally stressed during processing, which can lead to a degradation reaction, coupled with reduction of molecular weight. As known and also shown in Chapter 5, zero viscosity depends on molecular weight according to eq. 5.5. Therefore, any potential polymer degradation can be analysed prior to the micro-injection-moulding process by studying zero viscosity on PP powder and, subsequent to processing, on micro dumbbell specimens.

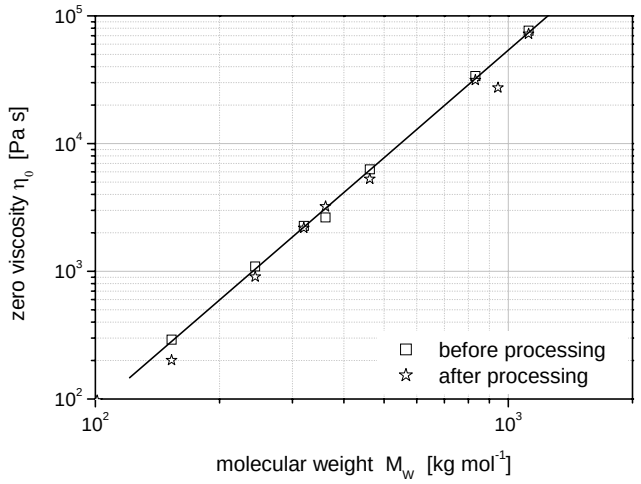

Figure 6.13: Zero viscosity versus average molecular weight of LP-PP, measured before processing on powder and after processing on micro dumbbell specimen (measurement temperature = 200°C)

Figure 6.13 shows zero viscosity (determined by applying the Carreau viscosity model) as a function of molecular weight, measured prior to and subsequently after the processing. A similar linear correlation between zero viscosity and molecular weight can be observed, so that polymer degradation during micro-injection moulding can be excluded. Therefore, this material characterisation of PP confirms the gentle processing provided by the newly developed micro-injection-moulding process.

6.3 Conclusion

The filling and solidification behaviour inside the mould during the manufacture of micro dumbbell specimens was studied. In particular, the shear rate during filling and the temperature gradient while cooling are key factors for developing the morphological structure inside the part. The shear rate was simulated using MPI flow analysis software. In contrast, the cooling behaviour of the polymer melt over the micro dumbbell specimens was calculated by solving the heat conductivity equation and by means of cavity pressure analysis.

Differences in shear rate transversely and parallel to the direction of flow of the molten polymer could be detected in relation to the molecular weight of the PP samples. Generally, the shear rate increases as the molecular weight increases up to a shear rate of $7.5 \cdot 10^5\ s^{-1}$ for the high molecular weight samples PP-L1600. However, shear rate strongly depends on part geometry. The shear rate in the parallel zone of the micro dumbbell specimen is approximately twice as high as at the shoulder. Furthermore, when comparing the shear rate inside the micro dumbbell specimen with an eight times larger dumbbell specimen, using the same material (PP-L1600) and the same processing conditions, the shear rate of the micro dumbbell specimens is 750 times higher than for larger “standard” specimens. Both the inhomogeneous distribution of the shear rate and the different maximum shear rate cause different crystallisation processes and, finally, result in different morphologies and properties, depending on the molecular weight.

Analysis of solidification behaviour shows that the acting cooling rate is very high, so that polymer crystallisation is almost completed after 1 s. This is supported by the fact that the cavity pressure, which continuously measures the pressure on the surface of the part, achieves ambient pressure after 1 s. This can be obtained only when the linkage between the injection moulding machine and the cavity, as well as the part, is solidified, so that no more material can be pushed into the mould.

Moreover, the calculated characteristic retardation time, indicating orientation retardation time, is much higher when the molecular weight is higher. For example, PP-L1600 exhibits a characteristic retardation time of 19.3 seconds. Hence, a highly oriented structure inside the micro dumbbell specimen is expected for high molecular weight samples. In particular at positions with high shear rates, such as in the straight parallel zone and close to the wall, oriented structures are to be anticipated.

Comparatively analysis of zero viscosity of PP powders and micro dumbbell specimens confirms that the polymer does not become degraded during injection moulding, in spite of high shear rates.

7 STRUCTURE AND MORPHOLOGY

The acting flow and cooling conditions prior to and during solidification of the molten polymer influence the crystallisation and govern, therefore, the formation of the final structure.[36,55,56,150-156] For example, when high flow and high cooling rates exist, oriented structures, such as shish kebab or lamellae row structures, are preferably formed. In addition, Varga et al.[73,81] found that the supermolecular structure formed in the vicinity of the sheared layer is generally rich in the β-modification of iPP. Moreover, Jay et al.[36] observed an increase in orientation as the molecular weight increases. One reason for this is an enhancement of the nucleation and the growth rate as a function of the molecular weight.

In contrast, spherulites are formed under quiescent crystallisation conditions. This type of superstructure depends also on the molecular weight. Woodward[84] studied the structure of fractionated polyethylene (PE) by means of TEM and found that isothermal crystallisation gives axialites at low molecular weights, sheet-like structures at moderate molecular weights, spherulites at moderate to high molecular weights and randomly positioned lamellae at very high molecular weights. A similar observation in the change of microstructure of PE samples, depending on the molecular weight was found by Michler[41]. He published a study on the influence of molecular weight on morphology by conventional and high-voltage transmission electron microscopy and found that with increasing molecular weight there is a change in morphology, from sheaf-like structures and banded spherulites to small bundles of parallel lamellae or randomly distributed lamellae.

Injection-moulded samples from semi-crystalline polymers usually show a multi-layered morphology. The composition of the morphology is finally responsible for the end-use properties of plastic parts. Parts with a thick skin layer show improved impact strength in association with poor dimensional stability. In contrast, highly crystalline samples possess high stiffness and strength, but tend to be brittle.

Furthermore, previous studies[164,165] on the influence of the injection-moulding process on the morphology and end-use properties of parts from polyformaldehyde (POM) and poly(butylene terephthalate) (PBT) show that variations of the injection speed, melt temperature, mould temperature and residence time of the melt inside the plasticising unit of the injection moulding machine affect the formation of the skin layer. The higher the injection speed, the thicker the skin layer of POM parts. In addition, the impact strength increases as the skin layer becomes thicker. It was also found that a long residence time leads to inhomogeneous morphology and, as result, to brittle PBT parts.

The morphology of injection-moulded semi-crystalline polymers is described mostly by different layers, across the wall thickness.[84,166] Generally, a 3-layered structure, consisting of an oriented skin layer, an intermediate layer (shear-induced structure) and a highly crystalline core can be observed in polarised light. Also structures with 6 or 7 layers can be observed microscopically.[43,167]

The skin layer is characterised by a high degree of orientation and lack of crystalline structures, such as spherulites. When hot melt is injected into the mould, the polymer freezes immediately upon contact with the cold cavity wall. Therefore, insufficient time exists for flow-induced orientations to relax. The molecule chains are orientated overwhelmingly in the direction of flow.[34,39] Typically, a well-formed spherulitic structure can be found in the core, which usually is totally unoriented.[168] Between the skin layer and the isotropic core exist several intermediate layers (shear and oriented layers).

Nowadays, it is well-known that the action of high shear rate and shear stress during filling results in orientation of macromolecules and hence in oriented morphological structures.[43,73,81,153,166] Keller et al.[49] have developed a model for the formation of structure during crystallisation under shear stress. They assume that row-nucleated columnar structures are formed, on which disc-shaped lamellar crystals grow under the acting shear stress. This type of crystallisation results in the so-called shish kebab structure. Shish kebab structures possess high stiffness and strength in and perpendicular to the direction of flow, due to their unique structures with several stretched macromolecules and circular folded lamellae. Furthermore, Keller et al. have found that the number of shish kebab structures increases with the increasing shear stress, while their diameter is reduced. As a result, an increasingly oriented fibrillar structure is formed.

In general, the formation of skin-core morphology is strongly affected by molecular structure and processing conditions.[39,52,53,169] In this part of the thesis, the influence of molecular structure on morphology is studied by means of light microscopy, scanning electron microscopy, transmission electron microscopy, wide-angle x-ray scattering, and differential scanning calorimetry studies. In addition, the entanglement molecular weight of PP is estimated, based on its viscoelastic behaviour.

7.1 Evolution of entanglement molecular weight

The average number of entanglements per chain, the so-called entanglement molecular weight ME, can be calculated based on the plateau modulus G_N^0, which reflects the molecular architecture of polymers. The ME is defined as the molecular weight between adjacent temporary entanglement points and can be determined by means of dynamic oscillation rheometry according to the following equation:

$$ME = \frac{\rho RT}{G_N^0} \qquad (7.1)$$

where R is the universal gas constant (R = 8.314 J mol^{-1} K^{-1}), and ρ is the density of the polymer at temperature T, at which the plateau modulus was measured.

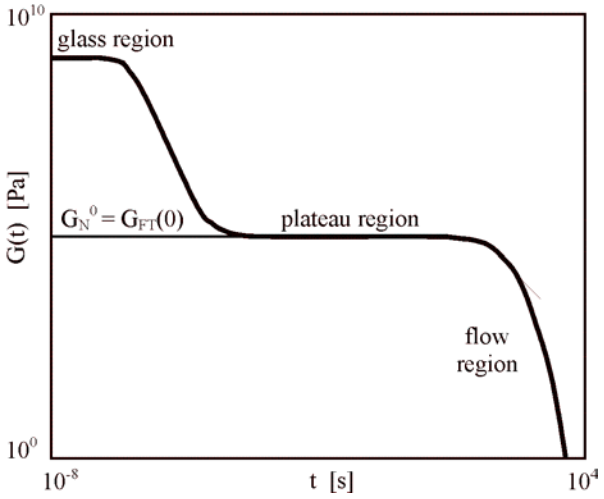

Figure 7.1: Schematic representation of relaxation function G(t) for a semi-crystalline polymer.

However, in the case of polyolefins, it is often difficult to measure the storage modulus G'(υ) and loss modulus G''(υ) of the plateau zone and, therefore, it is usually impossible to determine a significant onset of the plateau zone. For this reason, scanty information on plateau modulus analysis by means of rheological investigations of polyolefins is reported in literature. Recently, Eckstein et al.[170] discussed the advantage and disadvantage of several methods for determining plateau modulus by measuring the viscoelastic behaviour of polymer melts, especially of high molecular weight polymers. Primarily, plateau modulus can be experimentally obtained by linear extrapolation of the flow transition modulus G_{FT} to zero time, as shown schematically in Figure 7.1. However, using this method the extrapolation of the G_{FT} is difficult, because of the deficiency of an articulate transition from the plateau region to the glass region.

Moreover, the plateau modulus can be obtained from the frequency where the minimum of the loss tangent tan δ is located.[171,172]

$$G_N^0 = G'(\upsilon)_{\tan\delta_{min}} \qquad (7.2)$$

Experimentally, in the case of isotactic PP within only a small temperature range, it is possible to measure the viscoelastic properties of the molten polymer. This temperature range is limited to low temperatures since crystallisation begins at about 125°C and degradation can cause a failure of measurements at high temperatures, although nitrogen is used to avoid oxidative degradation.

However, the rheology of polymers largely depends on temperature. Thus the storage (elastic, solid-like) modulus G', and the loss (flow, liquid-like) modulus G'', can be superimposed by horizontal shifting along the frequency axis as described in eq. 7.3.

$$G\left(\upsilon\, a_T, T_0\right) = G\left(\upsilon, T\right) \qquad (7.3)$$

Using the Arrhenius equation, the horizontal shift factor a_T can be calculated as follows:

$$\log\, a_T = \frac{E_A}{2.303\,R}\left(\frac{1}{T} - \frac{1}{T_0}\right) \qquad (7.4)$$

where T_0 is the reference temperature, E_A is the activation energy of flow, and R is the universal gas constant.

Consequently, G' and G'' are analysable over a wide frequency range.

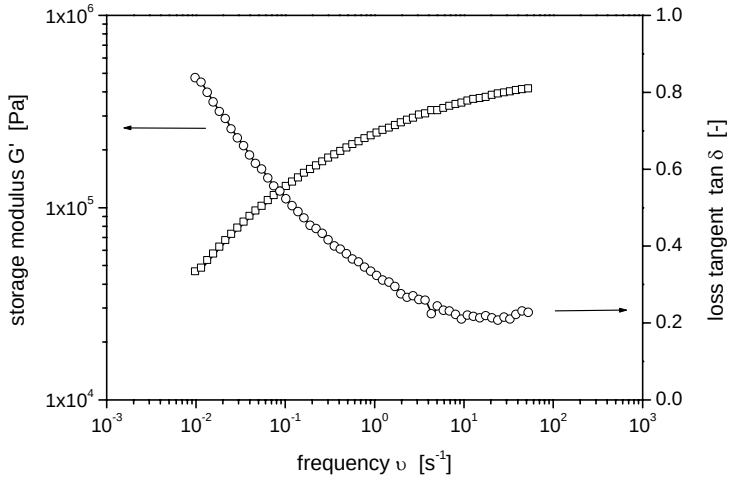

Figure 7.2: Master curve of storage modulus and loss tangent as a function of frequency for PP-L1600 at a reference temperature of 200°C

Figure 7.2 shows the master curve of the storage modulus G' and the loss tangent tan δ as a function of frequency for PP-L1600, shifted by means of the Arrhenius equation. A minimum of the loss tangent tan δ at 35 s^{-1} is clearly visible, and as a result, the plateau modulus of $4.5 \cdot 10^5$ Pa can be determined. By means of eq. 7.1 an entanglement molecular weight ME of 6 730 $g \cdot mol^{-1}$ is calculated.

Table 7.1: Number of entanglements per chain of the LP-PP series

Sample	*MW* *[kg mol^{-1}]*	*MW/MN* *[-]*	*MW/ME* *[-]*
PP-L1600	1 600	na	238
PP-L1120	1 120	6.4	166
PP-L833	833	6.6	124
PP-L462	462	7.2	69
PP-L361	361	6.8	54
PP-L320	320	6.8	48
PP-L244	244	7.3	36
PP-L153	153	7.3	23
PP-L101	101	na	15
PP-M256	256	5.7	na
PP-B445	445	6.9	na

ME = entanglement molecular weight, MN = number average molecular weight, MW = weight average molecular weight, MW/MN = molecular weight distribution, MW/ME = numbers of entanglements per chain, na = not available

This result is in strong agreement with data found in literature. Eckstein et al.[170], for instance, recently presented an entanglement molecular weight value of 6 900 $g \cdot mol^{-1}$ for isotactic LP-PP with a molecular weight of 871 $kg \cdot mol^{-1}$ and a polydispersity of 2.4, as well as a value of ME for atactic PP of 7 050 $g \cdot mol^{-1}$. They found that isotacticity is one of the most important parameters governing the entanglement density in PP. Using the analysed ME for iPP, the number of entanglements per chain can be calculated by dividing the molecular weight of the samples by the entanglement molecular weight. Table 7.1 presents the number of entanglements per chain for the PP series. There is a significant difference between the value of MW/ME of the high molecular weight samples and the low molecular weight samples; in the case of PP-L1600 there are 238 entanglements per chain against 15 for PP-L101, although these entanglements and tie molecules are the load-bearing elements between the crystallites when stress is applied.

7.2 Differential scanning calorimetry

The melting behaviour and structure of injection-moulded LP-PP micro dumbbell specimens were characterised by means of their melting point, crystallinity and lamellar thickness distribution, using DSC. In addition, two commercially-available industrial samples, synthesised in liquid phase, were studied comparatively. Furthermore, the injection-moulded LP-PP micro dumbbell specimens, which were annealed at temperatures of 100°C and 140°C, were additionally analysed by DSC.

7.2.1 Crystalline fraction

The first heating scans for the untreated series of injection-moulded LP-PP samples are shown in Figure 7.3 and the corresponding first cooling scans are presented in Figure 7.4. In addition, the calorimetric parameters determined from the thermograms for unannealed and annealed injection-moulded LP-PP samples are collected in Table 7.2.

The dashed line in Figure 7.3 at 165°C serves to highlight the variation in the peak maximum (representing the melting point) with changing molecular weight. The DSC thermograms show a characteristic melting behaviour of the monoclinic α-form of crystals in isotactic PP with a monomodal peak at a temperature of about 162 to 165°C.[139-143] All samples with a molecular weight of higher than 244 kg·mol^{-1} (up to 1 600 kg·mol^{-1}) exhibit no significant difference in melting point, but the two samples with low molecular weight (below 153 kg·mol^{-1}) exhibit a melting point at the lower temperature of 162 °C.

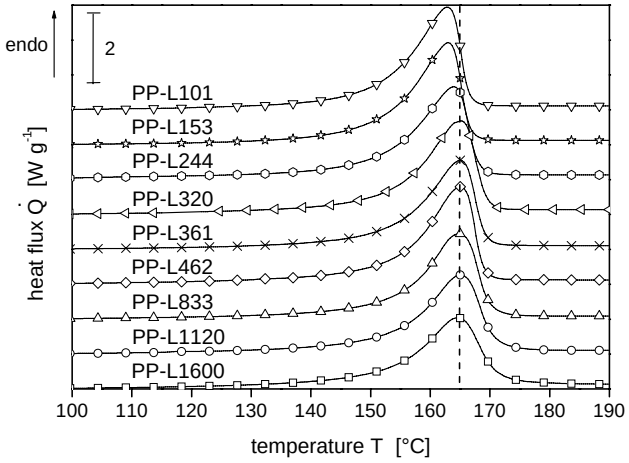

Figure 7.3: DSC scans of the unannealed injection-moulded LP-PP series with various molecular weights (1st heating, heating rate: 20 K/min, N_2 atmosphere)

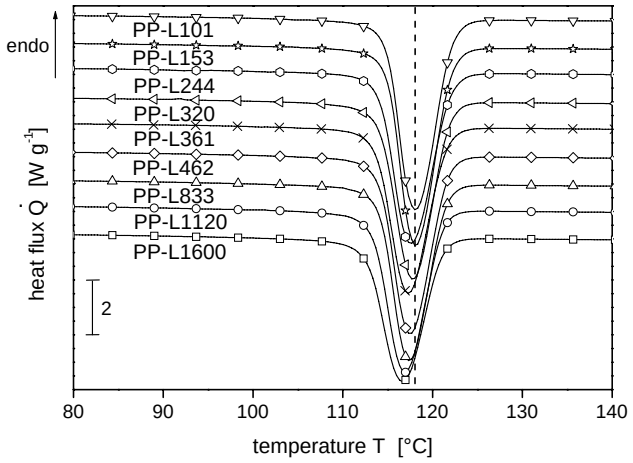

Figure 7.4: DSC scans of the unannealed injection-moulded LP-PP series with various molecular weights (1st cooling, cooling rate: 20 K/min, N_2 atmosphere)

Moreover, there are notable differences in crystalline fraction as the molecular weight of the samples changes. As expected, crystallinity sinks from 50 % in the case of PP-L101 to 41 % for PP-L1600. The reason for this is the presence of a large number of entanglements per chain for the higher molecular weight polymers, as determined in Chapter 7.1. The entanglements lead to high viscosity in the long polymer chains, so that the high molecular weight polymers are hindered from forming crystals and causing, furthermore, lowered crystallisation temperature. From Figure 7.4 it is clearly recognisable that the crystallisation peak shifts slightly to a lower temperature as the molecular weight increases; the peak maximum varies from 119.4°C (PP-L101) to 117.7°C (PP-L1600).

In addition, the crystallinity of the annealed injection-moulded PP micro dumbbell specimens is counterable higher as the annealing temperature increases. In the case of the high molecular weight sample PP-L1600, even an increase in crystallinity of 11 % occurs after annealing at a temperature of 140°C for 1 hour. In contrast, the crystallinity of all other samples increases by approx. 5 to 7 % as a result of an improvement in crystalline structure during thermal treatment.

The crystallinity of the industrial samples, PP-M256 and PP-B445, are similar to the crystallinity of the micro dumbbell specimens, PP-L244 and PP-L462, having almost the same molecular weights. However, the melting temperatures of the industrial samples are approx. 3°C lower than those of the comparable LP-PP samples. The reason for this might be an unknown additive formulation in the commercially-available industrial samples.

As shown in Figure 7.3 the melting endotherms of the higher molecular weight samples are broader than those of the lower molecular weight samples. Furthermore, the endset temperature becomes lower as the molecular weight decreases, also in the case of thermally treated samples. The beginning of the melting of crystalline fraction occurs at a temperature of about 120°C. There, the small crystalline lamellae begin to melt and continue to melt as the temperature increases. At higher temperature the thicker and bigger lamellae start to melt completely. Hence, the melting peak characterises the distribution of the crystalline fraction inside the polymeric sample, as presented schematically in Figure 7.5. Consequently, endothermic behaviour in the melting range can be considered to analyse and describe lamellae thickness and distribution.

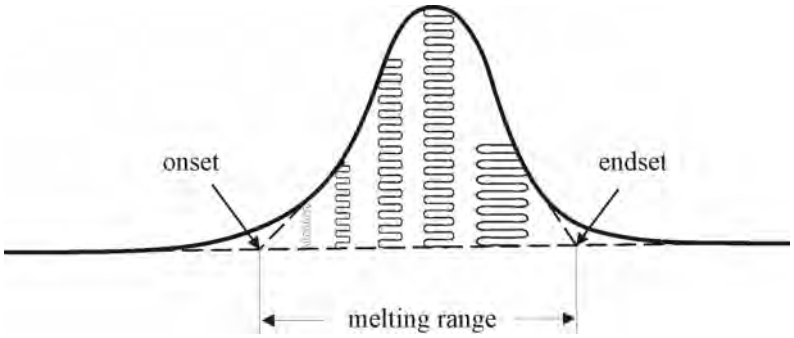

Figure 7.5: Schematic drawing of the melting zones of crystalline lamellae

Table 7.2: Thermal properties and crystallinity of unannealed and annealed injection-moulded LP-PP samples, determined by DSC

Sample	ΔH_m [J g^{-1}]	X_c [%]	T_m [°C]	T_{me} [°C]	T_c [°C]	$\Delta H_{m,100}$ [J g^{-1}]	$X_{c,100}$ [%]	$T_{m,100}$ [°C]	$T_{me,100}$ [°C]	$T_{c,100}$ [°C]	$\Delta H_{m,140}$ [J g^{-1}]	$X_{c,140}$ [%]	$T_{m,140}$ [°C]	$T_{me,140}$ [°C]	$T_{c,140}$ [°C]
PP-L1600	81.2	41	164.7	172.5	117.7	92.3	47	165.4	173.5	117.7	101.3	52	165.5	175.4	114.5
PP-L1120	88.9	45	165.0	171.1	118.1	93.1	48	165.3	172.1	117.7	98.2	50	165.3	171.3	118.1
PP-L833	88.9	45	165.3	170.7	118.9	92.7	47	165.6	171.6	116.0	101.4	52	164.9	171.8	118.4
PP-L462	92.9	47	165.3	170.2	118.4	96.6	49	165.5	169.9	118.8	102.8	52	165.2	169.6	118.5
PP-L361	90.0	46	164.9	169.8	118.1	94.8	48	164.5	169.1	117.5	105.1	54	164.8	169.0	117.2
PP-L320	94.3	48	165.2	170.3	118.4	96.7	49	163.6	169.0	119.6	106.0	54	165.1	169.3	119.6
PP-L244	94.5	48	163.9	168.7	118.5	95.8	49	163.2	168.1	119.2	107.1	55	163.2	167.9	118.5
PP-L153	95.8	49	162.5	166.9	119.4	94.2	48	162.9	167.5	118.5	112.2	57	161.9	166.5	119.3
PP-L101	97.1	50	162.5	166.8	119.3	100.5	51	162.8	167.3	119.5	108.8	56	162.6	167.2	120.3
PP-M256	91.2	47	162.3	167.0	111.3	90.1	46	163.0	167.2	111.3	102.6	52	162.7	167.1	112.0
PP-B445	88.9	45	161.1	166.2	110.7	89.6	46	161.1	166.2	111.4	96.0	49	160.7	166.2	111.7

ΔH_m = melting enthalpy, X_c = crystallinity, T_m = melting temperature, T_{me} = endset melting temperature, T_c = crystallisation temperature, 100 = annealing at temperature of 100°C for 1 hour, and 140 = annealing at a temperature of 140°C for 1 hour

7.2.2 Evolution of the lamellae thickness and lamellae thickness distribution

According to the relationship stated by Thomson and Gibbs, average lamellar thickness can be estimated by relating melting temperature to lamellae thickness of a polymer as follows:

$$L = \frac{2\varphi_e T_m^0}{\Delta H_f \left(T_m^0 - T_m\right)} \tag{7.5}$$

where L is the lamellae thickness (longitudinal dimensions of the crystal), T_m is the melting temperature of the investigated polymer, T_m^0 is the equilibrium melting temperature of α-phase iPP (= 464 K [109]), ΔH_f is the melting enthalpy of a perfect crystal (= 196 J·cm^{-3} [109]), and φ_e is the free surface energy of the end faces at which chains fold (= 102.9 J·cm^{-2} [109]).

Based on eq. 7.5, the thickness distribution of crystalline lamellae can by related to the form of the DSC curve by the following equation:

$$f(L) = \frac{1}{M}\frac{dM}{dL} \tag{7.6}$$

where crystalline mass dM in a temperature range between T and T+dT can be described as follows:

$$dM = \frac{dE}{dT}\frac{dT}{\Delta H_f}\rho_c \tag{7.7}$$

with

$$\frac{dM}{M} = \frac{dE}{dT}\frac{dT}{\Delta H_f M}\rho_c \tag{7.8}$$

and

$$dT = dL\frac{\left(T_m^0 - T_m\right)^2}{T_m^0}\frac{\Delta H_f}{2\varphi_e} \tag{7.9}$$

Combining eq. 7.5, 7.8, and 7.9 finally results in eq. 7.10.

$$\frac{1}{M}\frac{dM}{dL} = \frac{\frac{dE}{dT}\left(T_m^0 - T_m\right)^2 \rho_c}{2\varphi_e T_m^0 M} \tag{7.10}$$

with

$$\frac{dE}{dT}\frac{1}{M} = \frac{\dot{Q}}{\dot{H}} \tag{7.11}$$

where ρ_c is the density of the crystal phase (= 0.936 g·cm^{-3} [109]), dE is the energy necessary to melt the crystalline mass dM in the temperature range between T and T+dT, $\dot{H}$ is the heating rate for DSC measurements, and $\dot{Q}$ is the measured heat flux.

The heat flux used here is the total heat flux on the DSC scan subtracted by a linear baseline.

This relationship of the lamellae thickness distribution linked to DSC measurements is described in greater detail by Romankiewicz and Sterzynski.[173]

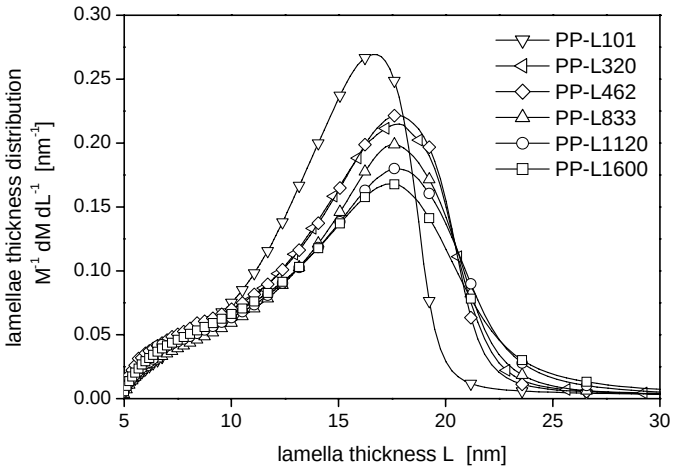

Figure 7.6: Lamellae thickness distribution of the unannealed LP-PP series with various molecular weights

Figure 7.6 shows the calculated lamellae thickness distribution of the untreated series of injection-moulded LP-PP samples based on molecular weight. In addition, Table 7.3 presents the average lamellae thickness calculated from the melting temperature, as well as the maximum lamella thicknesses determined from the endset temperatures of the unannealed and the annealed injection-moulded PP samples. From Figure 7.6 it is obvious that especially the unannealed samples of low molecular weight (PP-L101 and PP-L244) exhibit thinner lamellae with narrow distribution. In contrast, the other samples (molecular weight from 320 to 1 600 kg·mol^{-1}) exhibit increasing lamellae thickness and distinctive broadening of lamella thickness distribution as the molecular weight increases. Particularly, the thickness of the thicker lamellae (maximum lamella thickness L_{max}) obtained from the evaluation of the endset temperature increases drastically with increasing molecular weight. These phenomena have been observed in the past[174,175] and are a result of the reduction in crystallisation rate with increasing molecular weight due to entanglements and viscosity effects, which can be verified above.

Moreover, lamella thickness and, of course, crystallinity also increase due to the increasing mobility of the polymer chains when injection-moulded samples are thermally treated at elevated temperature. Non-crystalline fractions continue to crystallise slowly to improve the perfection of their crystals inside the superstructure. This effect occurs especially for polymers cooled quickly below glass transition temperature (for example during the injection-moulding process), thereby depressing the crystallisation process.

Table 7.3: Lamella thickness of unannealed and annealed injection-moulded LP-PP samples

Sample	L_m *[nm]*	L_{max} *[nm]*	$L_{m,100}$ *[nm]*	$L_{max,100}$ *[nm]*	$L_{m,140}$ *[nm]*	$L_{max,140}$ *[nm]*
PP-L1600	18.5	26.3	19.0	27.8	19.1	31.2
PP-L1120	18.7	24.5	19.0	25.8	19.0	24.7
PP-L833	19.0	24.0	19.2	25.1	18.7	25.4
PP-L462	19.0	23.4	19.1	23.1	18.9	22.8
PP-L361	18.7	23.0	18.4	22.2	18.6	22.1
PP-L320	18.9	23.5	17.8	22.1	18.8	22.5
PP-L244	18.0	21.8	17.5	21.3	17.5	21.1
PP-L153	17.1	20.2	17.3	20.7	16.7	19.9
PP-L101	17.1	20.1	17.3	20.6	17.2	20.5
PP-M256	17.0	20.3	17.4	20.5	17.2	20.4
PP-B445	16.3	19.6	16.3	19.6	16.1	19.6

L_m = average lamella thickness, L_{max} = maximum lamella thickness, 100 = annealing at a temperature of 100°C for 1 hour, and 140 = annealing at a temperature of 140°C for 1 hour

7.3 Polarisation microscopy

Figure 7.7 shows the optical cross-section micrographs of the unannealed injection-3moulded LP-PP specimens taken transverse to the direction of flow and magnified 200 times.

An oriented skin layer and a spherulitic structure in the core are clearly obvious on all samples, with the exception of the PP-L1600 sample with the highest molecular weight. In addition, the shear layer can also be partially recognised in the cross-sections of the samples, but is most distinctive in the case of the lower molecular weight samples, such as PP-L101. Between the skin layer, the shear layer, and the core there are intermediate layers, which can be seen more clearly in the SEM images.

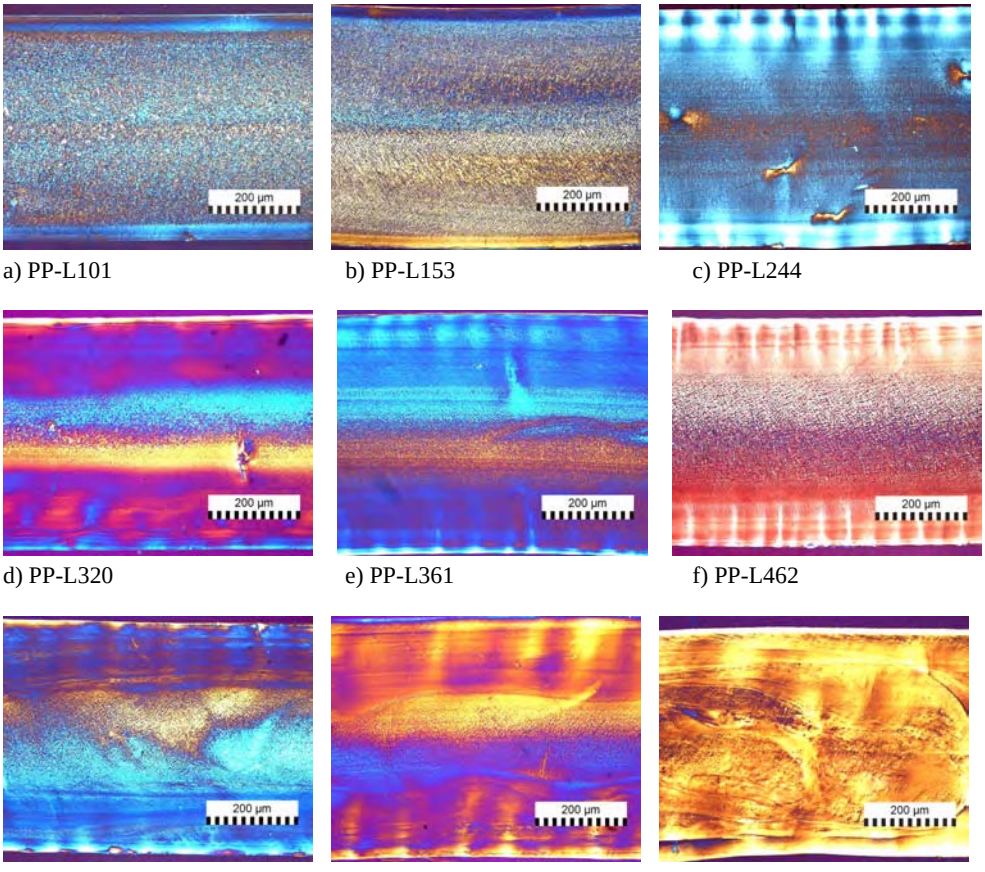

a) PP-L101 b) PP-L153 c) PP-L244

d) PP-L320 e) PP-L361 f) PP-L462

g) PP-L833 h) PP-L1120 i) PP-L1600

Figure 7.7: Optical micrographs of cross-sections of unannealed injection-moulded LP-PP samples with various molecular weights viewed in cross polarisation and magnified 200 times.

The lower molecular weight samples exhibit very thin skin layers with distinctive crystalline core regions. In contrast, the cross-sections exhibit a reduction in the spherulitic core and a considerably more inhomogeneous structure as the molecular weight of the PP samples increases. It can be recognised more clearly from Figure 7.8 that the oriented skin layer increases the more the molecular weight increases. An increase in skin layer thickness from a minimum of 30 µm for PP-L101 to a maximum of 170 µm for PP-L1600 is visible, which in the case of the high molecular weight PP-L1600 samples, makes up almost 70 % of the overall cross-section (total thickness = 500 µm). The reason for this is the high viscosity of the high molecular weight PP; the long macromolecules are hindered from crystallising to spherulites in the time available, so that no spherulitic structure is visible at all, even in the core. However, oriented crystalline structures with dimension less than the resolution level of the optical microscopy used, are present, as observable in the TEM pictures (see Figure 7.12).

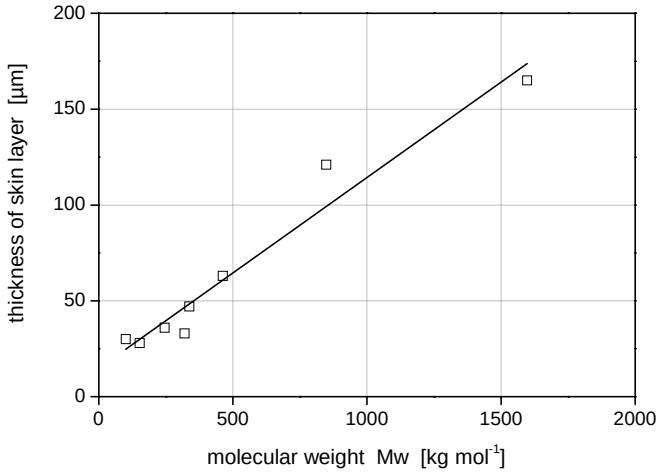

Figure 7.8: Dependence of skin thickness on molecular weight for unannealed injection-moulded LP-PP samples

A more highly oriented morphology is to be expected for the PP sample of the highest molecular weight, which comes from the fact that the injection speed is constant during processing, although the viscosity increases as the molecular weight increases and, in consequence, the shear stress, particularly on the cavity wall, increases too. The appearance of highly oriented layers can be observed by the existence of partial delamination of the layers in the case of PP-L1600.

Furthermore, 'temperature rings' can be observed on the PP samples PP-L833. As is known, when hot polymer melt comes into contact with the cavity wall during the filling procedure, the polymer solidifies and orientates abruptly and, as a result, a non-crystalline layer is formed. A similar process occurs more or less abruptly, when the flowing hot melt

hits an already crystallised layer. Consequently, intermediate layers appear between the “frozen” layer and the slowly crystallising polymer. This is usually the result of the presence of high shearing, which causes additionally a local temperature rise in the flowing melt, thereby inducing temperature differences inside the cavity.

However, when melting PP powder PP-L1600 between two glass plates and subsequently crystallising the quiescent molten polymer isothermally, classic spherulitic superstructures are formed. The development of the superstructure was observed while crystallising at a temperature of 130°C using a hot stage coupled with a polarisation microscope. Figure 7.9 shows the optical micrographs, depending on the crystallisation time. As a result, it is clearly visible that the high molecular weight sample PP-L1600 crystallises preferably to α-modified spherulites under isothermal and quiescent conditions, when sufficient time is available.

In addition, from Figure 7.9 a spherulite growth rate of approx. 20 $\mu m \cdot min^{-1}$ can be determined. This result is in strong agreement with data found in literature.[173]

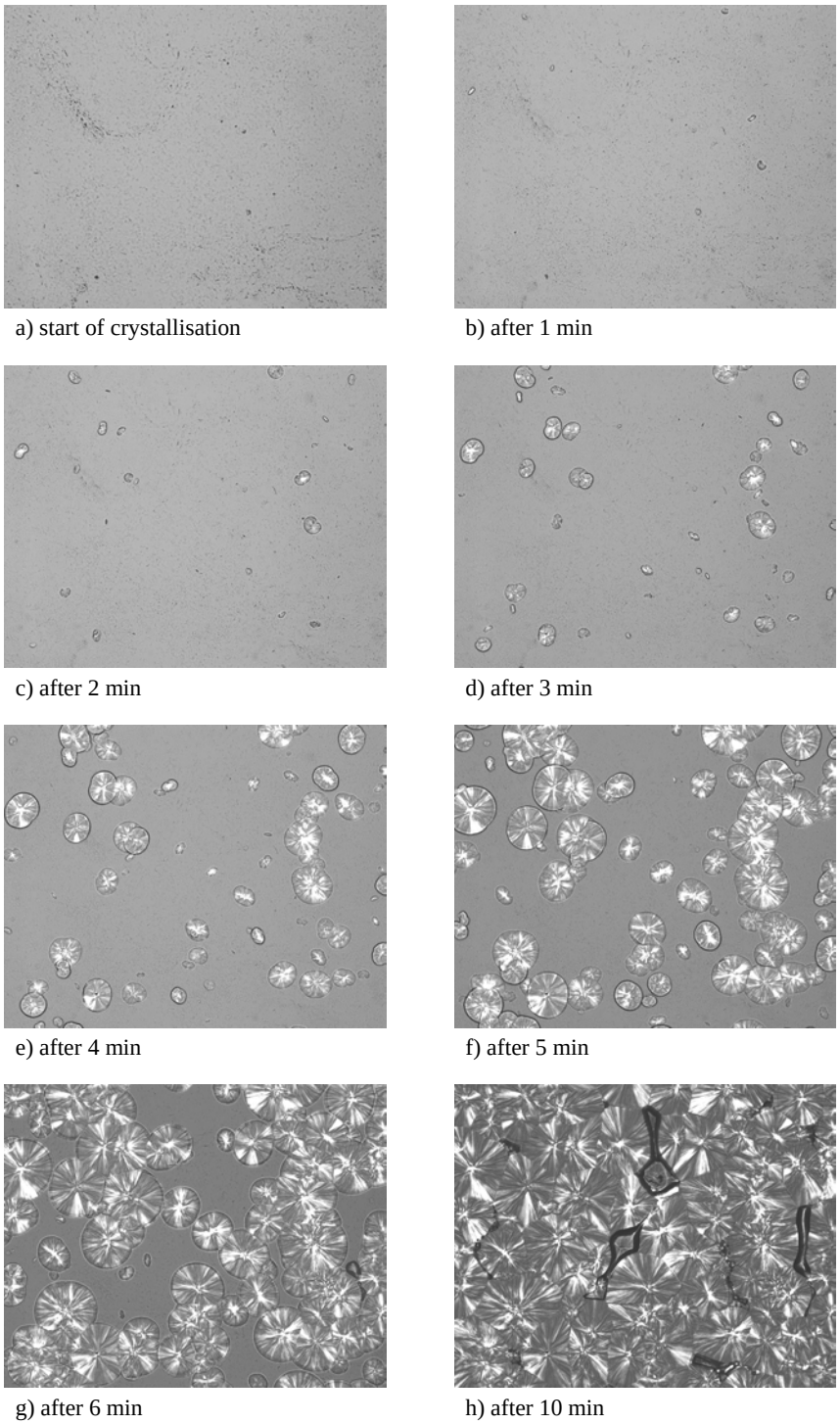

a) start of crystallisation
b) after 1 min
c) after 2 min
d) after 3 min
e) after 4 min
f) after 5 min
g) after 6 min
h) after 10 min

Figure 7.9: Growing of spherulites under isothermal and quiescent conditions at a crystallisation temperature of 130°C; sample used for analysis was PP powder PP-L1600

7.4 Scanning electron microscopy

Figures 7.10 and 7.11 present the scanning electron micrographs of the two samples PP-L320 and PP-L833. The investigations were performed on the skin and core area of the moulded PP samples at the small, parallel zone of the dumbbell, as well as at the shoulder.

Both samples exhibit layered structure, as previously suggested from the microscopic investigations in cross-polarised light. For example, several separate layers can be observed in Figure 7.11c – thin skin layer, shear layer, fibre-like layer, fine-grained layer, intermediate layer and spherulitic core – which are different in their orientation and homogeneity. The fibre-like layer exhibits extended parallel shish kebab structures lying ordered in the direction of flow, which can be confirmed by TEM analysis. The visible intermediate layer is mainly caused by strong local temperature differences.

When comparing Figures 7.11c and 7.11d, the differences are obvious in several layers along the micro dumbbell specimen. Within the shoulder of the specimen, the oriented skin layers with a thickness of between 100 to 150 µm are smaller than the skin layers of the parallel zone of the specimens with a thickness of about 200 µm. However, in the centre of the sample, classic spherulitic structures can be observed all along the specimen length. The diameter of the spherulites is approx. 5 µm. Furthermore, the fibre-like layer is more clearly pronounced in the parallel zone, i.e., orientation is higher in the narrow area of the specimen.

PP-L320 also exhibits several different layers on the skin of the shoulder, but to a lesser extent than does PP-L833. The skin layer here is about 30 µm thick and corresponds with the results obtained from optical-microscopic analysis. In the centre of the shoulder there are also spherulites with diameters of about 5 µm, similar to those in PP-L833. Besides, highly oriented structures, which are homogenous on the overall cross section, occur in the parallel zone of the micro dumbbell specimen, although a spherulitic core is expected to be similar to that of the higher molecular weight sample PP-L833 and this would correspond with the results of the optical-microscopy investigation.

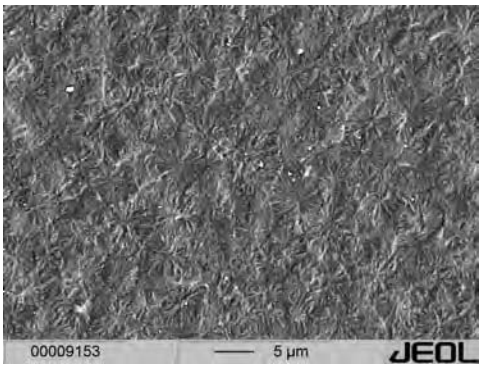

a) centre of the shoulder

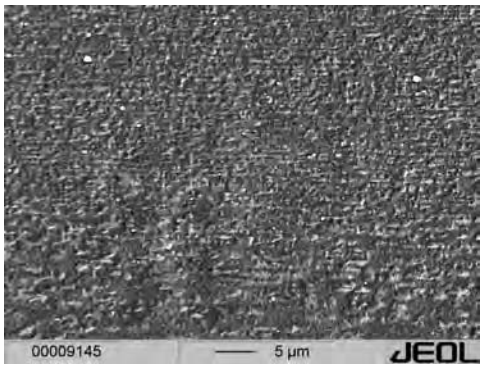

b) centre of the parallel zone

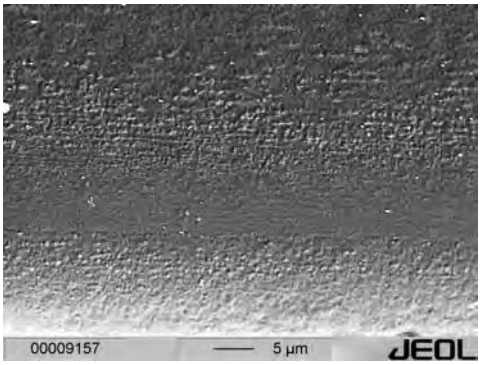

c) skin of the shoulder

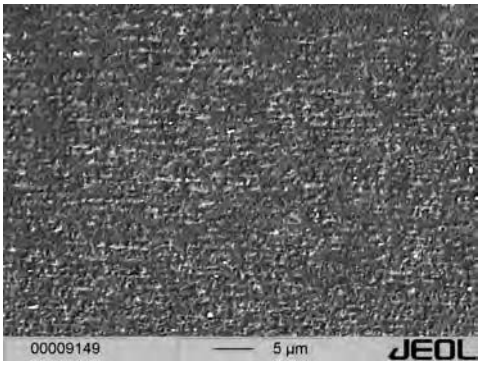

d) skin of the parallel zone

Figure 7.10: Morphology of injection-moulded micro dumbbell specimens from PP-L320 as observed by means of SEM. The investigated samples were taken from two different zones, a) and c) from the shoulder of the micro dumbbell specimen, and b) and d) from the parallel zone. Magnification is the same in all cases.

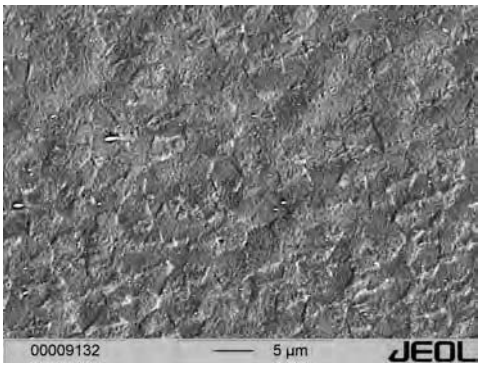

a) centre of the shoulder

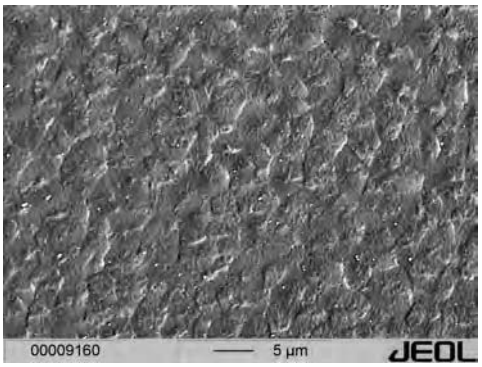

b) centre of the parallel zone

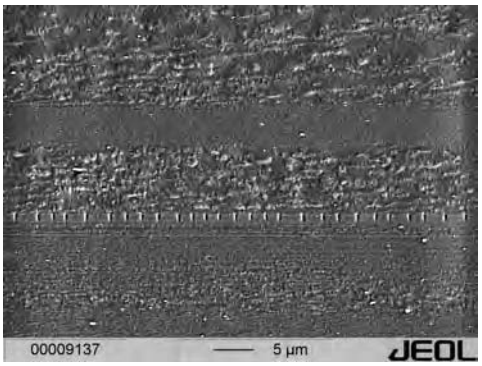

c) skin of the shoulder

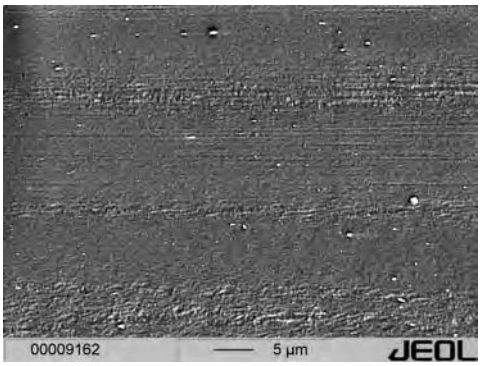

d) skin of the parallel zone

Figure 7.11: Morphology of injection-moulded micro dumbbell specimens from PP-L833 as observed by means of SEM. The investigated samples were taken from two different zones, a) and c) from the shoulder of the micro dumbbell specimen, and b) and d) from the parallel zone. Magnification is the same in all cases.

7.5 Transmission electron microscopy

Formation and order nanostructures (e.g. lamellae) as well as those of superstructures (e.g. spherulites, shish kebabs, etc.) can be analysed by means of transmission electron morphology (TEM), using ultra thin sections. The amorphous and crystalline structure is illustrated by different densities after contrasting by means of RuO_4. Crystalline fractions with high densities appear bright, whereas amorphous, less dense fractions are dark. Figure 7.12 illustrates TEM micrographs for a representative selection of untreated injection-moulded LP-PP samples, using two different magnifications. The samples for analysing were taken from the centre of the parallel zone (see Figure 3.6).

At higher magnification the PP samples with the lowest molecular weight, PP-L101, display long lamellae lying fairly straight perpendicular to the direction of flow, which is typical of injection-moulded semi-crystalline polyolefins.[169,176] The lamellae are tightly packed with few amorphous fractions between them. However, no superstructure can be recognised at lower magnification.

Sample PP-L320 exhibits an oriented superstructure even at low magnification, running in the direction of flow and indicating a shear-induced structure, which are in their nature either shish kebab or cylindrite (Figure 7.12c). However, the adjacent planar lamellae transverse to the direction of flow can also be observed at higher magnification; but in contrast to PP-L101, the visible lamellae are notably thicker.

PP-L462, PP-L833 and PP-L1120 exhibit a similar, highly oriented structure in the direction of flow with traversally aligned lamellae, like PP-L320. It seems that the number of oriented structure in direction of flow increases as the molecular weight increases. Furthermore, the thickness of the lamellae and the amorphous region between the lamellae increases as the molecular weight increases, which is obvious when comparing Figure 7.12f of PP-L462 and Figure 7.12h of PP-L833.

The structure observed on the highest molecular weight samples, PP-L1600, is very interesting. Even at low magnification, relatively thick lamellae-like structures lying parallel to the direction of flow can be recognised distinctively. This structure is different from the oriented structure in the cases of other samples shown. The thickness of this novel structure was determined at between 20 and 30 nm. Nevertheless, from Figure 7.12l it can be assumed that proper and short lamellae run transversely to the direction of flow here also.

However, when melting PP-L1600 between two glass plates and subsequently crystallising the completely molten material at a low cooling rate, the common, non-oriented monoclinic α-form of crystals can be observed. In Figure 7.13, sporadic cross-hatched structures are recognisable, which are known for having a spherulitic superstructure. Thereby, the main lamellae (mother lamellae) cross the lamellae (daughter lamellae) perpendicular to these main lamellae.[169] Hence, high molecular weight PP crystallises preferably to spherulites, under quasi isothermal and quiescent conditions when sufficient time is available.

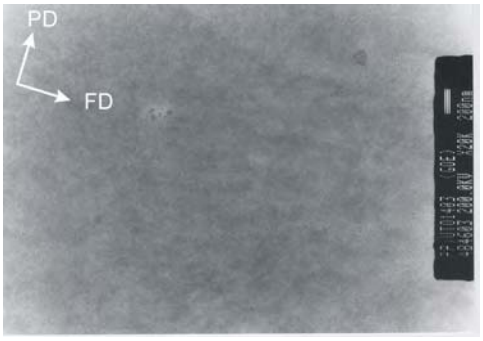

a) PP-L101 (20 000X)

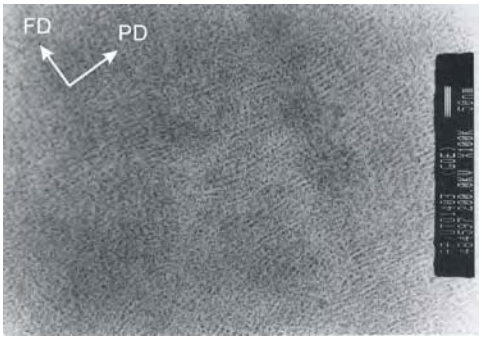

b) PP-L101 (100 000X)

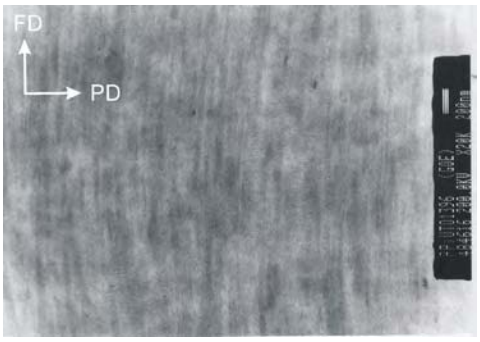

c) PP-L320 (20 000X)

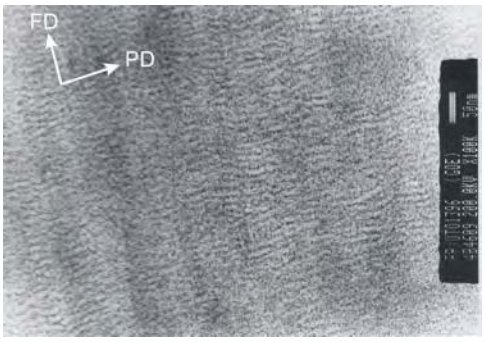

d) PP-L320 (100 000X)

e) PP-L462 (20 000X)

f) PP-L462 (100 000X)

Figure 7.12: TEM micrographs of a representative selection of injection-moulded PP micro dumbbell specimens with two different magnifications of 20 000X and 100 000X (FD = the direction of flow, PD = perpendicular to the direction of flow)

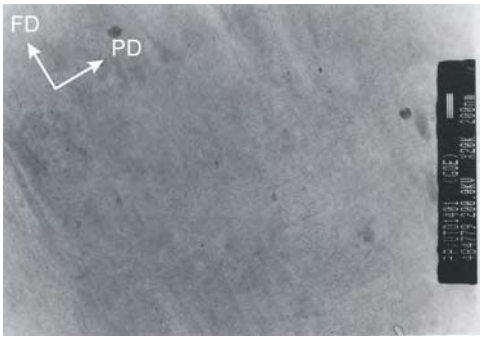

g) PP-L833 (20 000X)

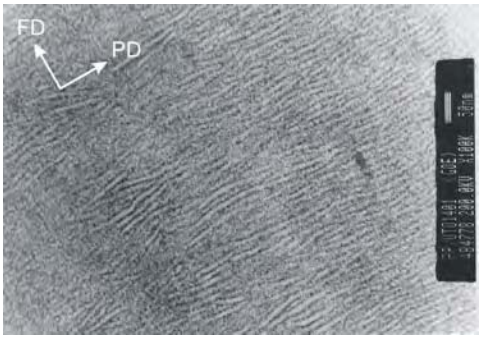

h) PP-L833 (100 000X)

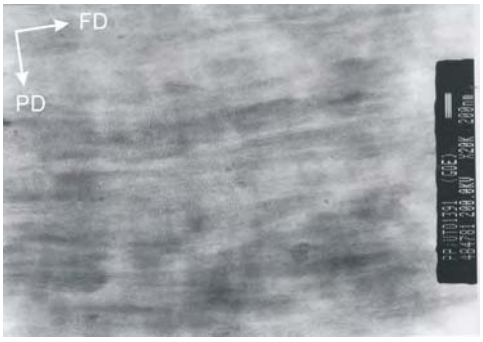

i) PP-L1120 (20 000X)

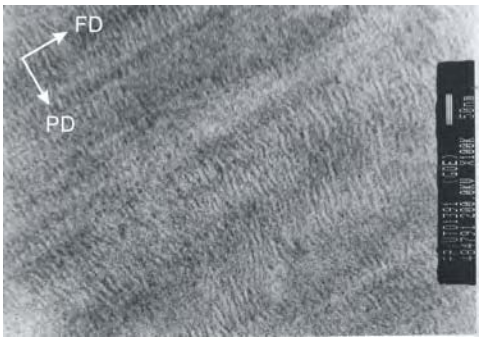

j) PP-L1120 (100 000X)

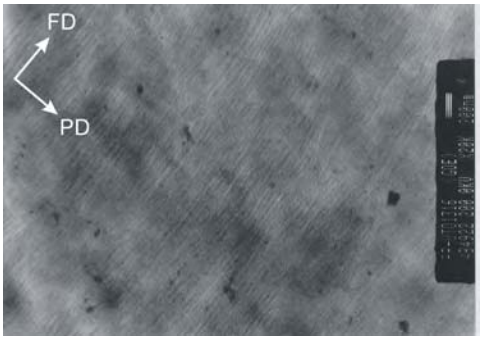

k) PP-L1600 (20 000X)

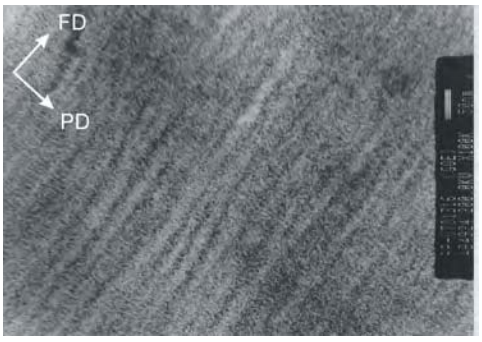

l) PP-L1600 (100 000X)

Continuation of Figure 7.12

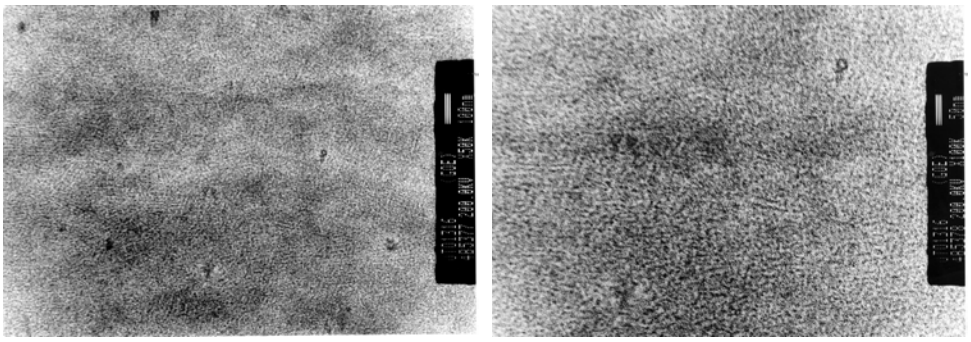

a) PP-L1600 re-crystallised (20 000X) b) PP-L1600 re-crystallised (100 000X)

Figure 7.13: TEM micrographs of the re-crystallised PP sample PP-L1600, using magnifications of 20 000X and 100 000X

Generally speaking, the low molecular weight injection-moulded samples possess fairly straight lamellae perpendicular to the direction of flow. Increasing the molecular weight leads to more highly oriented shear-induced structures. In most studies, the shear-induced structure is indicated as shish kebab. However, Varga[73] found that crystallisation under flow leads to a supermolecular structure of cylindric symmetry. These two types of supermolecular structures (shish kebab and cylindrite) differ in the dimension ratios of their building elements. Somani et al.[157] observed for shish kebabs a long period of kebabs between 60 and 70 nm, independent of the shear conditions, whereas the cylindrites are smaller in their dimensions and exhibit a size of 20 to 30 nm. Here, we found a maximum size of 30 nm for the oriented structure of PP-L1600; these results lead to the assumption that mainly cylindrical structures are present. However, WAXS studies (results shown in the next chapter) indicate that a shish kebab structure is more likely than cylindrical structure.

7.6 Wide-angle x-ray scattering

The WAXS images were taken from the centre position in the small parallel zone of the micro dumbbell specimens across the thickness of the samples in the direction of flow, and for PP-L1600 additionally from the shoulder of the micro dumbbell specimen.

Figure 7.14 shows the Debye pattern of a selection of the injection-moulded LP-PP. All samples exhibit similar Debye crystal reflection rings ((110), (040), (130) and (111), (041)), which originate from the α-form of iPP for highly oriented structures. This fact is consistent with the TEM micrograph (Figure 7.12), which shows that the parallel region of the micro dumbbell specimen is composed either of highly oriented shish kebabs or cylindrite.

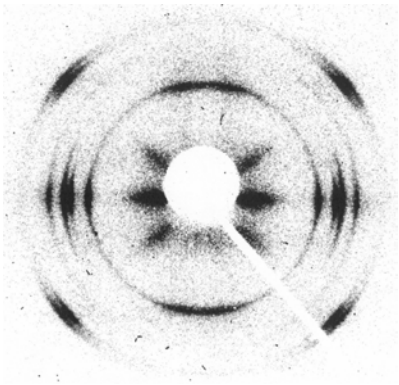

a) PP-L462 (parallel zone)

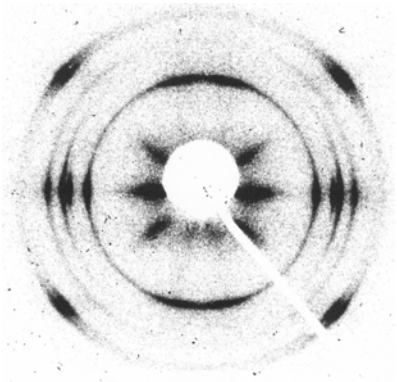

b) PP-L1120 (parallel zone)

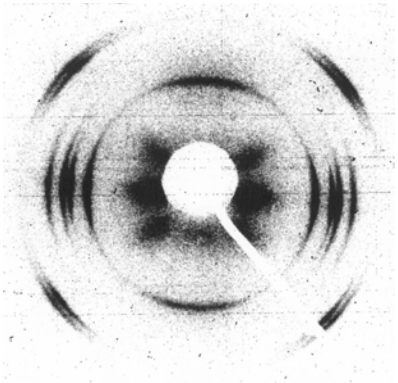

c) PP-L1600 (parallel zone)

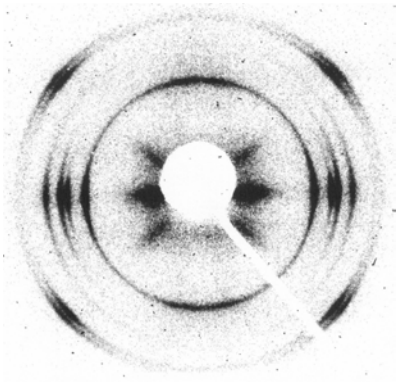

d) PP-L1600 (shoulder)

Figure 7.14: Wide-angle x-ray scattering patterns taken from different positions of a representative selection of the unannealed injection-moulded PP samples PP-L462, PP-L1120, and PP-L1600

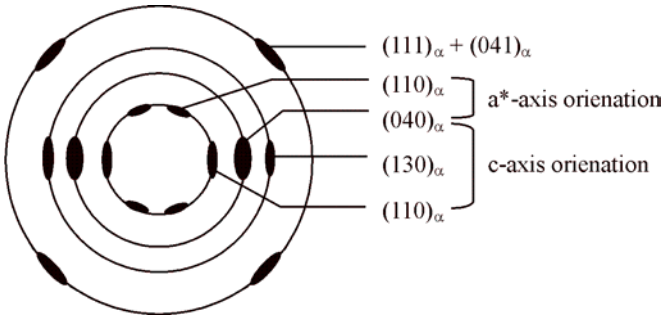

Figure 7.15: Schematic interpretation of the wide-angle x-ray scattering patterns after Fujiyama et al.[166]

Figure 7.15 illustrates schematically the wide-angle x-ray scattering patterns observed. As expected, 130, 110 and 040 reflections can be found for c-axis orientation of oriented columnar structures. However, an additional 110 reflection appears on the meridian. This reflection has been found by several authors[43,52,166] and is to be attributed to lamellae with lamellar axes almost parallel to the direction of flow. In fact, on extended-chain fibrillar crystals (i.e., shishs), grafting crystallisation causes the growth of secondary lamellae perpendicular to the direction of flow. These epitaxial oriented lamellae result in a*-axis orientation in flow. As a result, the Debye reflection 110 clearly indicates the existence of modified shish kebab structures.

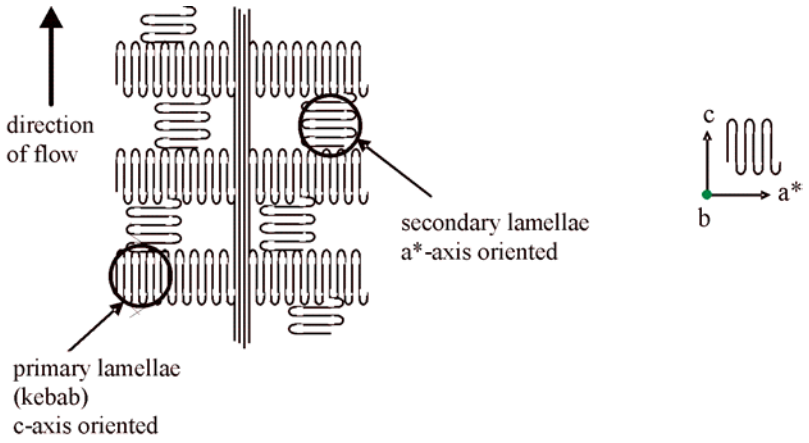

Figure 7.16: Shish kebab structure with epitaxial grafted secondary lamellae

Figure 7.16 shows the modified shish kebab structure schematically, taking the obtained results into consideration. In addition to the fibrous shishs and the disc-shaped crystalline lamellae (kebabs), a*-axis oriented crystallised lamellae pile epitaxially on the c-axis oriented shish kebab structure. Fujiyama et al.[166] found, that the a*-axis oriented lamellae are imperfect and rather greater in quantity than the c-axis oriented perfect lamellae.

7.7 Conclusion

The morphology of the injection-moulded LP-PP micro dumbbell specimens were studied, depending on their molecular weight.

From microscopical investigations it was found that superstructures differ across and along the micro dumbbell specimen. Those of inhomogeneous morphology can be best observed by polarisation and scanning electron microscopes. All samples exhibit more or less distinct skin-core morphology, typical of injection-moulded specimens from semi-crystalline polymers. In a total of six different layers, variations in superstructure and orientation are observed. Skin layers became thicker as molecular weight increases. In the case of PP-L1600 almost 70 % of the total micro dumbbell specimen thickness is composed of oriented layers, and no spherulitic core at all is noticeable. However, the morphology of the injection-moulded micro dumbbell specimens is dominated by a highly oriented shish kebab structure. In fact, the number of shish kebabs increases as the molecular weight increases. Only the low molecular weight sample PP-L101 exhibits a spherulitic superstructure and no oriented shish kebab structures. Also lamellae thickness increases as molecular weight increases, recognisable in the TEM micrographs. Here, a lamella thickness of between 10 to 30 nm is observed. Similar values of lamellae thickness can also be calculated based on melting temperature using the Thomson-Gibbs relation. However, it should be taken into account that Thomson-Gibbs involves the interfacial fraction and, thus, thicker lamellae will be calculated as compared to the lamella thickness determined by TEM micrographs.

Moreover, DSC analyses have shown that the crystallinity increases as the molecular weight decreases. This can be attributed to the presence of a larger number of entanglements for the higher molecular weight samples. Furthermore, annealing of the micro dumbbell specimens results in higher crystallinity, coupled with thicker lamellae due to improving perfection of the crystalline fraction. The industrial PP specimens show crystallinity similar to the laboratory LP-PP samples, but thinner lamellae. This is probably caused by additional unknown additives, such as stabilising agents or lubricants, which are added to the commercially-available industrial PP resins.

WAXS shows patterns identical to those of mixed c-axis and a*-axis orientation. For this reason, the interpretation of the WAXS investigations here leads to a shish kebab structure with additionally grown small lamellae which, being a*-axis oriented, are epitaxially crystallised on the kebabs.

8 END-USE PROPERTIES – MOULDED POLYPROPYLENE SPECIMEN

Use of polymer products depends essentially on their stiffness, strength, deformability, and temperature and chemical resistance. These properties are mainly influenced by molecular structure and processing conditions. For instance, the crystallinity and stiffness of a polymeric material is basically governed by molecular structure (molecular weight and molecular weight distribution). Additionally, the solidification process (crystallisation) strongly influences morphology and, thus, product performance.

The search for the relationship between structures and properties has motivated extensive studies in the past. In particular, many analyses have been carried out in order to understand the dependence of morphology on the deformation behaviour of semi-crystalline polymers.[43,64,91-95,101,102] Furthermore, there are many articles which study the influence of processing conditions on mechanical properties.[34,45,51-54,166] However, these studies are usually performed without any knowledge of the materials used, such as the polymerisation conditions used, additives, pre-treatment after polymerisation, etc., although the strong influence of these parameters on the properties studied is known, as is shown in Chapter 5.

Unless the basic data of an investigated material are known, it makes no sense to analyse its morphology and properties, nor even to correlate them, if additional influencing factors cannot be excluded.

Based on this, this chapter focuses on the influence of molecular weight on the end-use properties of a series of well-defined LP-PP's. A major object of focus is the analysis of the mechanical response to static and dynamic deformation, which is critically important in determining the suitability of a material for a given application. In addition, the mechanical properties of the injection-moulded LP-PP samples after annealing at temperatures of 100°C and 140°C was studied for the analysing of the effect of possibly changed morphology and for a better understanding of the structure-properties relationship.

8.1 Quasi-static tensile properties

The stress-strain behaviour of the injection-moulded LP-PP micro dumbbell specimens were analysed in order to describe their mechanical behaviour. Figures 8.1 and 8.2 represent detailed plots, ranging from 0 to 30 % strain, of the true stress-strain curves for the unannealed and annealed (140°C,1 h) injection-moulded PP samples. Correspondingly, the stress at 8 % strain, Young's modulus (tangent modulus) at 0.5 % strain, and the strain at break are shown in Table 8.1. The annealed injection-moulded PP samples were only measured up to a strain of 30 % and as a result no strain at break was determined.

In both Figures 8.1 and 8.2, the samples exhibit a stress-strain behaviour typical of ductile semi-crystalline polymers. At low strain, a nearly linear rise in stress characterises the major pure elastic deformation behaviour. This follows more or less distinctively the yielding of the samples, as indicated by deviation from linearity in the stress-strain curve at a strain of about 6 %. Here the polymer chains start to slip and usually necking occurs. As the strain level increases, strain hardening appears until the samples finally break.

In the case of high molecular weight samples (from 833 $kg \cdot mol^{-1}$ to 1 600 $kg \cdot mol^{-1}$) no distinctive yielding is detectable, but strain hardening becomes clearly noticeable at about 10 % strain. The effect of strain hardening (indicated by a progressive stress-strain curve) becomes more pronounced the higher the molecular weight. Similar behaviour has been observed by other scientists[43,166] and will be discussed in more detail below. Only sample PP-L244 shows distinctive yielding and peaking at 8 % strain. The low molecular weight samples PP-L101 and PP-L153 break brittle at strains of about 8 % and 11 %, respectively. Hence, there is a minimum molecular weight of 153 $kg \cdot mol^{-1}$, below which polymeric materials are brittle. From literature[177], it is known that the ductile-to-brittle transition usually appears when the molecular weight is twice the entanglement molecular weight ME. This theory is explained by the fact that the entanglements between lamellae are responsible for carrying a large amount of the stress during the tensile test, so that the absence of entanglements strongly affects fracture behaviour.

Based on an ME value of 6 700 $g \cdot mol^{-1}$ (calculated previously by means of viscoelastic data) the critical molecular weight Mc of iPP is about 13 400 $g \cdot mol^{-1}$, i.e, much lower than the molecular weights of the brittle samples, although by contrast the number of entanglements per chain of those samples is lower than that of the high molecular weight samples. In consequence, other factors must play a role in the transition from ductile-to-brittle behaviour as molecular weight decreases.

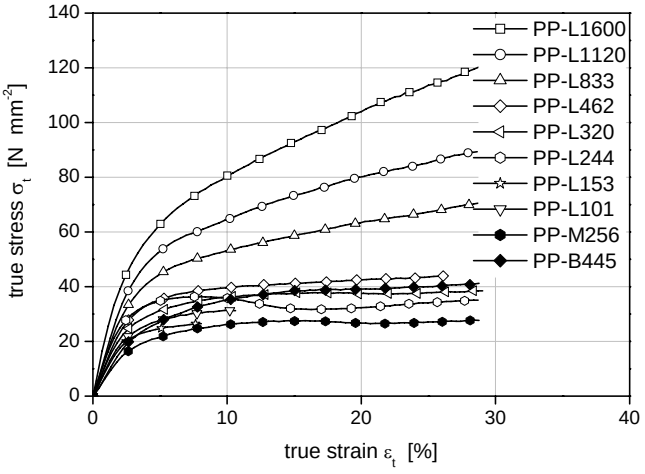

Figure 8.1: Stress-strain behaviour of unannealed injection-moulded LP-PP samples, depending on molecular weight (strain rate $3 \cdot 10^{-4}$ s^{-1}, contact force 1 N, temperature 25°C)

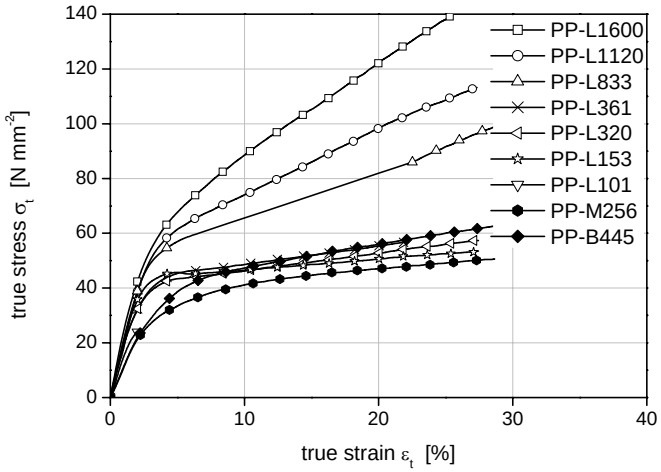

Figure 8.2: Stress-strain behaviour of annealed injection-moulded LP-PP samples at 140°C for 1h, depending on molecular weight (strain rate $3 \cdot 10^{-4}$ s^{-1}, contact force 1 N, temperature 25°C)

The fact that the low molecular weight samples PP-L101 and PP-L153 rupture just after yielding and fail to exhibit necking in tensile tests is assumed to be due to early (at low deformation) stretching of the short molecular chains to their maximum and the breaking of few entanglements per chain. Additionally, the formation of microvoids caused by initial stretching of the amorphous molecules lead to local stress concentration within the amorphous phase. Within the small amorphous fraction, the applied stress can be compensated to a lesser extent, so that growth of the microvoids into crazes is promoted, finally causing rupture.

Table 8.1: Mechanical properties of unannealed and annealed injection-moulded PP samples

Sample	$\sigma_{\varepsilon=0.08}$ $[N \cdot mm^{-2}]$	$E_{\varepsilon=0.005}$ $[N \cdot mm^{-2}]$	ε_B [%]	$\sigma_{\varepsilon=0.08,100}$ $[N \cdot mm^{-2}]$	$E_{\varepsilon=0.005,100}$ $[N \cdot mm^{-2}]$	$\sigma_{\varepsilon=0.08,140}$ $[N \cdot mm^{-2}]$	$E_{\varepsilon=0.005,140}$ $[N \cdot mm^{-2}]$
PP-L1600	75	2 330	44	79	2 350	83	2 320
PP-L1120	61	1 480	85	67	2 030	70	2 160
PP-L833	51	1 600	143	56	1 860	na	na
PP-L462	39	1 350	208	47	1 680	45	2 000
PP-L361	36	1 560	na	na	na	47	1 880
PP-L320	35	1 300	216	45	1 670	45	1 820
PP-L244	36	1 570	na	44	1 520	46	1 720
PP-L153	27	1 340	na	36	1 020	na	na
PP-L101	30	1 270	11	na	1 370	na	1 560
PP-M256	25	730	na	33	1 070	39	1 190
PP-B445	33	850	na	39	1 070	45	1 180

$\sigma_{\varepsilon=0.08}$ = stress at 8% strain, $E_{\varepsilon=0.005}$ = Young's modulus at 0.5% strain, ε_B = strain at break, 100 = annealing at a temperature of 100°C for 1 hour, 140 = annealing at a temperature of 140°C for 1 hour, and na = not available

To understand the stress-strain behaviour of the injection-moulded LP-PP series, the morphological structure found in Chapter 7 should be considered. As known from DSC measurements, the crystallinity of low molecular weight PP samples is higher than that of high molecular weight samples, and lamellae thickness increases, most notably in the case of thicker lamellae, as molecular weight increases. As a result, the amorphous fraction between the lamellae increase with molecular weight. Additionally, from the viscoelastic properties of PP the number of entanglements per chain can be estimated, exhibiting significant increase with increasing molecular weight.

From morphological studies, most observable by TEM analysis of the unannealed PP samples, it is obvious that microscopic structure changes in the micro dumbbell specimens depend on molecular weight. The low molecular weight samples clearly exhibit spherulitic

structure in the core and a thin, oriented skin layer. In contrast, highly oriented shear-induced structures (shish kebab) can be observed as molecular weight increases.

Based on these results and current understanding, a schematic model of the structural formation of low molecular weight and high molecular weight polymers can be postulated as shown in Figure 8.3. Figure 8.3 also presents schematically the micromechanical deformation and orientation processes of the amorphous and crystalline phase, assigned to the stress-strain curve.

First, elongation of the samples in tensile direction causes stretching of the amorphous molecules. This process is purely elastic; once the load on the sample is removed, it is stress-free. When the semi-crystalline polymer is further deformed, plastic yielding occurs where crystallite sliding takes places. Thus, the lamellae start to orientate themselves parallel to the deformation direction; correspondingly, interlamellar slipping occurs, coupled with the unfolding of lamellae until ultimate break. Peterlin[91-94] has described this mechanism as the breaking of the lamellae into microblocks and their reorganisation in microfibrils accompanied with interlamellar separation and insertion of unfolded molecule chains into the amorphous fraction. As a result, strain hardening occurs.

Based on the deformation processes explained, the difference in stress-strain behaviour of the different molecular weights of untreated and thermally treated injection-moulded samples can be explained.

Young’s modulus corresponds to the initial response of material to energy input (strain) and is attributed to stiffness of the material at low deformation. Therefore, from the point of view of material science it is decisive how stress will be transmitted through the crystalline and mainly the amorphous fraction.

Here, Young’s modulus is estimated as the tangent modulus at a strain of 0.5 %. Figure 8.4 shows that Young’s modulus increases as the molecular weight increases in a nearly linear fashion. Additionally, at the same molecular weight, Young's modulus is higher as crystallinity increases within the same sample. Increasing crystallinity is caused by annealing at higher temperatures, for which see Figure 8.6. However, when comparing Young’s modulus within the PP series, the higher molecular weight samples, which exhibit less crystallinity, are stiffer than the low molecular weight samples with more crystalline fraction. Therefore, the recognised and oft-reported phenomenon[43,44,178] that Young’s modulus usually rises continuously as crystallinity increases, is only correct with regard to one defined molecular weight sample. The high stiffness present of up to 2 300 $N \cdot mm^{-2}$ of the PP samples is caused by existing shish kebab structure. As observed by TEM analysis, the low molecular weight PP samples exhibit non-shish-kebab structures, but as molecular weight increases, the number of shish kebabs increases.

Due to their architecture the shish kebabs can sustain most of the stress. The shishs - consisting of fibrous crystals penetrating the texture - are responsible for high stiffness in the direction of flow (= tension, direction of load) and the kebabs - lamellae around the shish - are responsible for high stiffness transverse to the direction of flow.

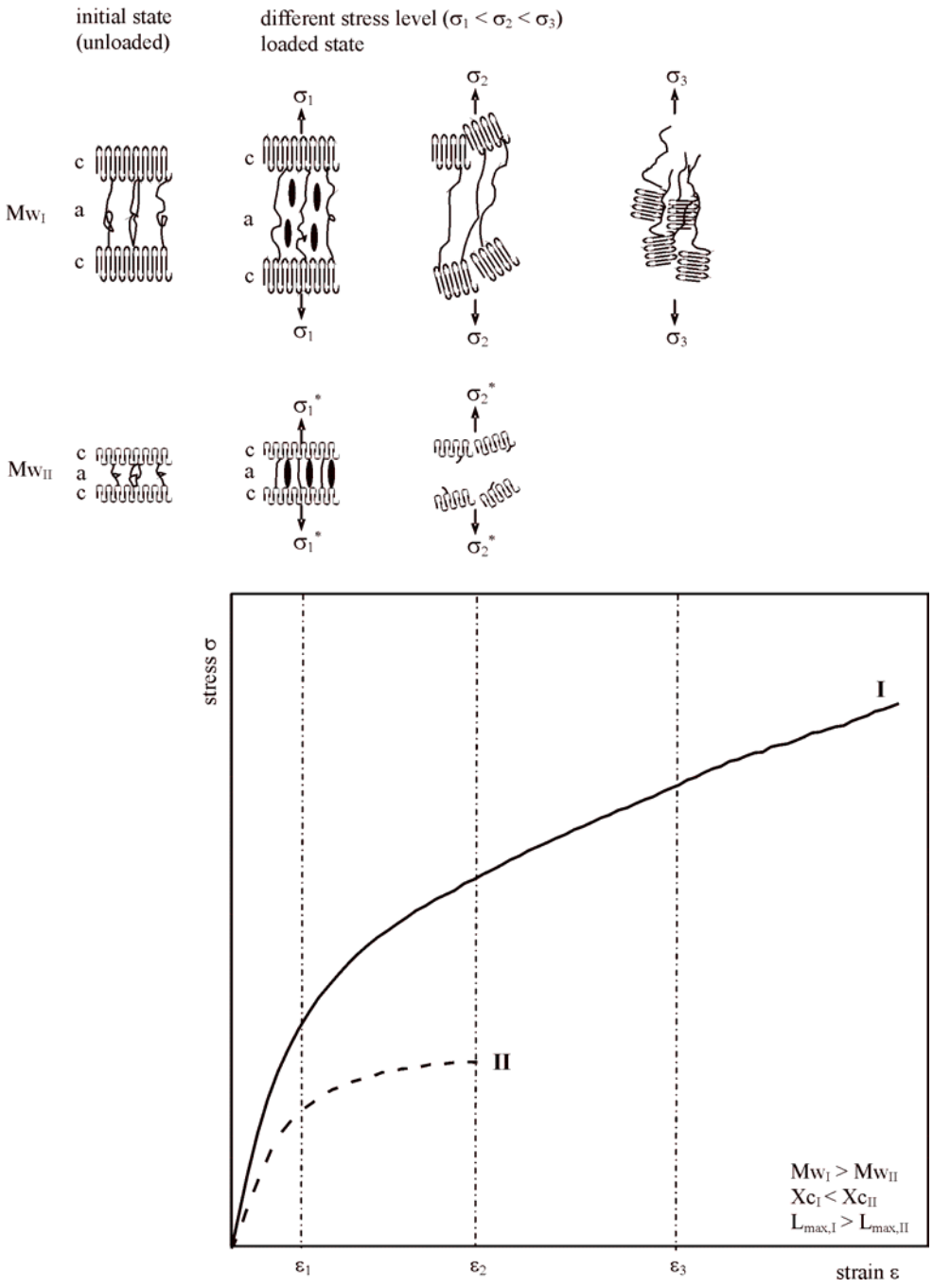

Figure 8.3: Schematic illustration of deformation behaviour (c = crystalline, a = amorphous)

However, there is another reason for the high stiffness of the PP samples. The stiffness of samples annealed at high temperatures, is greater than that of unannealed samples, although the proportion of shish kebab structures either remains the same, or is probably even smaller subsequent to the annealing of the samples. Therefore, another factor must be involved and it seems to be the mobility of the amorphous fraction. This can be explained by the different dynamic mechanical responses of the PP samples prior and subsequent to annealing as measured by DMA and described below.

Figures 8.5, 8.7 and 8.8 show the behaviour of tensile strength based on molecular weight, melting enthalpy (~ crystallinity) and lamellae thickness. The stress at a strain of 8 % (= yield point of PP-L244) is used as tensile strength, since not all of the samples show extensive yielding.

Similar to the behaviour of stiffness dependent on molecular weight, tensile strength increases proportionally as molecular weight increases. Furthermore, when comparing tensile strength dependent on crystallinity for the same molecular weight, tensile strength increases as the crystallinity increases as shown in Figure 8.7. However, considering that the crystallinity as analysed by DSC is lower for high molecular weight samples than for lower molecular weight samples, the tensile strength of PP-L1600 should be lower than that of PP-L101. However, the results presented in Figure 8.7 show the opposite. In consequence, and as found by the studies on stiffness, the well-known basic rule that the stiffness and tensile strength increase with increasing crystallinity, can be applied only for samples with the same molecular weight and is not transferable to samples with different molecular weights.

Highly oriented shish kebab structure also affects tensile strength and strain hardening occurring at higher deformation, as does stiffness. Although the number of shish kebabs is probably not influenced by thermal treatment, increasing strength and strain hardening after annealing indicates that an additional factor governs tensile strength.

The results found seem to be governed mainly by lamella thickness and lamella thickness distribution. This explanation can be affirmed by a linear relation between tensile strength and maximum lamella thickness, calculated from the DSC results, as shown in Figure 8.8. Therefore, thicker lamellae which are evolved from long molecule chains can sustain large deformations. This again explains why tensile strength is higher after thermal treatment of the samples, when comparing the tensile stress values at 8 % strain for the same molecular weight samples, as shown in Figure 8.7.

Similar behaviour was first observed by Young[179] for polyethylene (PE). He announced that tensile yield stress is activated by screw dislocation of the lateral surface of crystalline lamellae, indicating that lamella thickness influences considerably yield stress. Schrauwen et al.[64] confirmed this theory, finding that yield stress depends on lamella thickness. They found a fair correlation between the yield stress measured in polyethylene and that predicted by a mechanism involving the propagation of screw dislocation. Séguéla[180] has shown for PE and PP that tensile yield stress depends on lamella thickness, rather than crystallinity. He found the result to be consistent with Young's model of dislocation.

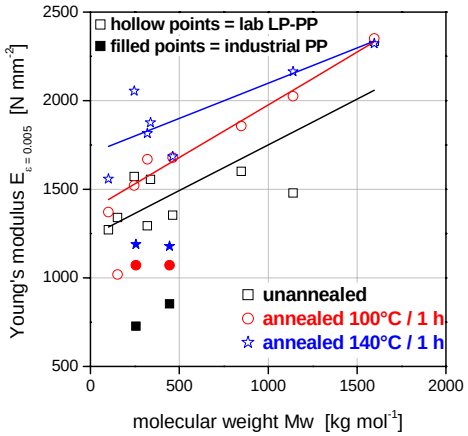

Figure 8.4: Dependence of Young's modulus on the molecular weight of unannealed and annealed injection-moulded LP-PP samples

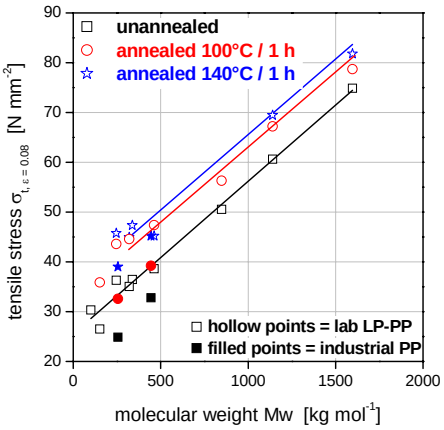

Figure 8.5: Dependence of tensile stress at 8 % strain on the molecular weight of unannealed and annealed injection-moulded LP-PP samples

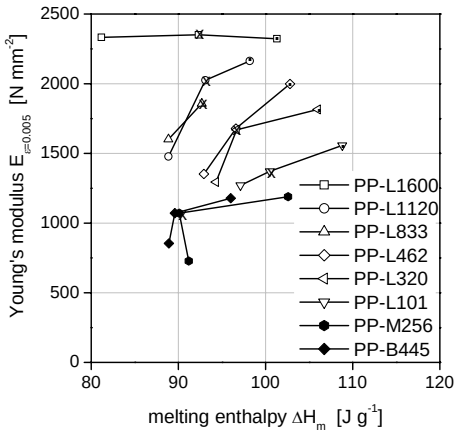

Figure 8.6: Dependence of Young's modulus on the melting enthalpy of unannealed and annealed injection-moulded LP-PP samples
(X = 100°C/1h, · = 140°C/1h)

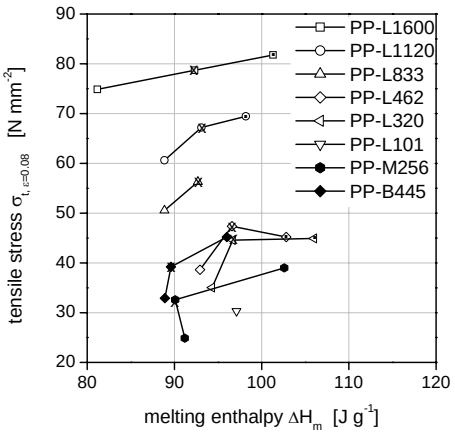

Figure 8.7: Dependence of tensile stress at 8 % strain on the melting enthalpy of unannealed and annealed injection-moulded LP-PP samples (X = 100°C/1h, · = 140°C/1h)

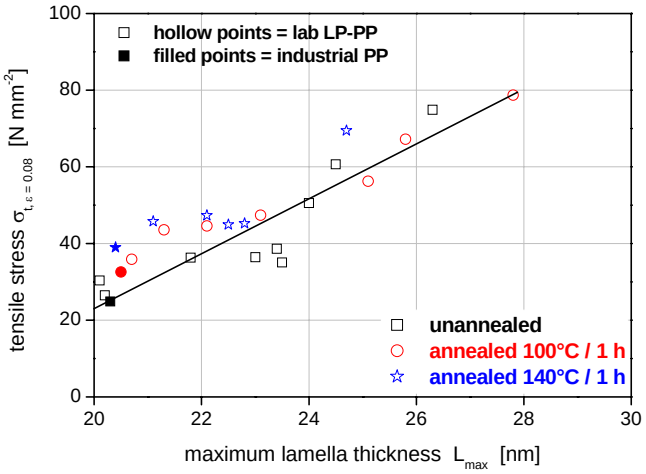

Figure 8.8: Tensile stress at 8 % strain as a function of maximum lamella thickness

In addition to the increase in tensile stress, a more pronounced strain hardening can be observed as the lamella thickness increases (see Figures 8.1 and 8.2). The reason for this is that the slipping and orientation of lamella become more difficult as thickness increases. Moreover, additional unfolding of longer molecule chains is more complicated in the case of high molecular weight polymers. This explanation is confirmed by the stress-strain behaviour of the samples annealed at 140°C for 1 hour, as shown in Figure 8.2. When the same molecular weight samples are compared before and after annealing, strain hardening is more pronounced for the thermally treated samples than for the untreated samples; this is due to growing lamella thickness during the annealing procedure.

Spectacularly, the high molecular weight sample PP-L1600 even achieves an unusual tensile stress of up to 120 $N \cdot mm^{-2}$ within the measured strain range. This high tensile strength, 3 times higher than the known tensile strength of a commercially-available PP, is atypical of PP. As far as it is known, such high tensile strength of injection-moulded dumbbell specimens has not been reported in literature until now.

Prox and Ehrenstein[45] found for PP with a molecular weight of 470 $kg \cdot mol^{-1}$ a maximum tensile strength of about 80 $N \cdot mm^{-2}$, but with low strain at break this was about 32 %. They studied injection-moulded PP dumbbell specimens within a molecular weight range of 240 $kg \cdot mol^{-1}$ to 653 $kg \cdot mol^{-1}$ and using extreme processing conditions, such as high injection speed (180 $mm \cdot s^{-1}$) and low melt (160°C) and mould temperatures (25°C), to obtain self-reinforcement. Analysing the dependence of molecular weight on mechanical properties, they found peak improvement of tensile strength at an average molecular weight of 470 $kg \cdot mol^{-1}$.

Furthermore, Kalay and Bevis[51] observed an increase in Young's modulus of mouldings produced by shear-controlled orientation injection moulding (SCORIM). By controlling the processing parameters it is possible to control and enhance stiffness without loss of tensile strength. They reported a maximum increase in Young's modulus of up to 2 600 $N \cdot mm^{-2}$ and a peak tensile strength of 55 $N \cdot mm^{-2}$ of mouldings, using iPP with an average molecular weight of 460 $kg \cdot mol^{-1}$, but linked with a reduction in strain at break of about 55 %.

Albano et al.[33] produced plaques from iPP within a molecular weight range of between 210 and 800 $kg \cdot mol^{-1}$ using conventional injection moulding. They studied the influence of molecular weight and thermal history on mechanical properties and obtained samples with a tensile strength of 58 $N \cdot mm^{-2}$ and strain at break of about 90 %, but with a low Young's modulus of about 830 $N \cdot mm^{-2}$.

However, extremely strong and stiff PP with a stiffness of up to several $kN \cdot mm^{-2}$ is known only in highly (biaxial) drawn and anisotropic PP films and fibres produced by special processing techniques. Here the disadvantage is low obtainable ultimate strain: lower than approx. 10 %.

For example, Suzuki et al.[181] reported on the mechanical properties and superstructure of isotactic PP fibers prepared by continuous vibration zone-drawing (CVZD). They found that the zone-drawn polymer with a low molecular weight of 30 $kg \cdot mol^{-1}$ and a draw ratio of up to 11 reached a tensile strength of about 1 000 $N \cdot mm^{-2}$ and a Young's modulus of 15 000 $N \cdot mm^{-2}$, but this was accompanied by a very low strain at break of 10 %. These strength data are due to highly oriented amorphous interphase.

Comparison of commercially-available industrial PP samples with the laboratory LP-PP samples shows that the industrial PP samples maintain less stiffness and strength, although their deformation behaviour is similar. The tensile stress at 8 % strain reaches a maximum of only 45 $N \cdot mm^{-2}$ for bimodal PP and about 38 $N \cdot mm^{-2}$ for monomodal PP. It should be noted that the yield point of the industrial samples at 14 % in the case of monomodal PP (PP-L256) and at 19 % for bimodal PP (PP-L445). Nevertheless, for defined comparison of the laboratory LP-PP samples with the industrial PP, a tensile stress at 8 % was used. However, it is a fact that tensile strength is also governed by lamellae thickness, as Figure 8.8 shows.

8.2 Dynamic mechanical properties

Semi-crystalline polymers show several types of relaxation phenomena which can be detected by dynamic mechanical analysis (DMA). As a result of certain molecular motions, storage modulus depression or a loss modulus peak appears on the mechanical relaxation curve.

In the case of isotactic polypropylene, dynamic mechanical relaxation processes can be observed from -50°C up to near the melting temperature. Typically for PP, there are three different relaxation processes due to molecular motions activated by thermal energy (see Figure 8.9).[181-184] Firstly, very short range motions, such as methyl group rotation in side chain ends, occur at approx. -50°C; this motion is termed the γ-relaxation process. The β-relaxation process at higher temperatures of about 0°C is the dominant relaxation and can be attributed to the transition from glassy to rubbery state in amorphous polymers, but it should be taken into account that the amorphous region in crystalline polymer is different from that in completely amorphous polymer, in that, the molecular motions of the amorphous phase are constrained by the crystallites. In the temperature region close to melting temperature, the α-relaxation process takes place due to motions in the interphase of crystallites. Although the reason for this α-relaxation process is still a subject of controvery, it is well documented [181-183] that the α-relaxation is strongly affected by orientation; on the one hand, this effect occurs primarily in temperature regions of above 30°C and, on the other hand, it is affected by the length of chain foldings at the interphase, which again depends on molecular weight and occurs at temperatures of about 100°C.

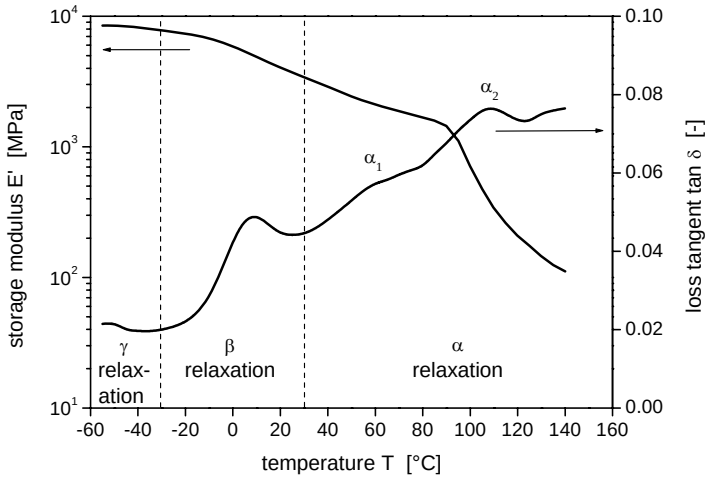

Figure 8.9: Typical dynamic mechanical relaxation processes of PP

8.2.1 Temperature dependency

Observing all three relaxation processes, measurements were performed from the very low temperature of -50°C up to 140°C. Detailed plots, ranging from -40 to 100°C, of the storage modulus E' and loss tangent tan δ as a function of the temperature, measured at 1 s^{-1} for a representative selection of the unannealed and annealed injection-moulded LP-PP samples are presented in Figures 8.10 to 8.13. Both Figures 8.10 and 8.11 show a very weak distinctive γ-relaxation, due to fewer CH3 motions.

In contrast, in the range of the β-relaxation, a vast peak can be observed between 0 and 10°C of the tan δ curve (Figure 8.10), which corresponds to the glass transition temperature Tg of iPP. Because of the dominant relevance of this β-relaxation, a detailed view of the tan δ curve for untreated injection-moulded LP-PP samples is shown in Figure 8.14. From there, the magnitude of the β-relaxation was determined after subtraction of a fitted linear baseline.

As shown in Figures 8.10, 8.11 and 8.14 a marked difference in the magnitude of the β-relaxation exists when comparing samples with different molecular weights. It is demonstrated in Figure 8.15, that the magnitude of the β-relaxation increases rapidly with increasing molecular weight toward asymptotic limits, which are reached at magnitudes of about 0.015 for the unannealed samples and 0.038 for the annealed (140°C, 1 h) samples. Despite this, only a weak difference in the maximum magnitude of the β-relaxation can be observed between the unannealed samples and the samples annealed at 100°C for 1 h. The reason for this seems to be the fact that minor changes in morphological structure occur when an annealing temperature of 100°C, which is below the crystallisation temperature of the LP-PP samples, is used. In contrast, when the injection-moulded LP-PP samples are annealed at temperatures of 140°C, which is above the crystallisation temperature of the PP samples (T_c ~ 120°C, see Table 7.2) post-crystallisation is promoted and, in consequence, the nanostructure is changed. In fact, a decrease in the mechanical relaxation of the β-process is associated with a reduction in the mobility of polymer chains in the amorphous phase.[181,183,184]

On one hand, the reason may be lower amounts of amorphous fraction, but this explanation is not totally consistent with the result found in Figure 8.16. The magnitude of β-relaxation increases as the content of amorphous fraction decreases after annealing of the injection-moulded LP-PP samples. For example, when comparing the magnitude of β-relaxation and the amount of amorphous fraction of the injection-moulded samples PP-L320 before and after annealing –

	unannealed	annealed, 140°C/1h
X_a	52 %	46 %
magnitude of β-relaxation	0.005	0.022

– the magnitude of β-relaxation increases 4 times, although the content of amorphous fraction decreases from 52 % to 46 %.

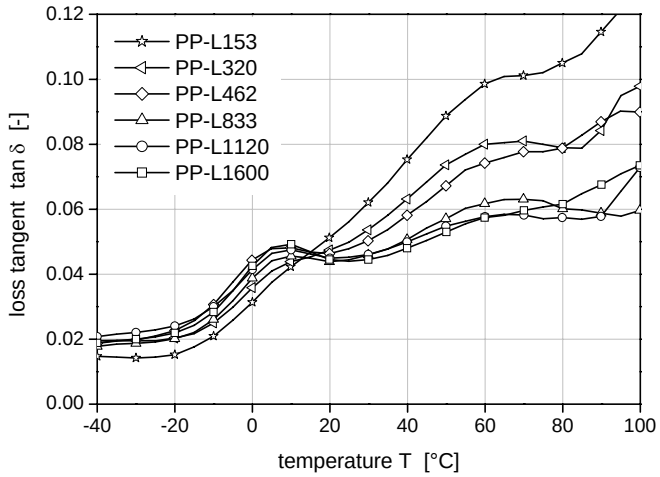

Figure 8.10: Loss tangent tan δ as function of temperature for unannealed injection-moulded LP-PP samples with various molecular weights (static strain 1 %, dynamic strain 0.1 %, frequency 1 s^{-1}, heating rate 5 $K \cdot min^{-1}$)

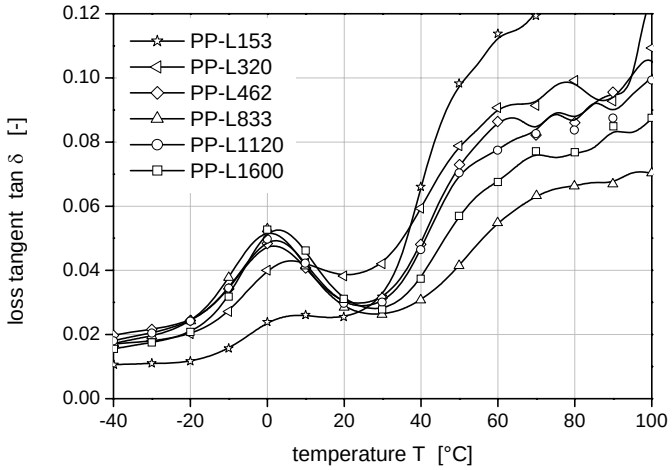

Figure 8.11: Loss tangent tan δ as a function of temperature for annealed injection-moulded LP-PP samples at a temperature of 140°C for 1h with various molecular weights (static strain 1 %, dynamic strain 0.1 %, frequency 1 s^{-1}, heating rate 5 $K \cdot min^{-1}$)

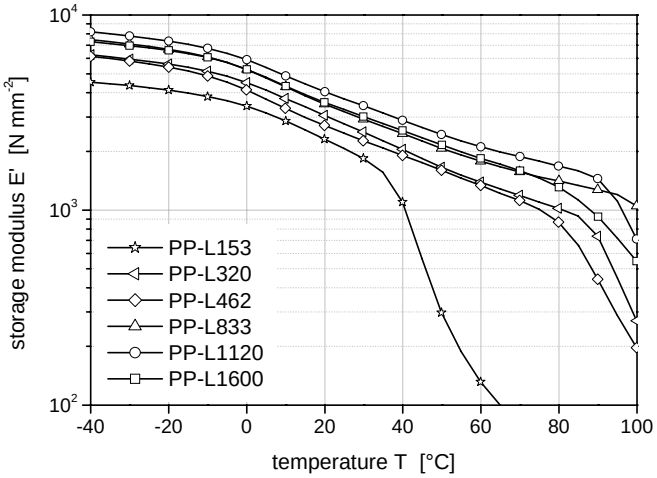

Figure 8.12: Storage modulus as a function of temperature for unannealed injection-moulded LP-PP samples with various molecular weights (static strain 1 %, dynamic strain 0.1 %, frequency 1 s^{-1}, heating rate 5 $K \cdot min^{-1}$)

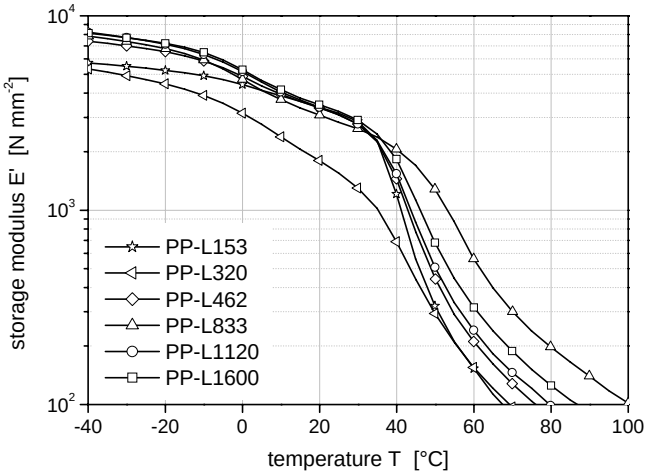

Figure 8.13: Storage modulus as a function of temperature for PP samples with various molecular weights and annealed at 140°C for 1h (static strain 1 %, dynamic strain 0.1 %, frequency 1 s^{-1}, heating rate 5 $K \cdot min^{-1}$)

However, when comparing the magnitudes of β-relaxation for the untreated high molecular weight sample PP-L1600 and the low molecular weight sample PP-L101 –

	PP-L1600	PP-L101
X_a	58 %	51 %
magnitude of β-relaxation	0.015	0.002

– it turns out, as expected, that the β-relaxation is higher with the higher content of amorphous fraction. Therefore, the way the content of the amorphous phase is changed should be taken into account in this explanation.

On the other hand, another reason may be a change in molecular packing in the amorphous phase. Denser packing of the molecular chains leads to a reduction in molecular motion. As can be observed in Figure 8.15, when comparing the magnitudes of β-relaxation in unannealed and annealed (mainly at 140°C for 1 h) samples, an obvious rise in the magnitude of β-relaxation can be noticed, although there is a reduction in amorphous fraction after the annealing procedure. Furthermore, stiffening of the amorphous components can usually be observed after annealing.[87] Therefore, not only the amount of amorphous phase, but also the structure of amorphous fraction, mainly between the lamellae, governs the relaxation process. Particularly, within the thicker lamellae there are considerably more mobile interlamellar amorphous components, which are not limited in their motions by crystallites. This implies a rapid rise in the magnitude of β-relaxation as a function of maximum lamella thickness, as shown in Figure 8.17.

Moreover, a marked rise in magnitude of β-relaxation appears for all samples of the PP series which were thermally treated at 140°C for 1 h. This leads to the assumption that considerably freer molecular mobility exists due to reorganisation of structure, which can be further supported by the fact, that a shifting of the tan δ peak to 0°C from 10°C is observable, when comparing Figures 8.10 and 8.11. A reduction in glass transition temperature is generally caused by an increase in free volume, consequently enhancing the spatial mobility of the molecules and leading to a rubber-like behaviour at lower temperatures. As a further result, the stiffness of the material is influenced considerably by the mobility of amorphous components, as shown in Figure 8.18. In fact, linear correlation between Young's modulus and the magnitude of β-relaxation can be observed.

Of course the mobile, interlamellar amorphous fraction also influences the α-relaxation process intensively. In Figure 8.10, the α-relaxation clearly shows a broad peak with a weak shoulder at about 60°C. Thus, the loss tangent tan δ increases at a temperature of about 30°C, but this is more gradual for high molecular weight samples. In contrast, the low molecular weight sample shows a marked rise, beginning at a temperature of about 20°C with a much more progressive slope than that of the curves of high molecular weight PP. Such behaviour can be attributed to crystal-crystal sliding. This mechanism requires mobility in the interlamellar regions; otherwise the movement of crystals is hindered.

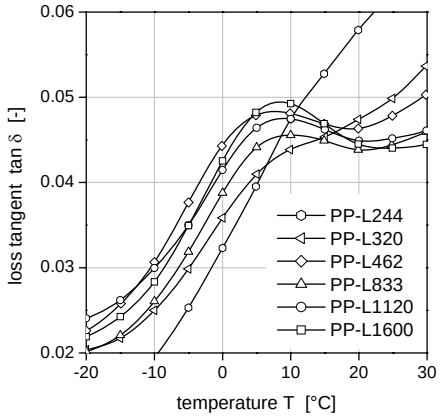

Figure 8.14: Detailed view of the β-relaxation process for unannealed injection-moulded LP-PP samples with various molecular weights

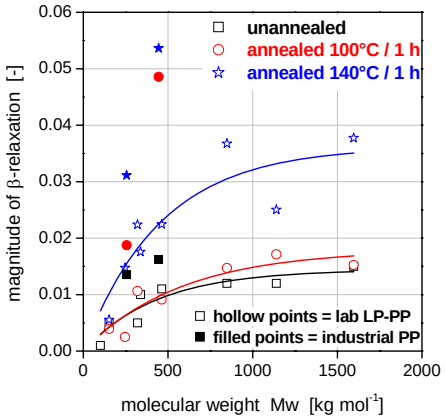

Figure 8.15: Dependence of the magnitudes of β-relaxation on unannealed and annealed injection-moulded LP-PP samples with various molecular weight

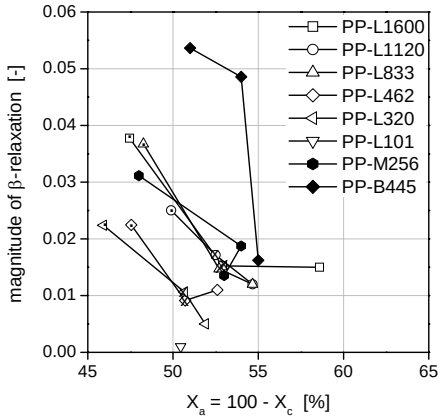

Figure 8.16: Dependence of magnitude of β-relaxation on amorphous fraction for unannealed and annealed injection-mouldedLP-PP samples (X = 100°C/1h, · = 140°C/1h)

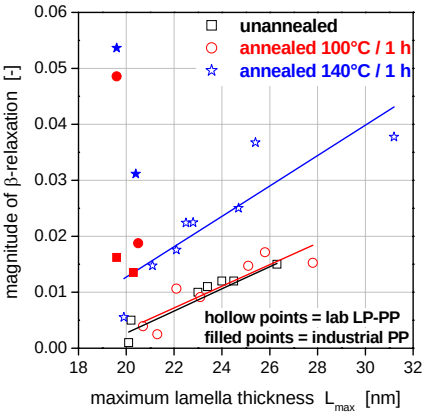

Figure 8.17: Dependence of magnitude of β-relaxation on maximum lamellae thickness for unannealed and annealed injection-moulded LP-PP samples

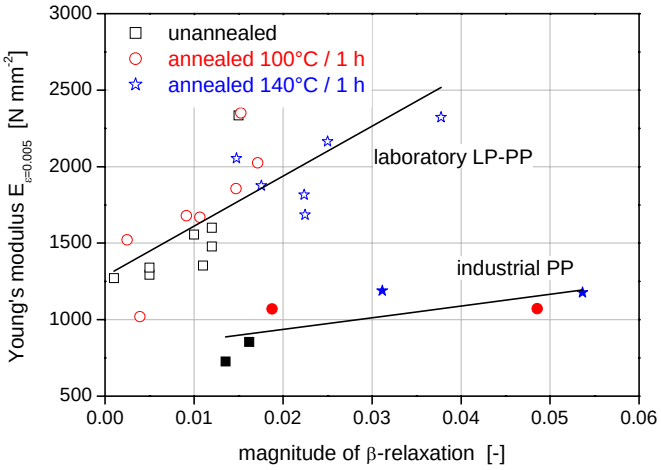

Figure 8.18: Young's modulus as a function of magnitude of β-relaxation

However, the untreated injection-moulded PP specimens in Figure 8.10 show that the samples with more mobile amorphous fraction exhibit a smaller α-relaxation peak. For example, PP-L1600 exhibits a pronounced β-relaxation peak at 10°C, but by contrast, almost no mechanical response in the α-relaxation range can be recognised.

Distinctive α-relaxation behaviour, as can be observed for the lower molecular weight samples in Figure 8.10, is well-known for oriented samples, for example, due to special drawing processes.[46,182,183] This is due to the fact that molecules arranged parallel to the direction of deformation can slip more easily.

Pluta et al.[183] investigated iPP samples compressed in a channel-die at 110°C up to a compression ratio of 6.6. They found that less deformation of iPP samples already influences the α-relaxation process and is noticeable by a marked increase in the tan δ curve at temperatures above 30°C. The main deformation mechanisms found were crystallographic slips along the chain direction.

Moreover, for highly zone-drawn PP fibres Suzuki et al.[182] noticed loss in β-relaxation and correspondingly, distinctive α-relaxation, starting at 20°C. To that they attributed an increase found in storage modulus E' as the drawing ratio increases. They implied that inter-crystalline bridges connect the crystal regions longitudinally and cause sliding processes.

Candia et al.[46] confirmed Suzuki's finding, also finding that the modulus is substantially a function of the drawing degree in the case of two-step drawn iPP. Additionally, they obtained increasing α-relaxation process for highly drawn PP fibres, starting at a temperature of 40°C.

Based on these findings and information available on the α-relaxation process, there have to be additional morphological effects hindering the slipping process as molecular weight increases. As known from morphological investigation, there are highly oriented shish kebabs

possessing high stiffness and strength due to extended molecule chains lying parallel to each other. Kebabs are formed radially around the oriented molecule chains which can interlock the shish kebabs, thus strongly limiting motion. Therefore, the shish kebabs increasing in number with increasing molecular weight cause an observable decline in the α-relaxation.

This explanation is further supported by the fact that the rise of tan δ in the α-relaxation process, starting at about 30°C, appears more distinctly, and the drastic storage modulus drop shifts to the lower temperature of 40°C; this can be seen by comparing the unannealed and annealed injection-moulded LP-PP samples in Figures 8.12 and 8.13. During annealing of the PP samples, the molecules are thermally stimulated to form thermodynamically stable structures, preferably the folding of chains to spherulites in the case of linear polymers, in consequence of which the shish kebabs structure is partially dissolved. This reorganisation of structure leads to a reduction in orientation and furthermore to easier crystal-crystal sliding processes.

In Figure 8.12 and 8.13, the storage modulus E' is plotted as a function of temperature of a representative collection of the annealed and unannealed injection-moulded LP-PP samples. The E'-temperature curve also reflects the β- and α-relaxation processes corresponding to tan δ curve (Figure 8.9), whereas the value of E' distinctly decreases for all samples in the temperature range in which β-relaxation occurs. Starting at a temperature of about 30°C, which is assigned to the α-relaxation process (see also Figure 8.10), E' decreases more slightly than at lower temperatures, but as the temperature reaches about 80°C, volatile decay is exhibited. Moreover, stiffness of the samples versus temperature is highest for the high molecular weight samples and decreases as molecular weight decreases. The explanation for this effect is discussed above and results in a higher number of oriented shish kebab structures in the case of high molecular weight samples.

Furthermore, the shift of the drastic storage modulus drop to lower temperatures can be most noticeably observed starting at 80°C for the unannealed and at 40°C for the annealed PP samples. When comparing storage modulus E' of the high molecular weight sample PP-L1600 at a temperature of 80°C, the storage modulus E' decreases from 1200 $N \cdot mm^{-2}$ in the case of the unannealed samples and to 120 $N \cdot mm^{-2}$ for the annealed samples, or about 100 times, as shown in Figure 8.19. The reason for this is re-organisation in the highly oriented shish kebab structure towards more spherulitic-like ordered morphology.

Commercially-available industrial PP behave differently from the laboratory PP series analysed, as shown in Figures 8.15 to 8.18. Overall β-relaxation of industrial PP samples is much higher than that of comparable laboratory LP-PP samples, although the magnitude of β-relaxation increases as the content of the amorphous fraction decreases, for which see Figures 8.16. Figure 8.18 shows that there also exists a linear correlation between stiffness and the magnitude of β-relaxation, but it does not match the results found for the PP series. Thus, other parameters, such as different molecular structure or additives, strongly affect the β-relaxation of the industrial samples.

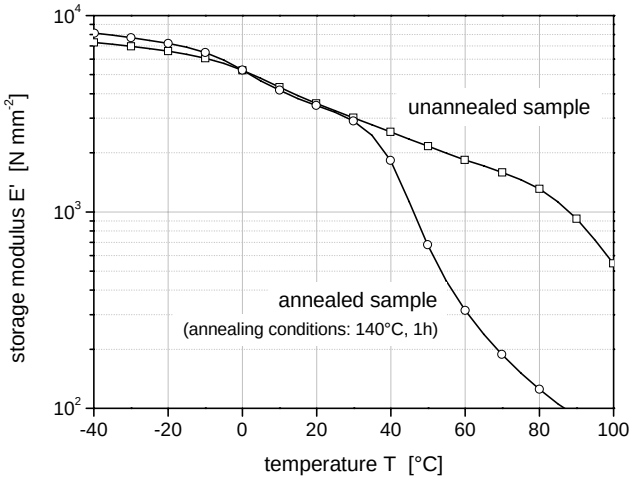

Figure 8.19: Comparison of storage modulus as a function of temperature for unannealed and annealed injection-moulded sample PP-L1600 (static strain 1 %, dynamic strain 0.1 %, frequency 1 s^{-1}, heating rate 5 $K \cdot min^{-1}$)

8.2.2 Time dependency

The suppression of the sliding effect in the case of the higher molecular weight LP-PP samples (see α-relaxation in Figure 8.10) is accompanied by the improved creep resistance of these materials. Figures 8.20 and 8.21 show the master curves over a wide frequency range of the storage modulus E' and loss tangent tan δ of a representative selection of the untreated injection-moulded LP-PP samples. The master curve was obtained by shifting the measured isotherms horizontally along the frequency axis at a reference temperature of 25°C.

In Figure 8.20 the relaxation process can be observed at low frequency (= long term loading), whereas a rise in the tan δ curves at different frequency is associated with variations in the molecular weights of the samples. This mechanical response (onset of the rising tan δ) denotes creep of the polymer chains. Correspondingly, a volatile depression of stiffness at different frequencies, also systematically changing with molecular weight, appears in Figure 8.21.

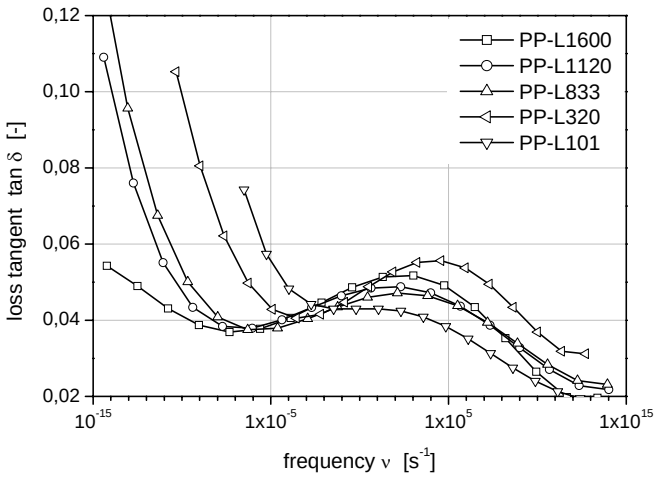

Figure 8.20: Master curve of the loss tangent tan δ for the unannealed PP samples versus frequency at a reference temperature of 25°C

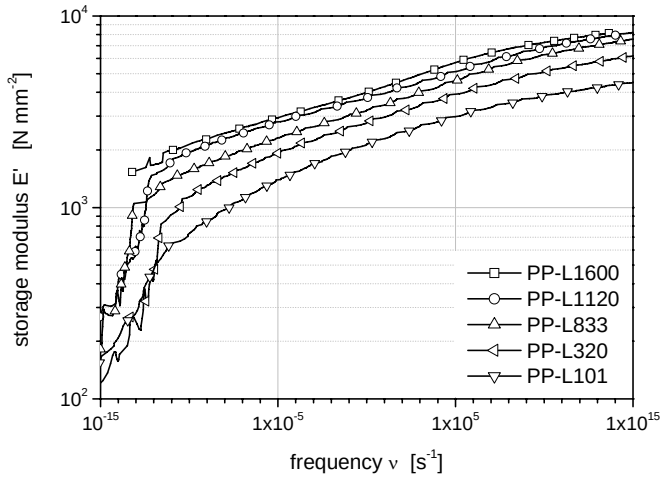

Figure 8.21: Master curve of the storage modulus E' for the unannealed PP samples versus frequency at a reference temperature of 25°C

8.3 Conclusion

The study of the mechanical deformation behaviour of the injection-moulded LP-PP specimens, depending on their molecular weight, has found that stiffness and tensile strength increase as molecular weight increases. PP-L1600 exhibits a tensile strength of approx. 120 $N \cdot mm^{-2}$, 3 times higher than the known tensile strength of commercially-available PP. The reason for this is the existence of highly oriented shish kebab structures and, in addition, an increase in lamella thickness as molecular weight increases. For the existing superstructure, maximum lamella thickness governs tensile stress as well as the strain hardening effect, rather than overall crystallinity. The recognised phenomenon that tensile strength and stiffness usually rises continuously as crystallinity increases, is only correct regarding one defined molecular weight.

The stiffness of the injection-moulded micro dumbbell specimens is determined by the mobility of the amorphous fraction. The magnitude of β-relaxation, measured by DMA indicates the mobility of the amorphous phase, i.e., the packing of the amorphous phase between the lamellae is more important than the overall content of the amorphous phase.

Furthermore, it has been found that the injection-moulded LP-PP samples rupture at lower strain as the molecular weight increases, with the exception of the injection-moulded specimens PP-L101 and PP-L153, which already break at an ultimate strain of 8 % and 11 %. As a result, a ductile-to-brittle transition occurs when the molecular weight passes 153 $kg \cdot mol^{-1}$.

By means of changed distinct β- and α-relaxation after the annealing procedure, dynamic mechanical analyses have indicated that thermal treatment of the PP samples at 140°C for 1 h in fact causes a rearrangement in morphological structure, but this does not adversely affect mechanical properties such as stiffness or strength at room temperature. In addition, there is an obvious improvement in tensile strength, stiffness and creep resistance in particular for the high molecular weight micro dumbbell specimens from novel synthesised PP.

The industrial PP specimens show lower tensile strength and stiffness than the laboratory LP-PP specimens, but their mechanical and viscoelastic properties depend similarly on molecular weight. This is probably caused by incorporated unknown additives, such as stabilising agents or lubricants, which are added to the commercially-available industrial PP resins.

Altogether the present investigation of mechanical properties shows that especially interlamellar amorphous fraction and lamella thickness, as well as highly oriented structures (e.g. shish kebab), are the main governors of the mechanical response of the samples and define their structural behaviour. If differences in morphology exist, then changes also arise in the mechanical and viscoelastic properties.

9 SUMMARISING DISCUSSION

In order to gain a fundamental understanding of the relationship between the molecular structure and end-use properties of semi-crystalline PP, it is of great importance to conduct a systematic analysis. Although, in the past, the search for a relationship between structure and properties of polymers has been a motive for extensive studies, the so-called "chain of knowledge" has never been followed until now.

Since several factors affect the properties of polymers, analysing the relationship between molecular structure and end-use properties makes sense only when one main parameter, which here is molecular weight, is studied and not, as usual, multiple parameters influencing each other and yielding undefined changes in properties.

The present study targets the discovering of "white spots on the map", exploring them accordingly. Therefore, a series of iPP's has been synthesised under defined polymerisation conditions and subsequently processed and tested with regard to final properties.

The characterisation of PP powder shows that the use of two different polymerisation techniques affects thermal, rheological and structural properties, even though identical catalyst and polymerisation temperatures of 70°C are used. There, differences between GP and LP polymerisation can be detected in the initial polymerisation rate, which reaches a maximum for LP of about 150 $kg_{PP} \cdot g_{cat}^{-1} \cdot hr^{-1}$ in contrast to the low GP initial polymerisation rate of about 45 $kg_{PP} \cdot g_{cat}^{-1} \cdot hr^{-1}$ (see Figure 5.3). This difference is caused by the higher monomer concentration on the catalysts' active sides in the case of liquid propylene polymerisation. Furthermore, different polymerisation techniques obviously result in different molecular structure of the synthesised PP powders (see Table 4.1). The GP samples exhibit broader PD due to the two-step polymerisation in this case. The change in molecular structure again affects thermal and rheological properties. DSC studies on the samples clearly show that the synthesised GP samples exhibit inhomogeneous crystalline structure (see Figure 5.13). Additionally, viscosity and viscoelastic behaviour of the PP samples are different. LP-PP samples exhibit higher zero viscosity and lower melt elasticity than GP-PP (see Figures 5.7 and 5.10).

These interesting new results prove the importance of knowing, describing and controlling the synthesis process exactly in order to obtain a polymer, defined in its basic properties.

Moreover, when using rheological measurement the recognised relationship between molecular weight and zero viscosity has been verified (see Figure 5.7). Additionally, it has been found that shear thinning behaviour is also strongly affected by molecular weight (see Figure 5.6). Such results, of course, are relevant to the melt processability of the samples. Low viscous PP materials are easier to process than high viscous one. For example, PP materials with high viscosity need a lower melt temperature for injection moulding at the same injection pressure. Moreover, simulation of the filling behaviour of the micro dumbbell specimens prepared shows that higher shear rates occur with increasing molecular weight (see Figure 6.4). On one hand, the high shear rates are caused by the very small geometry (in

particularly the small cross section of 1.25 x 0.5 mm^2 in the parallel zone) of the micro dumbbell specimens and, on the other hand, by the low viscosity of the PP samples investigated. Furthermore, the simulation of shear rate at filling of the mould cavity distinctively shows an inhomogeneous shear rate distribution across the micro dumbbell specimen (see Figures 6.5 and 6.6). Additionally, there is temperature distribution along the specimen's thickness (see Figures 6.8 and 6.9). Thus the molten polymer solidifies under inhomogeneous shear and cooling conditions, so that the inner structures (morphology) of the injection-moulded micro dumbbell specimens are inhomogeneous, as can be observed by morphological investigations under cross polarised light (see Figure 7.7).

High shear rates cause stretching of macromolecules in the direction of flow; thus a shear-induced crystallisation process during processing of the micro dumbbell specimen should be taken into account, as presented schematically in Figure 9.1. Since stretched macromolecules, row nuclei lying parallel, are formed, and lamellae start to grow around these, the formation of so-called shish kebab structures is promoted in consequence. These highly oriented structures exist in particular at phases where high shear rates exist, which usually means close to the cavity wall. Morphological investigations of the inner microstructure of dumbbell specimens confirm this assumption. SEM images clearly show shish kebab structures closest to the skin layer (where the highest shearing exists). This type of superstructure can be found favourably for the higher molecular weight samples (see Figure 7.11).

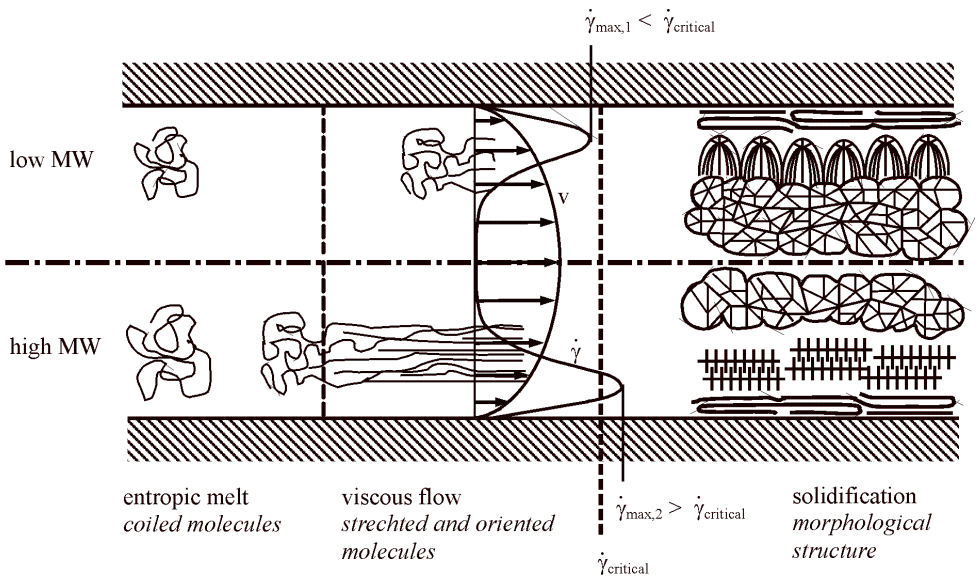

Figure 9.1: Schematic illustration of formation of morphological structure for low and high molecular weight samples

However, when the high molecular weight sample PP-L1600 is completely molten and subsequently crystallised under quiescent and isothermal conditions, the formation of spherulites of the crystalline α-form is promoted (see Figure 7.13). This result additionally confirms that shear-induced crystallisation is responsible for creating oriented shish kebab structures. In contrast to the high molecular weight samples, the low molecular weight sample PP-L101 exhibits predominantly spherulitic structure up to a thin, oriented skin layer which, however, exhibits no shish kebab structure. Consequently, a critical shear rate of about $3 \cdot 10^5\ s^{-1}$ exists at which shear-induced crystallisation to shish kebab structures prevails, instead of the formation of energetically more favourable spherulitic structures.

In addition, the characteristic retardation time depends on the molecular weight (see Table 6.2) and is much higher than the cooling time for high molecular weight samples; thus, retardation of shear-stretched macromolecules cannot take place and creation of spherulitic structure is prevented. For example, the highest molecular weight sample PP-L1600 possesses a calculated characteristic retardation time of 19.3 seconds, which is much higher than the calculated crystallisation time of approx. 1 second during processing of the PP samples. Figure 9.1 shows schematically the formation of structure as dependent on molecular weight. Processing of low molecular weight PP at moderate shear rates preferably creates a spherulitic type of morphology, in contrast to the shish kebab superstructure, which will occur when high shear rates exist or high molecular weight polymers are processed.

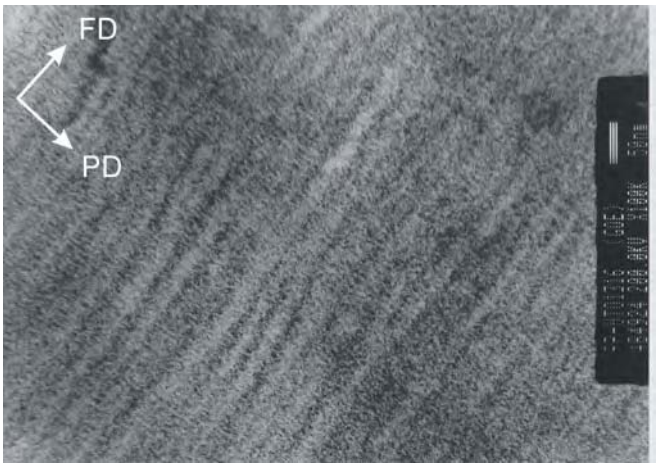

Figure 9.2: Novel morphology in injection-moulded micro dumbbell specimens of high molecular weight PP-L1600

The morphology of the injection-moulded PP samples is dominated by a highly oriented shish kebab structure (see Figure 7.12). The number of shish kebabs increases as molecular weight increases. In fact, the low molecular weight sample shows mainly spherulitic structures, as explained above. In the case of PP-L1600 even a novel morphology inside the injection-moulded micro dumbbell specimen can be observed, as shown in Figure 9.2. This

specimen even shows no separate layer in the core, but exclusively highly oriented layers over the entire cross section.

Analysing the microstructure of various injection-moulded PP specimens by TEM and DSC shows that both lamellae thickness and lamellae thickness distribution increase as molecular weight increases. The thickness of the thick lamellae varies from 20 to 26 nm (see Table 7.3).

Of course, the differences analysed in the morphological structure of micro dumbbell specimens injection-moulded from PP also drastically affect the final mechanical properties.

Tensile strength of more than 80 $N \cdot mm^{-2}$, coupled with high deformability to strains of more than 30 % was found first in injection-moulded PP specimens. The reason for this is a certain combination of PP polymer and the existence of highly oriented shish kebab structure, in association with a specific lamellar nanostructure. This morphology and not least lamellae thickness, together with the strain hardening effect, govern the tensile stress, rather than the overall crystallinity, as shown in Figure 9.3.

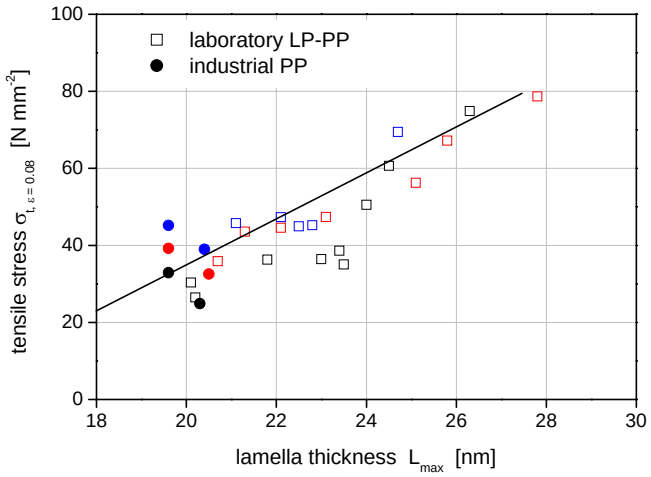

Figure 9.3: Tensile stress at 8 % strain as a function of maximum lamella thickness

By contrast, the stiffness of the injection-moulded micro dumbbell specimens is determined by the mobility of the amorphous fraction, for which see Figure 9.4. The magnitude of β-relaxation shown indicates the mobility of the amorphous phase. This means, the morphology of the interlamellar amorphous fraction is of greater importance than the overall content of the amorphous phase.

For the investigated PP specimens, crystallinity decreases as molecular weight increases, although tensile strength and stiffness increase. By contrast, when the crystallinity of the same molecular samples was increased by annealing at higher temperatures, tensile strength and stiffness also increased. Thus, the common assumption that the strength and stiffness of

polymers increase with increasing crystallinity is valid only when molecular weight remains the same.

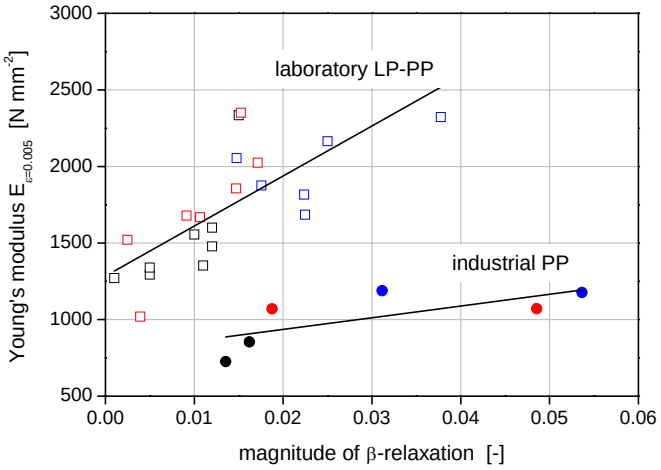

Figure 9.4: Young's modulus as dependent on the mobility of amorphous fraction, indicated by the magnitude of β-relaxation

Moreover, it has been found that highly oriented shish kebab structures are more temperature-resistant than, for example, spherulitic structures. This fact is supported by stiffness measured as dependent on temperature. Samples with shish kebab morphology show 100 times higher stiffness at temperatures of above 80°C than samples with classic spherulitic superstructure (see Figure 8.12). However, during annealing of the injection-moulded micro dumbbell specimens at 140°C for 1 hour some kind of superstructure re-arrangement takes place, coupled with distinctive stiffness loss starting at a temperature of 50°C (see Figures 8.12 and 8.13). Nevertheless, this structural reorganisation has no pronounced influence on tensile strength and stiffness, as measured at room temperature. On the other hand, changes in crystal-crystal sliding behaviour can be observed. The structure formed after annealing at elevated temperature behaves like spherulitic structure. Studies on the damping behaviour of LP-PP samples clearly show a change in α-relaxation behaviour. Crystals formed inside spherulites (in the case of low molecular weight samples) slide more easily than shish kebab structures. The shish kebabs interlock with each other due to their extended structure with circular grown lamellae. Thereby they are hindered from sliding between each other; the higher the number of shish kebabs, the worse the sliding, which is the case in particular for the highest molecular weight sample PP-L1600, where the lowest mechanical α-response is found (Figure 8.10).

In particular, Figures 9.3 and 9.4 clearly show that for industrial PP samples, additional influencing factors, such as extra additives or different synthesis conditions, should be taken into account for an understanding of strength and stiffness behaviour in relation to lamellar structure and magnitude of β-relaxation.

This again confirms that for a fundamental understanding of the relationship between structure and properties, systematic investigations should be carried out on well-defined samples polymerised and manufactured under recognised, precise, and controlled conditions. Only in this way is it possible to achieve a detailed basic understanding of the structure-properties relationship.

10 REFERENCES

[1] D. Ulbrich, M. Vollmer, *Makrom. Chem.* **2002**, *50*, 350.

[2] U. Reifenhäuser, *press conference K2004* Düsseldorf 12.10.**2004**.

[3] W. C. Kuhlke, *ANTEC* Dallas **2001.**

[4] W. C. Kuhlke, T. S. Walsh, *ANTEC* San Francisco **2002.**

[5] J. C. Chadwick, J. J. Heere, O. Sudmeijer, *Macromol. Chem. Phys*. **2000**, *201*, 1846.

[6] J. C. Chadwick, G. Morini, E. Albizzati, G. Balbontin, I. Mingozzi, A. Cristofori, O. Sudmeijer, G. M. van Kessel, *Macromol. Chem. Phys*. **1996,** *197*, 2501.

[7] G. B. Meier, G. Weickert, W. P. M. van Swaaij, *J. Polym. Sci. Part A: Polym. Chem.* **2001**, *39*, 500.

[8] U. Parasu Veera, G. Weickert, *Polym. React. Eng*. **2003**, *11*, 33.

[9] Y. V. Zakharov, G. D. Bukatov, Y. I. Yermakov, *Adv. Polym. Sci*. **1983**, *51*, 61.

[10] Y. V. Kissin, L. A. Rishina, *J. Polym. Sci., Part. A: Polym. Chem.* **2002**, *40*, 1353.

[11] Y. V. Kissin, R. Ohnishi, T. Konakazawa, *Macrom. Chem. Phys*. **2004**, *205*, 284.

[12] Y. V. Kissin, L. A. Rishina, E. I. Vizen, *J. Polym. Sci., Part A: Polym. Chem*. **2002**, *40*, 1899.

[13] J. J. Samson, P. J. Bosman, G. Weickert, K. R. Westerterp, *J. Polym. Sci., Part A: Polym. Chem.* **1999**, *37*, 219.

[14] J. J. C. Samson, G. Weickert, *SPE* **2000**, 333.

[15] J. T. M. Pater, G. Weickert, W. P. M. van Swaaij, *J. Appl. Polym. Sci.* **2003**, *87*, 1421.

[16] J. T. M. Pater, G. Weickert, W. P. M. Swaaij, *AlChE* **2003**, *49*, 180.

[17] G. B. Meier, G. Weickert, W. P. M. van Swaaij, *J. Appl. Polym. Sci*. **2001**, *81*, 1193.

[18] G. Natta, G. Mazzanti, P. Longi, F. Bernadini, *Chim. Ind. (Milan)* **1959**, *41*, 519.

[19] J. B. P. Soares, A. E. Hamielec, *Polymer* **1996**, *37*, 4607.

[20] J. B. P. Soares, A. E. Hamielec, *Polymer* **1996**, *37*, 4599.

[21] E. Martuscelli, M. Avella, A. L. Segre, E. Rossi, G. Di Drusco, P. Galli, T. Simonazzi, *Polymer* **1985**, *26*, 259.

[22] W. K. A. Shaffer, W. H. Ray, *J. Appl. Polym. Sci*. **1997,** *65*, 1053.

[23] E. P. Moore, "*Polypropylene Handbook – Polymerisation, Characterization, Properties, Applications*" Hanser Publisher, Munich, **1996**.

[24] M. K. Gosh, S. Maiti, *J. Polym. Mat*. **1999**, *16*, 113.

[25] N. Kashiwa, H. Kaneko, S. Kojoh, *Intern. Polym. Sci. Techn.* **2003**, *30*, 1.

[26] W. Kaminsky, *J. Polym. Sci. Part A: Polym. Chem.* **2004**, *42*, 3911.

[27] M. Lamberti, M. Mazzeo, D. Pappalardo, A. Zambelli, C. Pellecchia, *Macrom. Symp.* **2004**, *213*, 235.

[28] C. J. G. Plummer, *Adv. Polym. Sci.* **2004**, *169*, 75.

[29] P. Corradini, *J. Polym. Sci. Part A: Polym. Chem*. **2004**, *42*, 391.

[30] P. J. Flory, *J. Am. Chem. Soc.* **1945**, *67*, 2048.

[31] T. Ogawa, *J. Appl. Polym. Sci.* **1992**, *44*, 1869.

[32] S. Osawa, H. Mukai, T. Ogawa, R. S. Porter, *J. Appl. Polym. Sci.* **1998**, *68*, 1297.
[33] C. Albano, R. Sciamanna, D. Kaiser, G. Delgado, *Revista Facultad de Ingenieria* **2001**, *16*, 69.
[34] M. R. Kantz, H. D. Newman, F. H. Stigale, *J. Appl. Polym. Sci.* **1972**, *16*, 1249.
[35] F. Altendorfer, E. Seitl, *Kunststoffe* **1986**, *76*, 47.
[36] F. Jay, J. M. Haudin, B. Monasse, *J. Mat. Sci*. **1999**, *34*, 2089.
[37] R. Phillips, G. Herbert, J. News, M. Wolkowicz, *Polym. Eng. Sci.* **1994**, *34*, 1731.
[38] L. Incarnato, P. Scarfato, D. Acierno, *Polym. Eng. Sci.* **1999**, *39*, 749.
[39] M. Fujiyama, T. Wakino, *J. Appl. Polym. Sci*. **1991,** *43*, 57.
[40] M. Gahleitner, J. Wolfschwenger, C. Bachner, K. Bernreitner, W. Neißl, *J. Appl. Polym. Sci*. **1996,** *61*, 649.
[41] G. H. Michler, *Colloid Polym. Sci.* **1992**, *270*, 627.
[42] R. J. Young, *Phil. Mag.* **1974**, *30*, 85.
[43] B. A. G. Schrauwen, L. C. A. Breemen, A. B. Spoelstra, L. E. Govaert, G. W. M. Peters, H. E. H. Meijer, *Macromolecules* **2004**, *37*, 8618.
[44] D. W. van der Meer, B. Pukanszky, G. J. Vansco, *J. Macromol. Sci. Phys.* **2002**, *B41*, 1105.
[45] M. Prox, G. W. Ehrenstein, *Kunststoffe* **1991**, *81*, 11.
[46] F. de Candia, G. Romano, A. O. Baranov, E. V. Prut, *J. Appl. Polym. Sci.* **1992**, *46*, 1799.
[47] A. J. Pennings, A. M. Kiel, *Kolloid Z. Z. Polym.* **1965**, *205*, 160.
[48] A. Keller, *J. Polym. Sci.* **1955**, *15*, 31.
[49] A. Keller, M. J. Machin, *J. Macromol. Sci. Part B: Phys.* **1967**, *1*, 41.
[50] M. J. Hill, A. Keller, *J. Macromol. Sci. Part B: Phys.* **1971**, *3*, 591.
[51] G. Kalay, M. J. Bevis, *J. Polym. Sci. Part B: Polym. Phys.* **1997**, *35*, 241.
[52] G. Kalay, M. J. Bevis, *J. Polym. Sci. Part B: Polym. Phys.* **1997**, *35*, 265.
[53] A. I. Isayev, T. W. Chan, K. Shimojo, M. Gmerek, *J. Appl. Polym. Sci.* **1995**, *55*, 807.
[54] A. I. Isayev, T. W. Chan, M. Gmerek, K. Shimojo, *J. Appl. Polym. Sci.* **1995**, *55*, 821.
[55] P. Zhu, G. Edward, *Polymer* **2004**, *45*, 2603.
[56] M. Seki, D. W. Thurman, J. P. Oberhauser, J. A. Kornfield, *Macromolecules* **2002**, *35*, 2583.
[57] M. Fujiyama, Y. Kitajima, H. Inata, *J. Appl. Polym. Sci*. **2002** *84*, 2142.
[58] M. Gahleitner, C. Bachner, E. Ratajski, G. Rohaczek, W. Neißl, *J. Appl. Polym. Sci*. **1999,** *73*, 2507.
[59] M. Fujiyama, H. Inata, *J. Appl. Polym. Sci*. **2002,** *84*, 2157.
[60] M. Fujiyama, H. Inata, *J. Appl. Polym. Sci*. **2002,** *85*, 1851.
[61] P. Viville, D. Daoust, A. M. Jonas, B. Nysten, R. Legras, M. Dupire, J. Michel, G. Debras, *Polymer* **2001**, *42*, 1953.
[62] C. Stern, A. R. Frick, J. T. M. Pater, G. Weickert, *Macrom. Mat. Eng*. **2005**, *290*, 372.

[63] C. Stern, A. R. Frick, G. Weickert, G. H. Micher, S. Henning, *Macrom. Mat. Eng*. **2005**, *290*, 621.
[64] B. A. G. Schrauwen, R. P. M. Janssen, L. E. Govaert, H. E. H. Meijer, *Macromolecules* **2004**, *37*, 6069.
[65] A. Elmoumni, H. Henning Winter, A. J. Wadden, *Macromolecules* **2003**, *36*, 6453.
[66] K. Yamada, M. Hikosaka, A. Toda, S. Yamazaki, K. Tagashira, *J. Macrom. Sci. Part B: Phys.* **2003**, *42*, 733.
[67] R. Tiemblo, J. M. Gómez-Elvira, S. Garcia Beltran, L. Matisova-Rychla, J. Rychly, *Macromolecules* **2002**, *35*, 5922.
[68] J. Loos, M. Arndt-Rosenau, U. Weingarten, W. Kaminsky, P. J. Lemstra, *Polymer Bulletin* **2002**, *48*, 191.
[69] A. Marigo, C. Marega, R. Saini, I. Camurati, *J. Appl. Polym. Sci.* **2001**, *79*, 375.
[70] X. Guo, A. I. Isayev, M. Demiray, *Polym. Eng. Sci.* **1999**, *39*, 2132.
[71] A. O. Ibhadon, *J. Appl. Polym. Sci.* **1998**, *69*, 2657.
[72] E. R. Sadiku, *Acta Polym.* **1990**, *41*, 446.
[73] J. Varga, *J. Mat. Sci.* **1992**, *27*, 2557.
[74] D. C. Basset, *J. Macromol. Sci. Phys.* **1996**, *B35*, 277.
[75] G. W. Ehrenstein, "*Polymer-Werkstoffe, Struktur, Eigenschaften, Anwendung*" 2nd Edn., Hanser Publisher, Munich, **1999**.
[76] R. A. Campbell, P. J. Phillips, *Polymer* **1993**, *34*, 4809.
[77] B. Wunderlich, "*Macromolecular Physics*" Vol. 1, Academic Press, New York, **1973**.
[78] J. Radhakrishnan, K. Ichikawa, K. Yamada, *Polymer* **1998**, *39*, 2995.
[79] J. Varga, *J. Therm. Analysis* **1989**, *35*, 1891.
[80] J. Varga, G. Garzo, A. Ille, *Angew. Makrom. Chem.* **1986**, *142*, 171.
[81] J. Varga, J. Karger-Kocsis, *J. Polym. Sci. Part B: Polym. Phys*., **1996**, *34*, 657.
[82] B. Lotz, *Polymer* **1998**, *39*, 4561.
[83] V. Caldas, G. R. Brown, *Polymer* **1994**, *35*, 899.
[84] A. E. Woodward, "*Understanding Polymer Morphology*" Hanser Publisher, Munich, **1995.**
[85] K. Matsumoto, I. Miura, K. Hayashida, *Kobunshi Ronbunshu* **1979**, *36*, 401.
[86] I. K. Park, H. K. Noether, *Coll. Polym. Sci.* **1975**, *253*, 824.
[87] G. H. Michler, "*Kunststoff-Mikromechanik – Morphologie, Deformations- und Bruchmechanismen*" Hanser Publisher, Munich, **1992**.
[88] F. H. Müller, *Kunststoffe* **1954**, *44*, 569.
[89] T. Juska, I. R. Harrison, *Polym. Eng. Rev*. **1982**, *2*, 13.
[90] M. Aboulfaraj, C. G'Sell, B. Ulrich, A. Dahoun, *Polymer* **1995**, *36*, 731.
[91] A. Peterlin, *J. Mat. Sci.* **1971**, *6*, 490.
[92] A. Peterlin, *Int. J. Fract.* **1975**, *11*, 761.
[93] A. Peterlin, *Coll. Polym. Sci.* **1987**, *265*, 357.
[94] A. Peterlin, *Polym. Eng. Sci.* **2004**, *3*, 183.

[95] R. J. Samuels, "*Structured Polymer Properties*" John Wiley, New York, **1974**.
[96] H. J. Kestenbach, J. Petermann, *Polymer* **1994**, *35*, 5217.
[97] H. Zhou, G. L. Wilkes, *J. Mat. Sci.* **1998**, *33*, 287.
[98] F. H. Müller, *Mat. Prüf.* **1963**, *5*, 336.
[99] K. Jäckel, *Kolloid Z. Z. Polym.* **1954**, *137*, 130.
[100] P. I. Vincent, *Polymer* **1960**, *1*, 7.
[101] I. Naundorf, S. Osterloh, G. Fischer, *Plastverarbeiter* **1995**, *45*, 18.
[102] I. Naundorf, S. Osterloh, G. Fischer, *Plastverarbeiter* **1995**, *45*, 120.
[103] D. Göritz, F. H. Müller, *Coll. Polym. Sci.* **1974**, *252*, 862.
[104] D. Göritz, F. H. Müller, *Coll. Polym. Sci.* **1975**, *253*, 844.
[105] B. Cayrol, J. Petermann, *Coll. Polym. Sci.* **1975**, *253*, 840.
[106] M. Al-haj Ali, B. Roffel, G. Weickert, B. Bettlem, *AlChE,* submitted
[107] I. C. van Putten, "*Propylene polymerisation in a circulating slugging fluidized bed reactor*" Ph.D. Thesis, University of Twente **2004**.
[108] V. B. Mathot, L. Benoist, "*Calorimetry and thermal analysis of polymers*" Hanser Publisher, Munich **1994**.
[109] V. A. Bershtein, V. M. Egorov, *"Differential Scanning Calorimetry of Polymers. Physics, Chemistry, Analysis*" Ellis Horwood, London, **1994**.
[110] J. Brandrup, E. H. Immergut, "*Polymer Handbook*" 3rd Edn., Wiley, New York, **1989**.
[111] G. Kämpf, "*Characterization of plastics by physical methods: experimental techniques and practical application*" Hanser Publisher, Munich, **1986**.
[112] R. H. Olley, D. C. Bassett, P. J. Hine, I. M. Ward, *J. Mat. Sci.*, **1993**, *28*, 1102.
[113] G. Lawes, "*Scanning electron microscopy and x-ray microanalysis*" Wiley, Chichester, **1987**.
[114] C. L. Rohn, "*Analytical Polymer Rheology, Structure, Processing, Property Relationship*" Hanser Publisher, Munich, **1995**.
[115] K. P. Menard, "*Dynamic mechanical analysis: a practical introduction*" CRC Press LLC, Florida **1999**.
[116] H. V. Boenig, *Elsevier Publishing Company Amsterdam*, **1966**.
[117] M. A. Ferrero, M. G. Chiovetta, *Polym. Eng. Sci.* **1991**, *31*, 904.
[118] M. A. Ferrero, A. Koffi, R. Sommer, W. C. Conner, *J. Polym. Sci. Part A: Polym. Chem.* **1992**, *30*, 2131.
[119] A. S. Hoffman, B. A. Fries, P. C. Condit, *J. Polym. Sci.* **1963**, *4*, 109.
[120] G. Bourat, J. Ferrier, A. Perez, *J. Polym. Sci*. **1963**, *4*, 103.
[121] G. Guastalla, U. Giannini, *Makromol. Chem. Rapid Commun*. **1983**, *4*, 519.
[122] B. Boucheron, *Eur. Polym. J.* **1975**, *11*, 131.
[123] E. M. Pijpers, B. C. Foest, *Eur. Polym. J.* **1972**, *8*, 1151.
[124] P. Kittilsen, T. F. McKenna, H. Svendsen, H. A. Jakobsen, S. Fredrisken, *Chem. Eng. Sci.* **2001**, *56*, 4015.
[125] M. W. Murphy, K. Thomas, M. J. Bevis, *Plast. Rubber Process. Appl.* **1988**, *9*, 3.

[126] J. P. Trotignon, J. Verdu, *J. Appl. Polym. Sci.* **1987**, *34*, 1.
[127] J. P. Trotignon, J. Verdu, *J. Appl. Polym. Sci.* **1987**, *34*, 19.
[128] Y. Churdpunt, A. I. Isayev, *J. Polym. Eng.* **2000**, *20*, 77.
[129] J. H. Reinshagen, R.W. Dunlap, *J. Appl. Polym. Sci.* **1976**, *20*, 9.
[130] M. Gahleitner, *Prog. Polym. Sci*. **2001**, *26*, 895.
[131] G. Weickert, *Polymerisation technology (OSPT)*, Twente **2004**.
[132] C. Tzoganakis, J. Vlachopoulos, A. E. Hamielec, *Polym. Eng. Sci*. **1989**, *29*, 390.
[133] M. Minoshima, J. L. White, J. E. Spruiell, *Polym. Eng. Sci.* **1980**, *20*, 1166.
[134] S. E. Bechtel, V. T. Youssef, M. G. Forest, H. Zhou, K. W. Koelling, *Rheo. Acta* **2001**, *40*, 373.
[135] R. R. Rahalkar, *Rheologica Acta* **1989**, *28*, 166.
[136] H. K. Chuang, C. D. Han, *J. Appl. Polym. Sci.* **1984**, *29*, 2205.
[137] V. P. Privalko, V. B. Dolgoshey, E. G. Privalko, V. F. Shumsky, A. Lisovski, M. Rodensky, M. S. Eisen, *J. Macrom. Sci. Part B: Physics* **2002**, *3*, 539.
[138] E. R. Harrell, N. Nakajima, *J. Appl. Polym. Sci.* **1984**, *29*, 995.
[139] M. Aboulfaraj, B. Ulrich, A. Dahoun, C. G'Sell, *Polymer* **1993**, *34*, 4817.
[140] W. J. O'Kane, R. J. Young, A. J. Ryan, *J. Macrom. Sci. Part B: Physics* **1995**, *34*, 427.
[141] M. F. S. Lima, M. A. Z. Vasconcellos, D. Samios, *J. Polym. Sci., Part B: Polym. Phys.* **2002**, *40*, 896.
[142] H. Lu, J. Qiao, Y. Xu, Y. Yang, *J. Appl. Polym. Sci.* **2002**, *85*, 333.
[143] E. L. Heeley, A. V. Maidens, P. D. Olmsted, W. Bras, I. P. Dolbnya, J. P. A. Fairclough, N. J. Terrill, A. J. Ryan, *Macromolecules* **2003**, *36*, 3656.
[144] C. de Rosa, F. Auriemma, T. Circelli, *Macromolecules* **2002**, *35*, 3622.
[145] M. Kakugo, H. Sadatoshi, J. Sakai, M. Yokoyama, *Macromolecules* **1989**, *22*, 547.
[146] M. A. Ferrero, E. Koffe, R. Sommer, W. C. Conner, *J. Polym. Sci. Part A: Polym. Chem.* **1992**, *30*, 2131.
[147] F. Johannaber, H. Thoma, *Kunststoffe* **2000**, *10*, 48.
[148] I. Catic, *Gummi, Fasern, Kunststoffe* **2002**, *55*, 382.
[149] M. Koch, *Kunststoffe Plast Europe*, **2004**, *94*, 122.
[150] J.-M. Haudin, C. Duply, B. Monasse, J.-L. Costa, *Macromol. Symp.* **2002**, *185*, 119.
[151] R. H. Somani, L. Yang, I. Sics, B. S. Hsiao, N. V. Pogadina, H. H. Winter, P. Agarwal, H. Fruitwala, A. Tsou, *Macromol. Symp*. **2002**, *185*, 105.
[152] R. Pantani, V. Speranza, A. Sorrentino, G. Titomanlio, *Macromol. Symp.* **2002**, *185*, 293.
[153] W. Ren, *Col. Polm. Sci*. **1992**, *270*, 943.
[154] S. Piccarolo, *J. Macromol. Sci. Phys*. **1992**, *B31*, 501.
[155] G. Eder, H. Janeschitz-Kriegl, G. Krobath, *Col. Polym. Sci.* **1988**, *266*, 1087.
[156] B. de Carvalho, R. E. S. Bretas, *J. Appl. Polym. Sci.* **1998**, *68*, 1159.
[157] R. H. Somani, L. Yang. B. S. Hsiao, T. Sun, N. V. Pogodina, A. Lustiger, *Macromolecules* **2005**, *38*, 1244.

[158] G. Kumaraswamy, A. M. Issaian, J. A. Kornfield, *Macromolecules* **1999**, *32*, 7537.
[159] A. K. van der Vegt, P. P. A. Smit, SCI Monograph, **1967**, *26*, 313.
[160] A. Fasano, A. Mancini, S. Mazzullo, "Isobaric crystallisation of polypropylene", in: *Complex Flows in Industrial Processes*, A. Fasano, Eds., Birkhäuser, **1999**, *5*, 149.
[161] F. Johannaber, M. Walter, *"Handbuch Spritzgießen"* Hanser Publisher, Munich, **2001**.
[162] B. Möginger, C. Lutz, A. Polsak, U. Fritz, *Kunststoffe* **1991**, *81*, 251.
[163] G. Eder, H. Janeschitz-Kriegl, "Crystallisation", in: *Materials Science and Technology, A comprehensive Treatment*, R. W. Cahn, P. Haasen, E. J. Kramer, Eds., Vol. 18, VCH, Weinheim **1997**.
[164] A. Frick, C. Stern, *Kunststoffe* **2002**, *7*, 46.
[165] A. Frick, A. Rochman, C. Stern, *Kunststoffe* **2004**, *8*, 132.
[166] M. Fujiyama, T. Wakino, Y. Kawasaki, *J. Appl. Polym. Sci.* **1988**, *35*, 29.
[167] Z. Mencik, D. R. Fitchmun, *Polm. Sci.* **1973**, *11*, 973.
[168] D. Tartari, M. Bramuzzo, *Kunststoffe* **1993**, *83*, 6.
[169] S. Henning, R. Adhikari, G. H. Michler, F. H. Baltá Calleja, J. Karger-Kocsis, *Macromol. Symp.* **2004**, *214*, 157.
[170] A. Eckstein, J. Suhm, C. Friedrich, R.-D. Maier, J. Sassmannshausen, M. Bochmann, R. Mülhaupt, *Macromolecules* **1998**, *31*, 1335.
[171] S. Wu, *J. Polym. Sci. Part B: Polym. Phys.* **1987**, *25*, 557.
[172] S. Wu, *Polymer* **1987**, *28*, 1144.
[173] A. Romankiewicz, T. Sterzynski, *Macromol. Symp.* **2002**, *180*, 241.
[174] B. Heck, T. Hugel, M. Iijima, E. Sadiku, G. Strobly, *New J. Phys.* **1999**, *1*, 17.1.
[175] T. Dötsch, M. Pollard, M. Wilhelm, *J. Phys. Condens. Matter* **2003**, *15*, 923.
[176] G. H. Michler, K. Morawietz, *Acta Polym.* **1991**, *42*, 620.
[177] P. J. Barham, "Crystallization and morphology of semicrystalline polymers", in: *Materials Science and Technology, A comprehensive Treatment*, R. W. Cahn, P. Haasen, E. J. Kramer, Eds., Vol. 12, VCH, Weinheim **1993**.
[178] W. J. O'Kane, R. J. Young, *J. Mat. Sci. Letters* **1995**, *14*, 433.
[179] R. J. Young, *J. Phil. Mag.* **1974**, *30*, 85.
[180] R. Séguéla, *J. Polym. Sci. Part B: Polym. Phys.* **2002**, *40*, 593.
[181] N. G. McCrum, B. E. Read, G. Williams, *"Anelastic and Dielectric Effects in Polymeric Solids"* Wiley, New York, **1967**.
[182] A. Suzuki, T. Sugimura, T. Kunugi, *J. Appl. Poly. Sci.* **2001**, *81*, 600.
[183] M. Pluta, Z. Bartczak, A. Galeski, *Polymer* **2000**, *41*, 2271.
[184] C. Jourdan, J. Y. Cavaille, J. Perez, *J. Polym. Sci. Part B: Polym. Phys.* **1989**, *27*, 2361.

ACKNOWLEDGMENTS

The challenges which are experienced when entering a new field of experimental work, kept me going for the last five years was only possible due to the support and assistance of many people. I would like to acknowledge all persons who have seen it all materialise in the form of this work.

First, I would like to thank my promotors Prof. Dr. Günter Weickert and Prof. Dr. Achim Frick for their support and their guidance during the last years I have worked on this research.

I would like to sincerely thank Prof. Dr. Günter Weickert to give me an opportunity to perform my PhD at the University of Twente.

In particular, I would like to express my heartfelt gratitude to Prof. Dr. Achim Frick. Your faith and support have greatly encouraged me during the last years. Without the enthusiasm and inspiration, you have provided on an every day basis, this work would have been hardly possible.

I would like to direct acknowledgements to all my colleagues and diploma students of 'Polymer Sciences and Processing' at Aalen University for perfect working and social atmosphere. My specials thanks goes to Arif Rochman, Przemyslav Fleszar and Steffi Trey for their creative ideas in making research. I also want to thank Helmuth Mayer for providing me with flow analysis and his help in interpretation of the data.

Furthermore, my gratitude goes to Mohammad Al-haj Ali, Dr. Inge van Putten and all other peoples form the 'Industrial Polymerisation Processes' group at University of Twente for helping me with the experimental part of this thesis.

Also, work for completion of this thesis has been done in collaboration with the group of Prof. Dr. Goerg Michler (Martin-Luther University of Halle). I would like to thank him and Sven Henning for all the morphological analysis they carried out, their interpretations and comments were extremely helpful in bringing this thesis to the final form.

Finally, I want to thank my friends and family for supporting me during the time I worked on this thesis.

Claudia
October 2005

CURRICULUM VITAE

Claudia S T E R N

Date / Place of Birth: April 22nd, 1975 / Ellwangen (Germany)
Nationality: German

Education

May 2001 - Nov. 2005	University of Twente, Enschede (The Netherlands) Faculty of Science and Technology, PhD studies
Oct. 1994 - Apr. 1999	Aalen University (Germany) Faculty of Chemistry, diploma degree in chemistry
Aug. 1993 - Jun. 1994	College, Aalen (Germany) Fachhochschulreife (equivalent to Leaving Certificate)
Aug. 1991 - Jun. 1993	College, Ellwangen (Germany) Apprenticeship as a Chemical-Technical-Assistant
Aug. 1985 - Jun. 1991	Secondary School, Unterschneidheim (Germany)

Employment history

Since October 2000	Aalen University (Germany) Department of Polymer Technology, research assistant
May 2000 - Aug. 2000	University of Birmingham (England) Department of Chemistry, research assistant
Oct. 1999 - Apr. 2000	DaimlerChrysler AG, Research Centre Ulm (Germany) Department for Environmental Analysis and Hazardous Material Management, research assistant
Sep. 1998 - Sep. 1999	Fraunhofer Institute of Chemical Technology, Pfinztal (Germany), Member of Research Group “In-/On-Line Measurement Technology for Polymer Processing”
Mar. 1997 - Aug. 1997	Daimler-Benz AG, Research Centre Ulm (Germany) Department of Production and Environmental Technology, trainee

LIST OF PUBLICATIONS

Books

[1] A. Frick, C. Stern, "*DSC-Prüfung in der Anwendung*", Hanser Publisher, Munich, **2006**.

[2] A. Frick, C. Stern, "Neue Einsatzmöglichkeiten der dynamischen Differenzkalorimetrie zur Qualitätskontrolle von Präzisionsbauteilen aus Kunststoffen", in: *Kennwertermittlung für die Praxis*, H. Frenz, A. Wehrstedt, Eds., Wiley-VCH, Weinheim **2003**, 180.

[3] A. Frick, C. Stern, A. Rochman, "Prozessintegrierte Werkstoffprüfung in der Kunststofftechnik", in: *Herausforderung durch den industriellen Fortschritt*, O. W. Buchholz, S. Geisler, Eds., Verlag Stahleisen, Düsseldorf **2003**, 270.

Publications international

[1] C. Stern, A. R. Frick, G. Weickert: New Findings on the Performance of PP, *Macromolecular Rapid Communications* **2005**, submitted.

[2] C. Stern, A. R. Frick, G. Weickert: Relation between structure and mechanical proeperties of PP: effect of shear-induced crystallisation and molecular weight, *Polymer* **2005**, submitted.

[3] A. Frick, C. Stern, U. Berger: Manufacturing of high quality micro prototypes by injection moulding using hybrid mould technology, *Journal of Engineering Manufacture* **2005**, accepted.

[4] C. Stern, A. R. Frick, G. Weickert, G. H. Michler, S. Henning: Processing, morphology and mechanical properties of liquid pool PP with different molecular weight, *Macromolecular Materials and Engineering* **2005**, *290*, 621.

[5] C. Stern, A. R. Frick, J. T. M. Pater, G. Weickert: Comparison of gas and liquid propylene polymerization technique, *Macromolecular Materials and Engineering* **2005**, *290*, 372.

[6] A. Frick, A. Rochman, C. Stern: Material-based process control recommended, *Kunststoffe plast europe* **2004**, *8*, 132.

[7] A. Frick, C. Stern: Residence in Haste, Long residence times affect the properties of PBT parts, *Kunststoffe plast europe* **2002**, *7*, 18.

Publications national

[1] A. Frick, A. Rochman, C. Stern: Werkstoffbasierte Prozesskontrolle empfohlen, *Kunststoffe* **2004**, *8*, 132.

[2] A. Frick, C. Stern: Qualitätssicherung von Kunststoffformteilen mittels DSC, Teil 1: Wareneingangskontrolle, *UserCom* **2004**, *19*, 16.

[3] A. Frick, C. Stern: Qualitätssicherung von Kunststoffformteilen mittels DSC, Teil 2: Fertigungskontrolle, *UserCom* **2004**, *20*, 9.

[4] A. Frick, C. Stern, J. Vänskä, H.-U. Weidmann, M. Jeworski: Ohne Drehung – Lichtmikroskopie in der Kunststofftechnik, *Qualität und Zuverlässigkeit* **2004**, *49*, 37.

[5] A. Frick, A. Rochman, C. Stern: Influence of process conditions on morphology and properties of TPU, *horizonte* **2004**, *25*, 49.

[6] A. Frick, C. Stern: Neues im Zusammenhang mit Polypropylene, *horizonte* **2003**, *23*, 35.

[7] A. Frick, A. Rochman, C. Stern: Material characterization and quality control of TPU elastomers, *Kautschuk Gummi Kunststoffe* **2003**, *6*, 330.

[8] A. Frick, C. Stern: Qualitätssicherung von Kunststoffformteilen mit Hilfe der Thermoanalyse, *horizonte* **2003**, *22*, 48.

[9] A. Frick, C. Stern: Auf die Temperatur kommt es an. Einfluss der Konditionierungs- und Verarbeitungsbedingungen auf die Qualitaet von PBT-Bauteilen, *Kunststoffberater* **2002**, *12*, 36.

[10] A. Frick, C. Stern: Verweile mit Eile – Zu lange Verweilzeiten beeinflussen die Eigenschaften von PBT-Bauteilen, *Kunststoffe* **2002**, *7*, 46.

Proceedings

[1] A. Frick, C. Stern, U. Berger, Manufacturing of high quality micro prototypes by injection moulding using hybrid mould technology, *International Conference on Multi-Material Micro Manufacture (4M)*, Karlsruhe (Germany) 29.Jun-01.Jul **2005**.

[2] C. Stern, A. Frick, G. Weickert: Difference in quality of iPP synthesised in gas phase and liquid pool, *3rd European Conference on the reaction engineering of polyolefines (ECOREP III)*, Lyon (France) 20.-24.Jun **2005**, 85.

[3] A. Frick, C. Stern, S. Henning, G. Michler, G. Weickert: Auswirkungen der scher-induzierten Kristallisation auf die Morphologie und die mechanischen Eigenschaften von iPP, *10. Problemseminar, Deformation und Bruchverhalten von Kunststoffen*, Merseburg 15.-17.Jun **2005**, CD-ROM

[4] A. Frick, M. Schackmann, C. Stern: Fließwegabhängige Morphologie in Mikroteilen aus POM, *10. Problemseminar, Deformation und Bruchverhalten von Kunststoffen*, Merseburg (Germany) 15.-17.Jun **2005**, CD-ROM

[5] C. Stern, A. Frick, G. Weickert: Influence of molecular weight on melt and solid state properties of new PP generation, *International conference on Polymeric materials 2004 - properties, processing, modification, application*, Halle (Germany) 29.Sep-01.Oct **2004**, CD-ROM

[6] C. Stern, A. Frick, I. C. van Putten, G. Weickert: Characterization of PP, Relationship between structure and properties, *9. Problemseminar, Deformation und Bruchverhalten von Kunststoffen*, Merseburg (Germany) 25.-27.Jun **2003**, 425.

[7] C. Stern, A. Frick: Zerstörungsfreie Bauteilprüfung in der Kunststofftechnik mittels Nah-Infrarot Spektroskopie, *9. Problemseminar, Deformation und Bruchverhalten von Kunststoffen*, Merseburg (Germany) 25.-27.Jun **2003**, 241.

[8] A. Frick, C. Stern: NIR-Spectroscopy, A new chance to quality management in polymer, *International conference on Materials Testing (TEST 2003)*, Nuernberg (Germany) 13.-15.May **2003**, 49.

[9] C. Stern, A. Frick: Investigations and modelling of structure-properties correlations of semi-crystalline polymers, exemplified with PBT, *International conference on Polymeric materials 2002 - properties, processing, modification, application*, Halle (Germany) 25.-27.Sep **2002**, 187.

[10] A. Frick, C. Stern: Influence of the production induced morphology on end-use properties of molded parts, *International conference on Polymeric materials 2002 - properties, processing, modification, application*, Halle (Germany) 25.-27.Sep **2002**, 191.

[11] A. Frick, C. Stern: Influence of injection moulding processing conditions on mechanical and thermal properties of poly(butyleneterephthalate) PBT, *University Journal Zeszyty Naukowe Pol. Ol., Chemia* **2001**, *146*, 199.

[12] C. Stern, A. Frick: Auswirkung hochwirksamer heterogener Nukleierung auf die Verarbeitungs- und Gebrauchseigenschaften von PBT, *8. Problemseminar, Deformation und Bruchverhalten von Kunststoffen*, Merseburg (Germany) 20.-22.Jun **2001**, 161.

[13] A. Frick, J. Lenza, C. Stern: Einsatz der dynamischen Differenzkalorimetrie zur Prüfung von spritzgegossenen Bauteilen aus Kunststoffen, *8. Problemseminar, Deformation und Bruchverhalten von Kunststoffen*, Merseburg (Germany) 20.-22.Jun **2001**, 197.